frontiers | Frontiers in Earth Science

TYPE Review
PUBLISHED 04 September 2023
DOI 10.3389/feart.2023.1159430

OPEN ACCESS

EDITED BY
James D. Muirhead,
The University of Auckland, New Zealand

REVIEWED BY
Lluis Fontboté,
Université de Genève, Switzerland
Matias Ghiglione,
University of Buenos Aires, Argentina

*CORRESPONDENCE
Daniel Wiemer,
daniel.wiemer@uwa.edu.au

RECEIVED 05 February 2023
ACCEPTED 16 August 2023
PUBLISHED 04 September 2023

CITATION
Wiemer D, Hagemann SG, Hayward N, Begg GC, Hronsky J, Thébaud N, Kemp AIS and Villanes C (2023), Cryptic trans-lithospheric fault systems at the western margin of South America: implications for the formation and localization of gold-rich deposit superclusters.
Front. Earth Sci. 11:1159430.
doi: 10.3389/feart.2023.1159430

Cryptic trans-lithospheric fault systems at the western margin of South America: implications for the formation and localization of gold-rich deposit superclusters

Daniel Wiemer[1]*, Steffen G. Hagemann[1], Nicholas Hayward[1,2], Graham C. Begg[1,3], Jon Hronsky[1,4], Nicolas Thébaud[1], Anthony I. S. Kemp[1] and Carlos Villanes[5]

[1]Centre for Exploration Targeting, School of Earth Sciences, University of Western Australia, Perth, WA, Australia, [2]Predict Ore Pty Ltd., Perth, WA, Australia, [3]Minerals Targeting International Pty Ltd., Perth, WA, Australia, [4]Western Mining Services Pty Ltd., Perth, WA, Australia, [5]Compañia Minera Poderosa S.A., Lima, Perú

We present a review of frontier research advances in the investigation of cryptic structures that transect the South American Andes at oblique strike directions. The intersections between these cryptic structures and the superimposed Andean belt correlate with the spatial distribution of gold-rich mineral deposit clusters. The deposit clusters can be described as superclusters, as they comprise various gold deposit types that formed at multiple times throughout the Phanerozoic, impinging repeatedly on the structural intersections. However, the cryptic inherited fault structures are difficult to detect, because their deeper-seated roots are often overlain by younger supracrustal successions, and/or their exposed surface manifestations are structurally obscured by subsequent tectonic-magmatic activity. Thus, it also remains a challenge to constrain the nature and timing of formation, and the respective subsequent evolutionary path, of these proposed pre-Andean structures. Based on various case studies, we demonstrate that the localization of identified Phanerozoic gold deposit superclusters along the western South American margin is fundamentally controlled by structural inheritance often dating back to at least the Mesoproterozoic. Integration of multi-approach observations and datasets allows insights into a larger-scale tectonic history that showcases the successive inheritance of major structures originating from the Amazonian Craton, over the Paleozoic Gondwana margin, into the Cenozoic magmatic belts of the Andes, and even into recent fractures within the subducting oceanic Nazca plate, recording >1.2-billion-years of progressive structural inheritance and growth at one of the longest-lived tectonic margins in Earth history. In contrast to previous models of the spatial distribution of gold deposits, based on statistical approaches and spatial periodicity in self-organized systems focusing on single subduction and/or accretion episodes and belts, we propose that the structural inheritance and intersections are key to the localization of gold deposits in the Andes. In combination with bulk-geochemical data from magmatic rocks, we suggest that inherited structures maintained a trans-lithospheric connectivity to pre-fertilized gold enriched upper mantle reservoirs, which were tapped during multiple tectono-magmatic reactivation episodes.

KEYWORDS

South America, Gondwana margin, Andes, structural inheritance, mineral systems, gold deposits, translithospheric fault, geodynamics

1 Introduction

The spatial distribution of economic ore deposits at tectonic margins remains a hotly debated subject with significance for the exploration of base and precious metals, such as copper and gold, respectively (e.g., Bierlein et al., 2006; Wyman et al., 2016; Groves et al., 2018; Hayward et al., 2018; Wiemer et al., 2022). Following early advances in the definition of favourable tectonic settings for specific deposit types, metals and metal associations (e.g., porphyry copper; Sawkins, 1972; Sillitoe, 1976; 2008; orogenic gold; Goldfarb et al., 1998), the advent of the *mineral system* concept provided a break-through recognition of essential underlying genetic processes and parameters for the formation of ore deposits within independent spatial-temporal frameworks (i.e., source—pathway—trigger; e.g., Wyborn et al., 1994; Hagemann and Brown, 2000; McCuaig et al., 2010; Hagemann et al., 2016). This allowed for a more holistic perspective on the relationship between the genesis of ore-deposits and their distribution that spawned a fruitful new era of *unifying models*, improving the translation of common geological processes and features into applicable target criteria (e.g., gold in accretionary orogens; Hronsky et al., 2012).

However, insights into both the genesis and the distribution of ore deposits are often still based on the investigation and understanding of individual deposits, with a common focus on the largest (i.e., world-class) known examples to derive unifying frameworks that are relevant at the regional to global scale (e.g., Jiadong orogenic gold province; Groves and Santosh, 2016). Furthermore, the identification of spatial controls is frequently based on hindsight recognition, with limited significance for future greenfield exploration targeting. In addition, as most of Earth's near-surface (<100 m) economic potential is known, the frontiers of metal ore exploration require advanced predictive targeting strategies, aiming for discoveries of evermore deeper (i.e., concealed) crustal ore deposits blind to conventional exploration methods, or in more remote and historically inaccessible jurisdictions, and/or satellite expressions of larger-scale deposit clusters of a particular mineral system.

Indeed, one of the main shortcomings of predictive power seems to lie in the lack of understanding the causative relationships between spatial, temporal, and genetic processes within broader geodynamic contexts. Whereas the importance of first-order, arc- or greenstone belt -parallel faults as primary, trans-lithospheric pathways for metal-bearing magmas and ore-fluids is commonly accepted (e.g., Neumayr et al., 1998; Haeberlin et al., 2002; Sillitoe and Perello, 2005; Bierlein et al., 2006; Goldfarb et al., 2008; Groves et al., 2018), the along-strike spatial distribution of deposits commonly remains poorly studied or controversial (e.g., Angerer et al., 2018). Various studies attest to the presence of major deposit clusters located at sites of structural complexity along, and/or in vicinity to, their first-order fault system (e.g., Eisenlohr et al., 1989; Neumayr et al., 1998; Thébaud et al., 2018; Piquer et al., 2021a; Wiemer et al., 2021a; 2022). Importantly, however, the recognition of sites of structural complexity as favourable ore deposit "hot-spots," invoked the emanation of two endmember hypotheses: i) the emergence of self-organized systems and spatial periodicity (e.g., Hronsky, 2011; Hayward et al., 2018), and ii) ancient structural inheritance (e.g., Chernicoff et al., 2002; McCuaig and Hronsky, 2014; Wiemer et al., 2021a; 2022). Both these hypotheses are based on well-recognized processes in the *natural sciences*, and ultimately may not necessarily operate mutually exclusive. Nevertheless, their role in ore deposit formation and distribution, and thus predictive target solutions, requires further research.

This review paper summarizes the general endmember models for the spatial distribution of ore deposits, while keeping in mind the possibility of syn-mineralization structure development, followed by a critical review on the tectonic and metallogenic evolution of South America, focussing on gold-rich porphyry, intrusion related and orogenic mineral systems along the western Gondwana margin and subsequent Andean belt. The distribution of ore deposits and deposit clusters along the western South American margin was used previously to demonstrate both endmember modes of spatial-genetic control, as the region represents a suitable natural laboratory to test respective hypotheses, due to the presence of extensive and well-preserved ore-rich arc segments (i.e., metallogenic belts) on the one hand (e.g., Sillitoe, 1976; 2008; Sillitoe and Perello, 2005; Carlotto et al., 2009; Hayward et al., 2018), and the notion of cryptic ancient lineaments and inherited Andean cross-faults, on the other hand (e.g., Chernicoff et al., 2002; Richards, 2003; Love et al., 2004; Ramos, 2008; McCuaig and Hronsky, 2014; Wiemer et al., 2022).

To this end, we present a synthesis of the >1 billion year tectonic-metallogenic evolution of western South America, highlighting the emergence of continent-scale structural patterns and ore-associated corridors, which are discussed in the light of cryptic structural inheritance as a result of a long-lived and complex history of cratonic boundary reactivation, micro-terrane dispersal and (re-)accretion. In addition, we present both new and compiled (global) geochemical data, addressing critical characteristics of mafic parental magmas associated with gold-rich deposits. The data support the notions of trans-lithospheric permeability and the inheritance of pre-fertilized mantle domains, in conjunction with polyphase structural-tectonic inheritance (e.g., Hronsky et al., 2012; Xiong et al., 2021; Wiemer et al., 2022).

2 Endmember models for the distribution of mineral deposits at tectonic margins

2.1 General perspective within the mineral system concept

The *mineral system* concept is based on the recognition of four essential ingredients, i.e., i) an ore-fertile source, ii) structural pathways to carry metal-bearing magma or fluid from source to sink, iii) a geodynamic trigger event that provides required energy to initiate and maintain magmatic source-extraction and magma/fluid

transport, and iv) an efficient metal trap to concentrate and preserve ore. Because Earth's mantle and crust are not readily enriched in economic concentrations of metals (e.g., McDonough and Sun, 1995), respective ore-fertile sources, or reservoirs, require either a *pre-enrichment* of metal (i.e., potentially multiple ancient/pre-mineralization geologic processes), and/or a *selective extraction* of metal (e.g., as incompatible species at low degrees of partial melting, i.e., a combination of source and trigger process; e.g., Hronsky et al., 2012). Similarly, the origin of structural pathways may be temporally and genetically unrelated to the processes that drive their (re-) activation at the time of ore deposit formation (e.g., earthquakes along pre-existing structures to cause fault-valve style fluid ascent and associated mineralization; e.g., Sibson, 1985; 1992). In fact, the geodynamic trigger is often cited as a reactivation event, and mostly documented as part of a transient tectonic switch (e.g., transpression to transtension; e.g., Goldfarb et al., 2008; Voute et al., 2019; Trunfull et al., 2020; Trevisan et al., 2021; Wiemer et al., 2021a; Bogossian et al., 2021; Loucks, 2021). Specific geodynamic triggers may drive fertility in magmas through the creation of transient compressive stress traps in the lower crust that localize sustained magma replenishment and batch fractionation (e.g., Loucks, 2021).

The most fundamental factor is the sequence of past geodynamic processes, which shape the evolutionary path that ultimately leads to the confluence of favourable parameters, at which point in time the formation of an ore deposit seems inescapable (e.g., Hronsky et al., 2012; Wiemer et al., 2022). But, *where exactly do deposits form along their principal first-order, arc-parallel fault zone structure?* Deposits and deposit clusters are often situated at sites of structural complexity or damage zones (i.e., reactivated fault intersections, jogs, bends, relays) characterized by increased permeability and connectivity, which promote the accumulation of magma and/or hydrothermal fluids (e.g., McCuaig and Hronsky, 2014; Wiemer et al., 2021a; 2022). Damage zones may arise during i) one-event systems, in which reactivation directly follows upper mantle fertilization and development of structural architecture during a single subduction episode. In this case *self-organization* may play a critical role in the distribution of zones of high permeability and increased magma/fluid flux. On the other hand, ii) geodynamic trigger events can cause the re-activation of structures (and fossil fertile mantle domains) that were already established during a former tectonic event. In this case *structural inheritance* may dictate the location of increased mass and energy fluxes. Importantly, structural inheritance, or the location and spacing of pre-existing structures, may have been subject to self-organization (Hayward et al., 2018). Hence, to advance predictability and refine exploration strategies, a comprehensive knowledge of the tectonic history of a respective region is necessary.

2.2 Self-organized systems and spatial periodicity

Self-organization and criticality, explaining the behaviour of complex natural systems, have been applied to the distribution of mineral deposits (Chadam and Ortoleva, 1990; Bak, 1996). Hronsky (2011) noted that deposits may exhibit a power law distribution and fractal geometry. Additionally, he argued that the formation of mineral systems often involves rapid focussed release of a large amount of energy after a slow build-up, indicating criticality. This concept encompasses three key ideas: the self-organization of energy and mass fluxes to maximize entropy production (seen in regular/power law spacing), the degree of order or size of the potential energy gradient that a system seeks to remove (explored through fractal geometry and resource endowment), and the spontaneous emergence of spatial patterns once a threshold barrier is surpassed (Schneider and Dorion, 2005).

Hayward et al. (2018) explored geological phenomena (e.g., hydrothermal convection cells, magmatic diapirism, crustal fault segmentation, and buckling instabilities) and their interaction in higher-level self-organization. They concluded that the intersection of fault systems with inherited spatial periodicity plays a significant role in shaping the distribution of periodic deposit clusters. However, whereas the presence of these phenomena (i.e., lower-level system components) may be identified, our present lack of knowledge of complex interactions and feedback loops between these components hampers predictability (Hayward et al., 2018).

Case studies demonstrate a rough spatial periodicity in the distribution of regions of high energy and mass flux, and/or associated structural complexity, along linear, arc-parallel fault zones, based on empirical data sets. For example, the distribution of volcanic centres along the Cocos-Caribbean arc displays spatial periodicity (~150-km wavelength), over a strike length of >1,000 km (Figure 1A; Hayward et al., 2018). In the case of ore deposits, spatial periodicity has been documented, for example, in the Archean Yilgarn Craton, Australia (e.g., Weinberg et al., 2005; Bierlein et al., 2006; Micklethwaite, 2007; Doutre et al., 2015). Here, world-class gold deposits along the Boulder-Lefroy Shear Zone in the Eastern Goldfields Superterrane are regularly spaced at intervals of ca. 35 km and focus on intersections with regional anticlines and dilational fault jogs (Bierlein et al., 2006; Hayward et al., 2018). Similarly, Eocene-Oligocene porphyry Cu deposit cluster centroids along the Domeyko fault system, northern Chile, may display a periodic distribution corresponding to a spacing of ca. 100–130 km (Figure 1B; Hayward et al., 2018). Other, global examples of spatial periodicity in the distribution of various deposits and deposit styles along respective major fault zones can be found in Hayward et al. (2018).

2.3 Structural inheritance and deposit supercluster

In contrast to the endmember model of *self-organization* in one-event systems (see Section 2.2), the distribution of deposits and deposit clusters may be explained by *structural inheritance* and ongoing reactivation through the superimposition of tectonic events. Generally, the recognition of inheritance of "structure," *sensu lato*, dates to, at least, the formulation of the Wilson-Cycle plate tectonic paradigm, which explains the current *modus operandi* of our planet's internal heat dissipation. As such, the current thermal state of the Earth system may be regarded as a snapshot of a much larger *self-organizing* system. However, the application of such idea is highly impractical, when concerned about the regional-scale distribution of deposits along plate boundaries and accretionary arcs. Instead, we must consider the most significant effect (i.e., control) of a particular crustal or trans-lithospheric

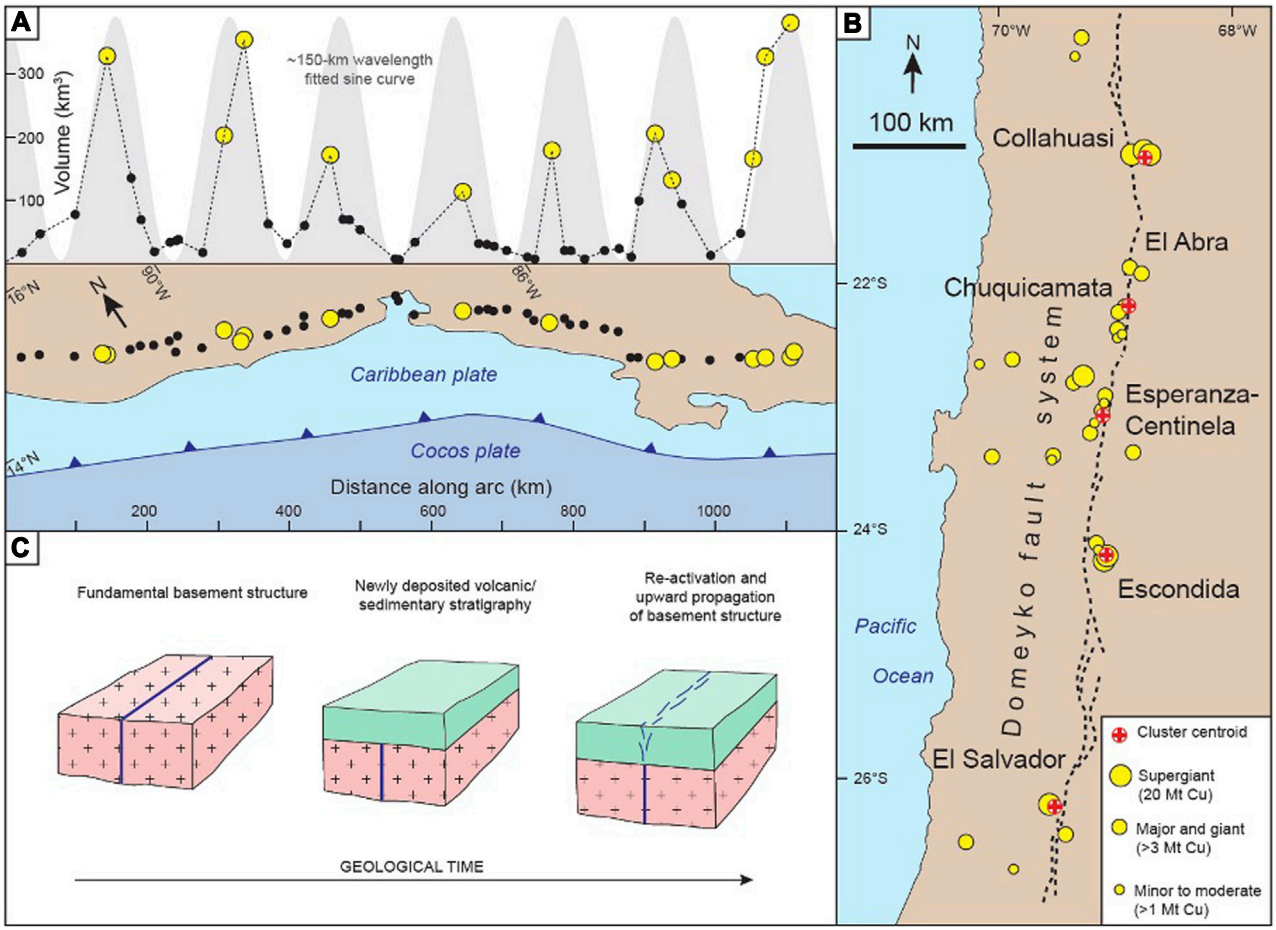

FIGURE 1
(A) Depiction of spatial periodicity (~150-km wavelength) in the distribution of highly productive Quaternary volcanic centers along the Cocos-Caribbean volcanic arc (redrawn from Hayward et al., 2018). **(B)** Statistical evaluation of the spatial distribution of porphyry Cu deposit cluster centroids along the Domeyko fault system, northern Chile (redrawn from Hayward et al., 2018). **(C)** Schematic block diagram illustrating vertical propagation and inheritance of basement structures into younger cover during tectonic re-activation (redrawn from McCuaig and Hronsky, 2014).

structure on the subsequent tectonic evolution of a region. In other words, the presence of a pre-existing structure determines the evolutionary path of successive events (see bifurcation theory; Nicolis and Prigogine, 1977).

Indeed, the initiation of plate tectonics, itself, and/or the initiation of new subduction zones (e.g., Stern and Gerya, 2018), the "seeding" of intracratonic rifts (e.g., Ukrainian Dniepr-Donets basin; Stephenson et al., 2021; see also Phillips et al., 2019; Muñoz-Barrera et al., 2020, and the analogue modelling by Zwaan et al., 2021), the ultimate break-up of continents (e.g., North Atlantic, Schiffer et al., 2020; Laurentian margin of eastern North America, e.g., Thomas, 2006), and the formation of micro-terranes and continental fragments (e.g., Mediterranean, van den Broek et al., 2020), have been proposed to require and/or impinge on, pre-existing lithospheric weak zones. Similarly, the structural inventory, and/or the shape and geometry of incoming lithosphere in continent-continent collisional orogens (e.g., India-Himalaya; Valdiya, 1976), or the structure and topography of oceanic crust in oceanic-continental accretionary orogens (e.g., aseismic seamount or ridge subduction in Ecuador, Marcaillou et al., 2016; or central Peru; Rosenbaum et al., 2005), have been proposed to significantly affect the structural-kinematic response and resulting lithospheric-crustal anatomy of resulting orogens.

With regards to ore deposit distribution in the South American Andes, *structural inheritance* was first documented by Sillitoe (1976), who documented the presence of lineaments and/or transverse boundaries that crosscut and segment prominent, arc-parallel metallogenic belts. Across the transverse boundaries, there are subtle changes in the distribution, lateral width, metal endowment, and overall presence or absence of metallogenic belts of a specific mineralization episode. Furthermore, it was noted that deposits cluster in vicinity to these transverse boundary structures (Sillitoe, 1976; 2008; Sillitoe and Perello, 2005). Meanwhile, other studies focussing on Cu and Cu-Au porphyry and related epithermal deposits in northern Chile found that major deposits are located at intersections between principal arc-parallel structures and other, cryptic major lineaments of supposedly more ancient origin (e.g., Salfity, 1985; Chernicoff et al., 2002; Richards, 2003; Gow and Walshe, 2005).

In central Peru, Love et al. (2004) and McCuaig and Hronsky (2014) demonstrated that arc-perpendicular transfer zones controlled the localization of Miocene mineralization (e.g.,

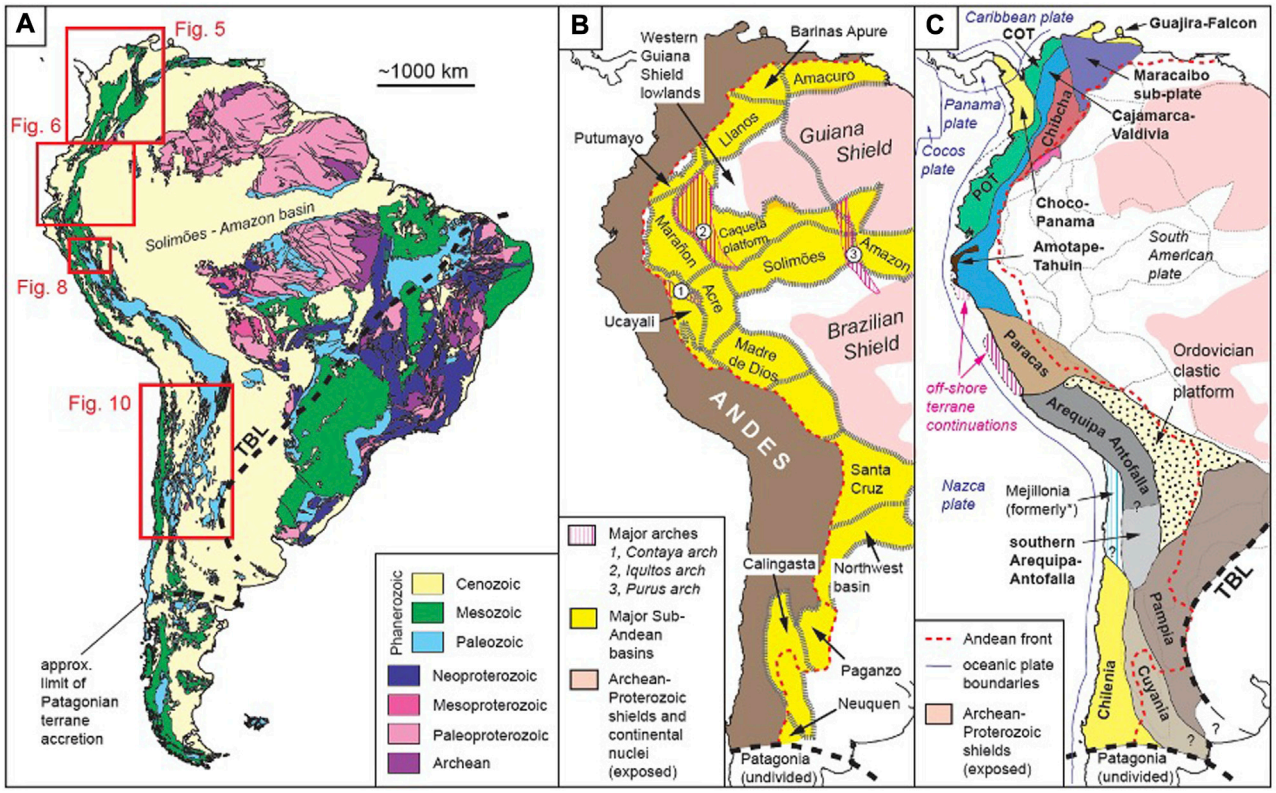

FIGURE 2
(A) Simplified geologic map of South America showing the distribution of surface lithologic ages (map based on Gómez et al., 2019); TBL, Trans-Brasiliano Lineament; Red rectangles indicate the location of maps presented in Figures 5, 6, 8, 10. **(B)** Outline of major Sub-Andean basins (modified after Jacques, 2003; Wesselingh et al., 2006). **(C)** Outline of basement blocks and micro-terranes along the western South American margin (compiled and modified after Mourier et al., 1988; Cediel et al., 2003; Loewy et al., 2004; Ramos, 2009; Cordani et al., 2010; Willner et al., 2011; Romero et al., 2013; Cingolani and Ramos, 2017; Wiemer et al., 2022); COT, Caribbean oceanic terranes; POT, Pacific oceanic terranes.

Antamina polymetallic skarn deposit) and represent inherited basement structures that date back to at least the Mesozoic. Noting the mere subtle, cryptic, and relatively broad expression of respective inherited transfer zones, McCuaig and Hronsky (2014) established a conceptual model of vertically accretive structural inheritance and fault propagation (Figure 1C). The model describes the upward propagation of re-activated deeply rooted basement structures into younger, overlying volcanic-sedimentary stratigraphy, whereby the newly propagated near-surface structural expression may be characterized by only cryptic and broader, often anastomosing and/or discontinuous fault networks.

A more recent study from northern Peru demonstrated the inheritance of basement structures in controlling the geometry of the Carboniferous Pataz gold vein system (Wiemer et al., 2021a). In the latter case, a switch in the far-field stress orientation during re-activation induced a strike-slip Riedel-type fault system, further obscuring the cryptic nature of inferred underlying basement faults. In a follow-up regional-scale investigation, Wiemer et al. (2022) suggested that the inferred cryptic pre-Carboniferous Pataz basement structures continue to the west and north-west, where at their intersection with much younger NNW-striking Andean arc-parallel fault zones clusters of Miocene Au-Cu porphyry and related epithermal deposits are located. Whether the pre-Carboniferous basement continues below the Andean belt to the west (i.e., vertically accretive inherited fault propagation), or the inherited structures were propagated laterally, will be discussed in Section 4.3. Nevertheless, Wiemer et al. (2022) coined the term "deposit supercluster" to describe the spatial association of deposits that belong to different metallogenic age-provinces but are controlled by the same inherited ancient structure or structural corridor. The concept of deposit supercluster will be used in the remainder of this paper to highlight possible similar cases of structural inheritance.

3 Critical review of the tectonic evolution of South America

As discussed in Section 2, tectonic history is key to identify endmember scenarios of the distribution of deposits, and/or deposit supercluster. Therefore, it is crucial to review the tectonic evolution of South America, in the light of possible inheritance of trans-lithospheric fault systems. The South American lithosphere evolved over much of Earth's geologic history, and witnessed all major supercontinent cycles (i.e., Columbia, Rodinia, Gondwana-Pangea), and comprises the longest-lived presently active tectonic margin at its western margin. The present distribution of surface lithologic ages is shown in Figure 2A.

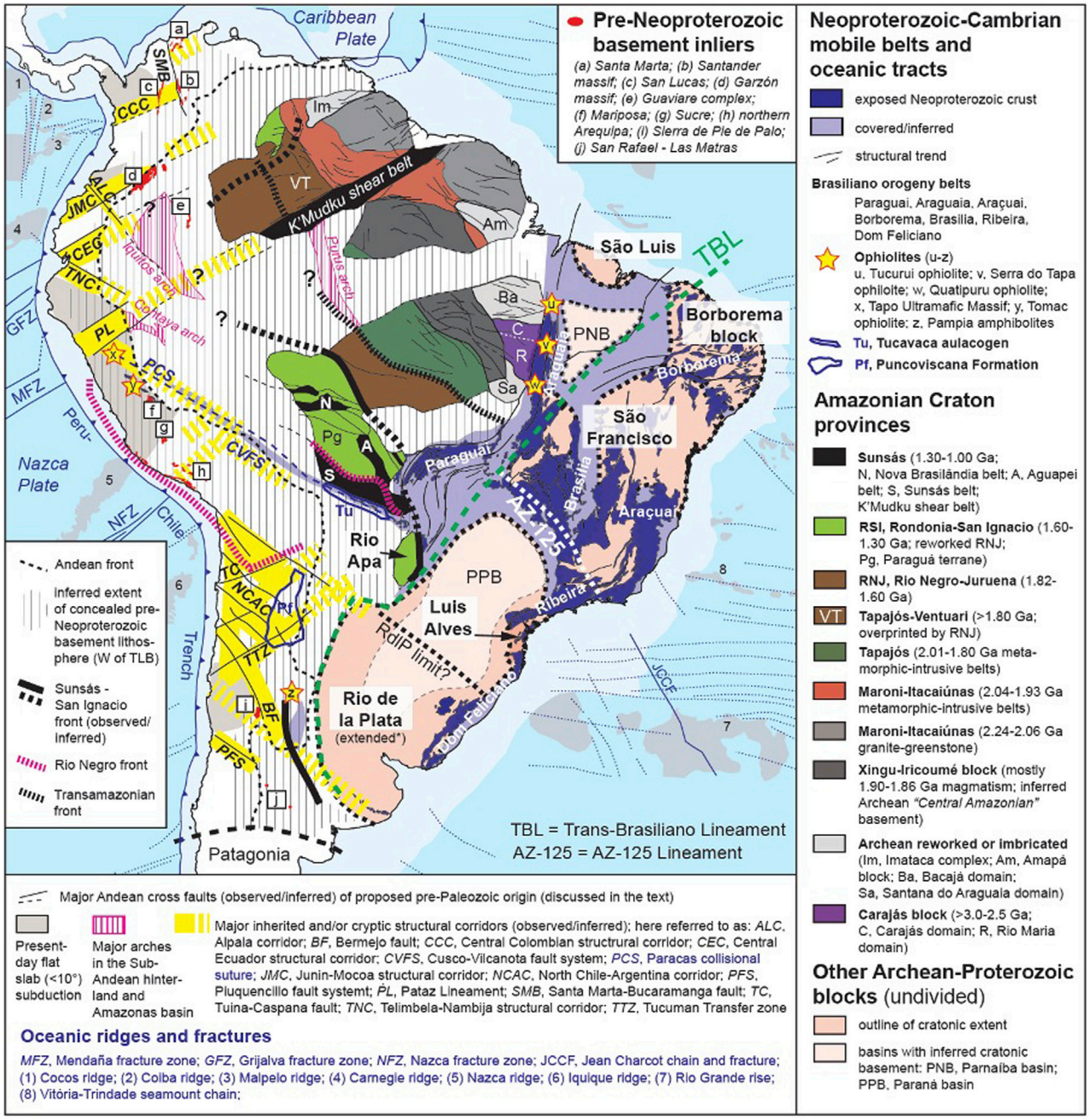

FIGURE 3
Map of South America showing the outline of Archean-Proterozoic cratons, the main geochronologic provinces of the Amazonian craton, the limits of orogenic fronts (i.e., Transamazonian, Rio Negro, Sunsás-San Ignacio, Andes), the location of pre-Neoproterozoic basement inliers within the Andes (*a-j*), the location of Neoproterozoic ophiolites (*u-z*) and oceanic tracts, and recent oceanic ridges and fracture zones (compiled and modified after Jacques, 2003; Loewy et al., 2004; Santos et al., 2004; 2008; Mišković et al., 2009; Cordani et al., 2010; 2013; 2016; Teixeira et al., 2010; Bettencourt et al., 2010; Rapela et al., 2010; Ibanez-Mejia et al., 2011; Escayola et al., 2011; Tassinari et al., 2011; Casquet et al., 2012; Rizzotto and Hartmann, 2012; de Castro et al., 2014; Ramos et al., 2015; Kroonenberg et al., 2016; Ramos, 2018; da Silva et al., 2018; Gómez et al., 2019; Motta et al., 2019; Rocha et al., 2019; López et al., 2020; Nedel et al., 2021; Assis et al., 2021; Wiemer et al., 2022). Note: both the extended (including the Parana basin, PPB; Santos et al., 2019), and the limited extent (*RdlP limit*; Rapela et al., 2011) of the Rio de la Plata craton are indicated. See text for discussion.

Focussing on the identification of possible ancient structural inheritance within the western South American margin (i.e., Andean orogenic belt), the problem in linking interior continental architecture with possible related, inherited structures in the basement of the Andes, is amplified by the vast sedimentary cover sequences that form large basins in the Andean hinterland (e.g., Solimões—Amazon basin; Figure 2A). Therefore, it is equally important to consider the outlines and margins of sub-basins that lie in-between the Andes and the exposed Archean-Proterozoic continental interior (Figure 2B). The outlines of sub-basins and/or major arches, may inform about the existence and lateral continuity of deep-seated basement structures (Figure 2B). In

fact, the boundaries of sub-Andean basins have been correlated with the structural segmentation of the Andes (e.g., Jacques, 2003). Furthermore, basin formation in the sub-Andes has been ascribed to early Permian-Triassic extension that was accommodated by inherited basement structural inhomogeneities, with major implications for oil and gas potential (e.g., Calderon et al., 2017; Zamora and Gil, 2018).

More importantly, however, we must appreciate the mosaic-like distribution of micro-terranes and crustal blocks, and their respective boundaries, along the western South American margin (Figure 2C). To understand this collage of tectonic entities, a critical review of the tectonic evolution of South America is presented below. To guide the reader in following data review, a compilation of main geological features, referred to and discussed in the following *Sections*, is presented in Figure 3.

3.1 Archean-Paleoproterozoic nuclei and the Amazonian Craton

The oldest fragments of continental lithosphere in South America are recognized in five major Archean-Proterozic cratonic blocks (Figure 3): 1) the Amazonian Craton (including the Rio Apa cratonic fragment), 2) the São Francisco Craton (including the Archean Goias block, and interpreted to correlate with the Congo Craton), 3) the São Luis Craton (interpreted to correlate with the West African Craton), 4) the Borborema Province basement (interpreted to correlate with the Sahara Metacraton), and 5) the Rio de la Plata Craton (interpreted to correlate with the Kalahari Craton). Furthermore, the crystalline basement of both the Parnaíba basin (e.g., de Castro et al., 2014) and the Parana (Paranampanema) basin are suggested to comprise Archean cratonic components. It remains contested whether the Parana basin basement (also including the Luis Alves cratonic fragment) forms part of the extended Rio de la Plata Craton (Santos and Oliveira, 2016), or forms a separate cratonic block (e.g., Rapela et al., 2011).

The Amazonian Craton is classically subdivided into ~NNW-trending geochronological provinces that correspond to an approximate E to W trend of decreasing crust formation ages (sub-divisions and references provided in Figure 3). Its Archean nucleus is formed by the Carajás block that largely comprises granite-greenstone belts of the >3.00–2.86 Ga Rio Maria domain and the ~3.08–2.73 Ga Carajás domain (e.g., da Silva et al., 2018; Motta et al., 2019; Trunfull et al., 2020). It is suggested that after proposed low-angle subduction between ca. 2.98–2.92 Ga, the two domains collided at ca. 2.87–2.86 Ga (e.g., da Silva et al., 2018). Early copper and iron-oxide-copper-gold (IOCG) mineralization is dated between ca. 2.76–2.68 Ga and associated with rifting and basin formation within the Carajás domain (Trunfull et al., 2020). Crust of similar Archean age has been reported from the Amapá, Bacajá, and Santana do Araguaia domains, and is inferred to form extensive basement to the Xingu-Iricoumé province, respectively, together forming the Central Amazonian province (Figure 3). The Central Amazonian province possibly formed a tectonic entity by the end of the Neoarchean and is enclosed by Paleoproterozoic ~2.26–2.06 Ga granite-greenstone belts of the Maroni-Itacaiunas province to the north-east (Figure 3; e.g., Kroonenberg et al., 2016; Kroonenberg, 2019; Tedeschi et al., 2020). During the major Transamazonian orogeny (correlated to the global assembly of the Columbia supercontinent) ~2.01–1.80 Ga juvenile crust of the Tapajós (and Tapajós-Ventuari) province to the west and south-west accreted, and magmatism, magmatic reworking and metamorphism affected large parts of the Central Amazonian and Maroni-Itacaiunas provinces (Figure 3). During this time the overall WNW- to NNW-trending structural grain of the western Amazonian Craton was likely established and correlates with the proposed south-westernmost front of the Transamazonian orogen, as shown in Figure 3. Indeed, significant orogenic gold deposits within the NE Guiana Shield formed at ca. 2.08 and 1.99 Ga and are associated with major NW-striking fault systems (e.g., Karouni deposit, Tedeschi et al., 2020). At its south-western extent, the Transamazonian event is represented by the ca. 2.05–1.87 Ga polyphase accretion to collisional Tapajonic (or Tapajós-Parima) orogeny (Tapajós province), during which gold-rich porphyry and epithermal mineral deposits formed in vicinity to major NNW- to NW-trending faults and arc-terrane boundaries (e.g., Santos et al., 2004; Bettencourt et al., 2016; Juliani et al., 2021). This event coincided with extensive (A-type) magmatism and hydrothermal activity within the Central Amazonian province (e.g., Xingu-Iricoumé province and Carajás block) and marked a major episode of diverse gold-rich mineral system formation (and remobilization) in the Carajás domain at ca. 1.88 Ga (e.g., Trunfull et al., 2020). The Tapajonic orogeny was shortly followed by the Rio Negro orogeny, including the ca. 1.81–1.74 Ga collisional Juruena orogeny with associated gold mineralization at ca. 1.79 Ga, at the SW margin of the Amazonian Craton (Rio Negro-Juruena province; Figure 3; e.g., Santos et al., 2004; Bettencourt et al., 2010; Casquet et al., 2012; Kroonenberg et al., 2016; Juliani et al., 2021; Nedel et al., 2021). Evidence for Rio Negro-Juruena basement has been detected in the Rio Apa cratonic fragment, and in the Paraguá terrane towards its southwestern limit (see Rio Negro front in Figure 3). The Rio Apa fragment and Paraguá terrane, however, were substantially reworked during the ~1.60–1.30 Ga Rondonian-San Ignacio orogeny (e.g., Bettencourt et al., 2010; Nedel et al., 2021), which marked the onset of the Mesoproterozoic Sunsás-San Ignacio orogenic cycles associated with the assembly of the Rodinia supercontinent (Section 3.2).

3.1.1 Paleoproterozoic crust and basement inliers within the Andes

Paleoproterozoic outcrops within the Andean belt are extremely scarce and restricted to the northern domain of the Arequipa-Antofalla terrane (Figure 2C; location "*h*" in Figure 3). Combined zircon geochronological and whole-rock Pb and Nd isotopic data attest to the presence of ca. 2.02–1.79 Ga juvenile intrusions that were metamorphosed at ca. 1.82–1.79 Ga (Loewy et al., 2004). Isotopic data from the central Arequipa-Antofalla terrane suggest that, here, Mesoproterozoic intrusions (Section 3.2) incorporated Paleoproterozoic components from the northern domain (Loewy et al., 2004). In the southern Arequipa-Antofalla terrane (Figure 2C), however, Paleoproterozoic zircon or isotopic signatures indicative of reworking of Paleoproterozoic components appear to be absent (Loewy et al., 2004). To the north, inherited ca. 1.99–1.81 Ga magmatic zircon have been

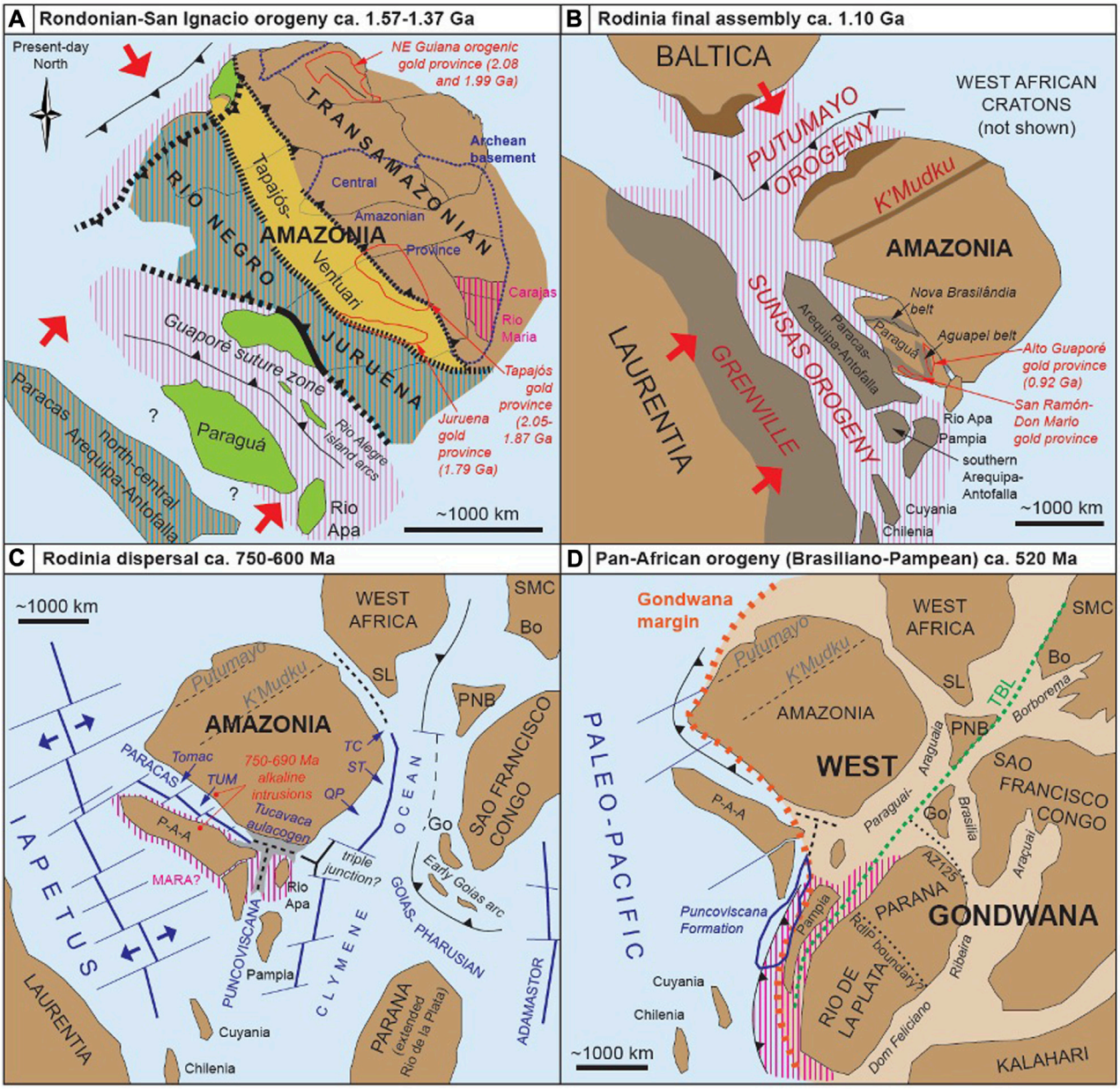

FIGURE 4
Continued.

reported from drill-cores in the Peruvian off-shore region and interpreted to represent basement to the Paracas terrane (Figure 2C), as a northern continuation of the central to northern Arequipa-Antofalla terrane (Romero et al., 2013). In addition, scarce Paleoproterozoic (ca. 1.75–1.90 Ga) detrital and inherited zircons have been found in Paleozoic intrusive and sedimentary rocks of the Eastern Andean Cordillera of Peru and southern Ecuador (e.g., Chew et al., 2007; Wiemer et al., 2022). A regional zircon Lu-Hf isotopic survey of the Peruvian Eastern Cordillera indicates contributions of reworked Rio Negro and Tapajós-Ventuari age crust (i.e., ca. 2.1–1.6 Ga), based on isotopic model ages (Mišković and Schaltegger, 2009). Overall, these data indicate that the Paracas and the northern-central Arequipa-Antofalla terranes may have originally formed part of the western Amazonian Rio Negro crust prior rift break-up and tectonic dispersal around ca. 1.74 Ga.

3.2 Mesoproterozoic Rodinia assembly: the Rondonian-San Ignacio and Sunsás orogenic cycles

During the Mesoproterozoic Rodinia assembly, the Amazonian Craton experienced two main stages of crustal growth and/or terrane accretion, both of which are recorded at the craton's NW and W/SW margins (present-day Northing; Figures 4A, B). The two

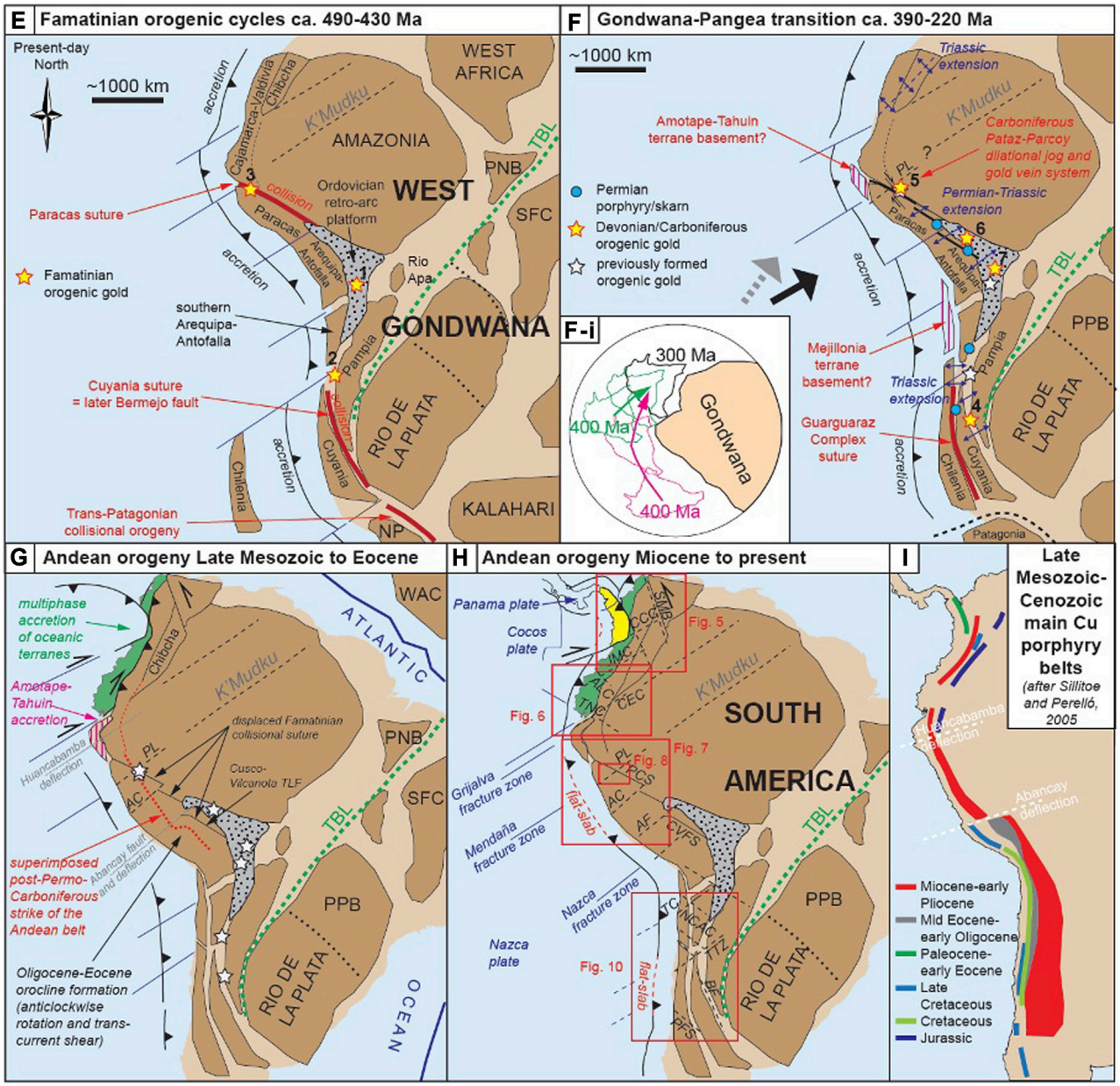

FIGURE 4
Schematic *freeform* illustrations of the paleogeographic-tectonic evolution of the South American Gondwana margin. Note that the reconstructions are based on the present-day Northing of the Amazonian Craton. The figures are based on information provided in: Mourier et al., 1988; Cediel et al., 2003; Loewy et al., 2004; Chew et al., 2007; 2016; Teixeira et al., 2007; Ramos, 2008; Mišković et al., 2009; Cardona et al., 2009; Cordani et al., 2010; Bettencourt et al., 2010; Ibanez-Mejia et al., 2011; Willner et al., 2011; 2014; Escayola et al., 2011; Roperch et al., 2011; Romero et al., 2013; Caxito et al., 2020; Casquet et al., 2014; Ramos et al., 2015; Granot and Dyment, 2015; Spikings et al., 2016; Cingolani and Ramos, 2017; Casquet et al., 2018; Young et al., 2019; Quadros et al., 2021; Nedel et al., 2021; Wiemer et al., 2021b; Wiemer et al., 2022. Discussion and further data sources are provided in the text. **(A)** The Amazonian Craton at the onset of the Mesoproterozoic, highlighting the established NW-trending structural grain of the cratonic interior, and the sub-parallel accretion-collision of both juvenile and reworked terranes (light green) during the Rondonian-San Ignacio orogeny. Note that the proposed composite Paracas—north-central Arequipa-Antofalla terrane comprises evidence for both Tapajós-Ventuari and Rio Negro-Ventuari basement, whereas no Rondonian-San Ignacio imprints have been detected. San Ignacio-age intrusions in the northwestern Amazonian Craton may indicate the onset of subduction accretion in this area. See text for discussion and references. **(B)** Collision of Laurentia and Baltica with the Amazonian Craton, leading to the Sunsás-Grenville and Putumayo orogens, respectively. Note that the K'Mudku shear zone is interpreted to have formed as a sub-parallel, and intra-cratonic response to the Putumayo orogeny. The Sunsás orogeny included a short-lived rifting of the former Guaporé suture zone (see **(A)**), followed by re-collision during which the Alto Guaporé gold province formed as part of the Aguapei belt. **(C)** The Neoproterozoic dispersal of Rodinia included the opening of the Iapetus Ocean and associated, possibly scissor-like, detachment of the Paracas-Arequipa-Antofalla (and/or MARA, see text) continental ribbon that led to the formation of the Paracas-Tucavaca ocean basin. Similarly, the Puncoviscana basin (and ocean?) opened, sub-parallel to the Clymene Ocean to the east, by rift-incision from a triple junction between the Tucavaca and Puncoviscana tracts (stippled lines). **(D)** Situation at the time of Pan-African West Gondwana assembly, which included the Brasiliano orogeny (see Brasiliano orogenic belts in italic fonts) and the Pampean orogeny (area marked by red stripe pattern). The Pampean orogeny included the collision of the Pampia terrane with the Rio de la Plata craton, but also an accretionary arc system, outbound of which the Puncoviscana Formation was deposited. Around the western and north-western Amazonian
(*Continued*)

FIGURE 4 (Continued)
Craton there is no evidence for collision at this time, but widespread detrital and inherited zircon from the Gondwana margin of Peru and Ecuador attest to the onset of Paleozoic subduction around the paleo-Gondwana margin. **(E)** The Ordovician-Silurian paleo-Gondwana margin (i.e., Famatinian orogeny) witnessed the collision of the Cuyania and Paracas (plus Arequipa-Antofalla?) micro-terranes, whereas sub-parallel magmatic belts formed as a result of coeval outboard subduction-accretion. The Famatinian orogeny marked the early formation of orogenic gold deposits (stars, numbers 1–3) that represent the oldest known localities associated with subsequent supercluster formation along the Gondwana and Andean margin throughout the Phanerozoic. **(F)** During the Devonian-Carboniferous, far-field stress regimes changed from NNE-to a NW/WNW-directed convergence direction (grey stippled arrow towards black arrow), as a response to the clockwise rotation of Laurentia around NW Gondwana (insert **(F–I)**), resulting in the oblique super-positioning of developing magmatic arcs (and associated docking of the Chilenia terrane) with regards to the former Famatinian structural grain, orogenic strike, and associated sutures. Orogenic gold formation in northern Peru (#5) was localized within a dilational jog at the intersection between the Pataz Lineament (PL), the Famatinian collisional suture, and the superimposed Carboniferous magmatic belt, and occurred during a Late Carboniferous (Pennsylvanian) tectonic switch from compression/transpression to transtension. The tectonic switch may have marked the very onset of following Permo-Triassic extension that appears to have developed in a scissor-like fashion, i.e., a southward increasing intensity and/or duration of extension (blue arrows). It is proposed that the extension dynamics resulted in the differential westward offset of the Famatinian suture, accommodated in pre-existing or newly formed transverse structures. Similarly, the spatially punctuated formation of Devonian-Carboniferous orogenic gold deposits in southern Peru, Bolivia, and Argentina (# 4, 6 and 7) may have been controlled by both newly established and pre-existing structures, as can be inferred by the reconstructed location of micro-terrane boundaries. **(G)** At the Late Mesozoic onset of the Andean orogeny, the docking of the Amotape-Tahuin terrane and subsequent multiphase accretion of the Pacific and Caribbean oceanic terranes appear to have been controlled by pre-existing faults within the continental interior and/or by the shape of either incoming oceanic lithosphere or the shape of the Gondwana margin continental lithosphere. **(H)** During the following Miocene to present, ongoing terrane accretion occurred along the western margin of central to northern Colombia, while the present-day Peru-Chile trench and subduction developed. The figure shows a compilation of identified present-day transverse structures along the Andean belt (compare with Figure 3) that are discussed in the light of (cryptic) structural inheritance and control on deposit localization with respect to more detailed maps shown in Figures 5–8, 10 (indicated). **(I)** Simplified distribution of Late Mesozoic to Cenozoic (to recent) major Cu porphyry belts of western South America (after Sillitoe and Perello, 2005).

main stages include: 1) the ca. 1.57–1.37 Ga Rondonian-San Ignacio orogeny, including the collisional Alto Guaporé orogeny in the SW Amazonian Craton, during which the Paraguá terrane ("*Pg*" in Figure 3) collided and was reworked (Bettencourt et al., 2010), and local granite intrusions between ca. 1.6–1.3 Ga that intrude the Rio Negro-Juruena province in the NW part of the Amazonian Craton (e.g., Cordani et al., 2016; Bonilla et al., 2021; Figure 4A); and 2) the ca. 1.30–1.00 Ga Sunsás-Putumayo orogeny that marks the South American equivalent to the Grenvillian orogeny in North America and Baltica during the final Rodinia assembly (Figure 4B). Overall, the main stages describe the stepwise approach and ultimate collision of Laurentia from the SW and Baltica from the NW. The approach and collision of Laurentia occurred sub-parallel to the previously established ~NW-striking structural grain of the Amazonian Craton, whereas Baltica and associated micro-terranes and arcs collided perpendicular to the NW strike of the Amazonian Craton (Figures 4A, B). The collision of Baltica involved a fringing arc system that marked the accretion of the Oaxaquian-Colombian terranes during the Putumayo orogeny at ca. 1.25–0.98 Ga (Figure 4A; Ibanez-Mejia et al., 2011). Evidence for Putumayo crust is represented in the ca. 1.20–1.00 Ga Santander, Santa Marta, and San Lucas inliers, together forming part of the Chibcha terrane, and the Garzón Massif (also referred to as the Andaqui terrane) in the Northern Andes of Colombia (Figures 2C, 3; e.g., Ramos, 2009). Zircon geochronological data from the Garzón Massif and from exploration wells in the Putumayo basin to the south attest to ca. 1.46–1.02 Ga magmatism, followed by ca. 0.99–0.97 Ga metamorphism (Figures 2B, C, 3; Ibanez-Mejia et al., 2011). Furthermore, at the NW edge of the Amazonian Craton, ca. 1.31 Ga magmatism and metamorphism affected the Guaviare complex (Figure 3; Cordani et al., 2016; López et al., 2020).

Importantly, based on a review of geochronological data of reset K-Ar and Rb-Sr mica ages within the Amazonian Craton Cordani et al. (2010) discuss the idea that thermotectonic reactivation focussed along structural corridors, such as the K'Mudku shear zone (Figure 3), as an intracratonic response to the Sunsás-Putumayo orogeny. The isotopic resetting of micas at ca. 1.20 Ga is partly associated with the development of mylonitic fabric development along the K'Mudku shear zone (Cordani et al., 2010 and references therein). In addition, A-type granites within the K'Mudku shear zone were emplaced at ca. 1.22 Ga (Souza et al., 2015). Given its sub-parallel alignment with the Putumayo orogen and/or its perpendicular relationship to the Sunsás orogeny, it may be inferred that the K'Mudku shear zone formed as an intracratonic response to the collision of Baltica, and/or as an intracratonic transfer zone in response to Laurentia collision (Figure 4B).

The final collision of Laurentia during the Sunsás orogeny along the W/SW Amazonian Craton margin included the formation of the ca. 1.14–1.01 Ga Nova Brasilândia belt, the ca. 1.30–0.92 Ga Aguapei belt, and the Sunsás belt, which roughly follow former sutures (e.g., Guaporé suture zone) that surround the Paraguá terrane and were established during the preceding Rondonian-San Ignacio orogeny (Figures 4A, B; e.g., Cordani and Teixeira, 2007; Teixeira et al., 2010; Bettencourt et al.,, 2010; Quadros et al., 2021). Final collision in the Aguapei belt at ca. 1.10–0.92 Ga followed rifting between ca. 1.15–1.10 Ga (Melo et al., 2022), possibly attesting to the notion that the Rondonian-San Ignacio and Sunsás orogenies were separated by a short-lived episode of extension. During the final collision, and/or post-collisional, the ca. 920 Ma Alto Guaporé gold belt formed along NNW-trending shear zones sub-parallel to the Aguapei belt ($^{40}Ar/^{39}Ar$ hydrothermal muscovite; Melo et al., 2022). The San Ramón gold province and the Don Mario Cu-Au-Ag mine may have formed at similar time within the Sunsás belt (Figure 4B).

Sunsás age basement inliers and/or sparse outcrops within the Andes include the Mariposa and Sucre inliers in central to south Peru, drill-cores from the Peruvian Paracas off-shore region, and basement inliers of the Arequipa-Antofalla terrane, overall attesting to magmatism and metamorphism between ca. 1.20–0.94 Ga. (Figure 3; Loewy et al., 2004; Mišković et al., 2009; Romero et al., 2013). Furthermore, widespread detrital and inherited ca. 1.30–0.95 Ga zircon ages in the Eastern Cordillera of Peru have been reported (e.g., Chew et al., 2007; Wiemer et al., 2022). These

data attest to the presence of extensive Sunsás basement in Peru, which included the Paracas and Arequipa-Antofalla terranes sandwiched in-between Amazonia and Laurentia (Figure 4B). To the south, widespread detrital and inherited zircon, and basement outcrops and xenoliths of the San Rafael, Las Matras and Sierra de Pie de Palo inliers suggest the presence of ca. 1.33–1.03 Ga basement to the Pampia, Cuyania, and Chilenia terranes (Figures 3, 4B; e.g., Sato et al., 2000; Ramos, 2009, and references therein; Rapela et al., 2010; Cingolani and Ramos, 2017).

3.3 Neoproterozoic Rodinia dispersal and oceanic tracts

The Neoproterozoic dispersal of Rodinia was largely marked by the opening of the Iapetus Ocean, following continental break-up that likely impinged on lithospheric weak zones sub-parallel to the Grenvillian/Sunsás orogen (Figure 4C). However, the Tomac ophiolite (Wiemer et al., 2022), and the Tapo Ultramafic Massif ophiolitic vestiges ("*x*" and "*y*" in Figure 3) attest to the formation of oceanic crust at 718 ± 47 Ma (Sm-Nd whole-rock isochron, Tassinari et al., 2011; Willner et al., 2014) in central to northern Peru. In combination with coeval local alkaline granite intrusions (ca. 750–690 Ma, U-Pb zircon, Mišković et al., 2009), and detrital zircon indicating a ca. 750 Ma maximum depositional age of marine sedimentary rocks ("Old" Marañon Complex; e.g., Chew et al., 2007), it has been proposed that a distinct Paracas oceanic basin formed sub-parallel to the Iapetus, resulting in the detachment of the Paracas and Arequipa-Antofalla terranes (Figure 4C; Wiemer et al., 2022). It is unclear whether the Paracas ocean formed an oceanic passage, or rather a scissor-like oceanic incision narrowing towards its proposed spatial correlation with the Tucavaca aulacogen to the SE (Wiemer et al., 2022; Figure 4C). Nevertheless, in this reconstruction, the extended Paracas-Arequipa-Antofalla terrane (including the juvenile Sunsás basement of the southern Arequipa-Antofalla domain) and the Rio Apa cratonic fragment may have formed the MARA composite terrane, as proposed by Casquet et al. (2012; Figure 4C). On the other hand, to the south, the ca. 750–630 Ma Puncoviscana Ocean basin may have separated the Arequipa-Antofalla terrane from the Rio Apa cratonic fragment and the Pampia terrane (e.g., Escayola et al., 2011). In this scenario, an additional rift triple junction would be situated at the intersection of the Paracas and Puncoviscana ocean basins with the Tucavaca aulacogen (e.g., Ramos, 2008; Figure 4C).

To the east of the Amazonian Craton, Neoproterozoic ophiolites ("*u-w*" in Figure 3) are interpreted to represent remnants of the Clymene Ocean (Figure 4C; 757 ± 49 Ma, Sm-Nd whole-rock Quatipuru ophiolite; Paixão et al., 2008; Cordani et al., 2013; Caxito et al., 2020). Whether oceanic crust fully separated the Amazonian Craton from the West African Craton remains unclear. However, the Clymene Ocean is interpreted to have separated the Amazonian Craton and associated dispersed micro-terranes to the south from the Rio de la Plata and/or Parana craton(s) and the São Francisco-Congo Craton to the east. The Rio de la Plata and the São Francisco-Congo cratons, in turn, were separated by the Goias-Pharusian Ocean that linked the Clymene and the Adamastor oceans (Figure 4C; e.g., Caxito et al., 2020).

3.4 Late Neoproterozoic to Cambrian Pan-African (Brasiliano-Pampean) orogeny

The following Pan-African assembly of West Gondwana was accomplished through multiple accretion and collision of cratonic blocks and magmatic arcs, referred to as the Brasiliano and the Pampean orogenies in South America. The West Gondwana assembly resulted in the establishment of a complex and extensive network of Neoproterozoic to Cambrian mobile belts to the east and south-east of the Amazonian Craton (Figure 3).

The Brasiliano orogeny included the collision of Archean-Paleoproterozoic cratonic blocks with, and to the east of, the Amazonian Craton, marking the closure of the Clymene and the Goias-Pharusian oceans, as well as the Adamastor Ocean further to the east (Figure 4D; e.g., Caxito et al., 2020). The polyphase orogeny included the formation of the Brasilia fold belt between the Goias Archean block and outboard magmatic arc and the São Francisco-Congo Craton, the collision of the São Francisco-Congo Craton with the Rio de la Plata-Parana cratonic block, which possibly led to the early establishment of the AZ125 lineament, and the formation of the Borborema belt between the northern São Francisco-Congo Craton and the Sahara Metacraton (e.g., Rocha et al., 2019; Caxito et al., 2020). The latter composite of tectonic entities collided with the Amazonian Craton and West African Craton during closure of the Clymene Ocean, which ultimately resulted in the formation of the Paraguai-Araguaia belts and the tectonic emplacement of Neoproterozoic ophiolites around the eastern margin of the Amazonian Craton. The Clymene Ocean suture has been proposed to be represented by the Trans-Brasiliano Lineament (TBL; Figure 4D; e.g., Paixão et al., 2008; Cordani et al., 2013; Caxito et al., 2020). Closure of the Adamastor Ocean to the east is recorded in the Dom Feliciano and Ribeira belts along the eastern margin of the Rio de la Plata Craton (Figure 4D).

The coeval Pampean orogeny records the accretion to collision of the Pampia terrane along the western Rio de la Plata Craton, marking the closure of the southern Clymene Ocean and associated development of the southern segment of the Trans-Brasiliano Lineament (Figure 4D). The Pampean orogeny led to ca. 540–515 Ma juvenile intrusions and metamorphism, documented in the Sierras Pampeanas (e.g., Rapela et al., 2010; Ramos et al., 2015). Neoproterozoic to Cambrian basement in the eastern Sierras Pampeanas comprise potential oceanic derived amphibolites (Ramos et al., 2015). The Pampean belt can be followed to the south, around the SW/S margin of the Rio de la Plata Craton (Tohver et al., 2021). Closure of the Puncoviscana Ocean is recorded in the Puncoviscana Formation with initially outbound sedimentation coeval with ca. 540–530 Ma arc magmatism, directly followed by collision of the Arequipa-Antofalla terrane with the northern Pampia terrane (Figure 4D; Ramos, 2008; Escayola et al., 2011).

To the north, no collisional orogeny has been documented. However, widespread inherited and detrital Pampean-age zircon are reported from the Peruvian Eastern Cordillera (e.g., Cardona et al., 2009; Wiemer et al., 2022). Hence, the Peruvian, Ecuadorian and Colombian Gondwana margin likely only witnessed the initiation of outboard subduction-accretion during the Pan-African Pampean orogeny (Figure 4D). On the other hand, there appears to be an absence of Pampean zircon in the off-shore Paracas and the

Arequipa-Antofalla terranes (e.g., Loewy et al., 2004; Romero et al., 2013). This indicates that Pampean subduction initiated in-between the Paracas-Arequipa-Antofalla blocks, likely reflecting the onset of NE-directed subduction of the Neoproterozoic Paracas oceanic crust (Figure 4D).

3.5 Famatinian accretion and micro-terrane collision

The Famatinian orogeny records extensive magmatic accretion along the West Gondwana protomargin during the Ordovician to Silurian (Figure 4E; e.g., Ramos, 2018). At the type locality in Argentina, a ca. 484–463 Ma continental arc complex developed on the older basement of the Pampia terrane and marks the docking of the Cuyania micro-terrane (e.g., Astini and Davila, 2004; Rapela et al., 2010; Cingolani and Ramos, 2017; Ramos, 2018). Further south, the coeval collision of the North Patagonia terrane resulted in the Trans-Patagonian orogeny (Figure 4E; González et al., 2021).

Along the preserved western margin of the Arequipa-Antofalla terrane, the Famatinian magmatic arc is represented by ca. 476–447 Ma granitoid intrusions that were metamorphosed at ca. 440 Ma (e.g., Loewy et al., 2004; Mišković et al., 2009). Famatinian-age magmatic zircon from off-shore drill-cores suggest the northward continuation of the magmatic arc, outbound along the western Paracas margin (Romero et al., 2013). In the hinterland, in present-day Bolivia and southern Peru, the Ordovician clastic retro-arc platform developed (Figure 4E; e.g., Ramos, 2018). Shortly after their deposition, the clastic sedimentary rocks were affected by folding and magmatic-hydrothermal activity that led to the formation of the Sierra Rinconada (e.g., Minas Azules) and the Incahuasi orogenic gold vein deposits (1 and 2 in Figure 4E; Rodríguez and Bierlein, 2002; Klipfel, 2007). The Ordovician retro-arc platform largely covers the proposed former rift triple junction, which connected the Tucavaca aulacogen with the Puncoviscana and the Paracas ocean basins (Section 3.3). Indeed, the Famatinian orogeny included the re-collision of the Paracas-Arequipa-Antofalla terrane(s) with the Gondwana margin, leading to the tectonic emplacement of the Tomac ophiolite and the Tapo Ultramafic Massif (TUM) ophiolitic vestiges in central to northern Peru ("*x*" and "*y*" in Figures 3, 4E; Tassinari et al., 2011; Willner et al., 2014; Wiemer et al., 2022). In central to northern Peru, *Early* Famatinian continental arc magmatism, and marginal to marine sedimentation (i.e., max. depositional ages of the Contaya Formation and the "Young" Marañon Complex, respectively), are recorded between ca. 480–465 Ma, followed by *Late* Famatinian intrusions, metamorphism, and associated deformation (D_2 after Wiemer et al., 2021a) ascribed to the Paracas collision at ca. 462–437 Ma (Chew et al., 2007; 2014; 2016; Cardona et al., 2009; Willner et al., 2014; Ramos, 2018; Wiemer et al., 2022). Wiemer et al. (2022) proposed that the northern limit of the Paracas collision was accommodated in oceanic transform faults, which represent the propagated oceanic extension of the Mesoproterozoic K'Mudku shear zone corridor in the Amazonian Craton (Figure 4E; discussed in more detail in Section 4.3). At the intersection of the extrapolated K'Mudku shear zone with the collisional Famatinian suture, D_2 deformation-related orogenic quartz-pyrite veins have been observed in the Pataz region of northern Peru (St. Filomena, 3 in Figure 4E; Wiemer et al., 2021a; 2022).

Further to the north, ca. 484–461 Ma igneous rocks, and metamorphic imprints record the continuation of the Famatinian orogen in the Chibcha and Cajamarca-Valdivia terranes of Ecuador and Colombia (e.g., Ramos, 2018). In this northern West Gondwana margin segment, the Famatinian orogeny was likely non-collisional (Figure 4E).

3.6 Late Paleozoic Gondwanide orogenic cycles and Permian-Triassic extension

After a short episode of apparent tectonic quiescence, the Late Paleozoic Gondwanide resurgence of subduction-accretion along the West Gondwana margin was characterized by an overall switch in the far-field principal stress regime towards a more E-directed orientation that can be ascribed to the clockwise rotation of Laurentia around NW Gondwana (insert Figures 4F–I; e.g., Young et al., 2019). The *Early* Gondwanide orogeny included the mid-Devonian to early Carboniferous collision of the Chilenia terrane. The event is recorded in the high-pressure metamorphic belt of the Guarguaraz Complex, Chile (Figure 4F; Willner et al., 2011). Further inland, Devonian-Carboniferous orogenic gold systems formed in the Sierra de las Minas, Sierra de Córdoba and Sierra Culampaja districts of the Sierras Pampeanas (4 in Figure 4F; ca. 393–351 Ma; $^{40}Ar/^{39}Ar$ hydrothermal mica; Skirrow et al., 2000). These gold deposits are spatially associated with Devonian granites, and/or associated with newly established conjugate NW- and NE-trending fault networks that intersect reactivated older (Famatinian and/or Pampean) shear zones (Skirrow et al., 2000).

Carboniferous granitoid intrusions at the western Chilenia margin attest to the presence of an outbound accretionary arc system. This accretionary magmatic belt can be followed northward of the Chilenia collisional orogen along the entire Peruvian, Ecuadorian and Colombian Gondwana margin (Figure 4F). The magmatic accretion may have led to the formation of the Carboniferous basement to the Amotape-Tahuin terrane in south-western Ecuador (Figure 4F; e.g., Mourier et al., 1988). Evidence for Late Paleozoic basement to the suspect Mejillonia terrane of north-western Chile (Figure 4F) is not confirmed, and the Mejillonia terrane may have formed during later Triassic-Jurassic magmatic arc accretion (Casquet et al., 2014).

Along the Peruvian Eastern Cordillera, an extensive Carboniferous to Permian magmatic belt formed (Chew et al., 2007; 2016; Cardona et al., 2009; Mišković et al., 2009; Witt et al., 2013a; Angerer et al., 2018; Voute et al., 2019). A superimposed relationship to the former Famatinian orogen (i.e., crosscutting obliquely aligned strike trend) is best documented in structural relationships in northern Peru (Wiemer et al., 2021a; 2022).

The Carboniferous to Permian magmatic belt hosts numerous intrusion-related orogenic gold districts (5 in Figure 4F) along the Eastern Cordillera of central to northern Peru (e.g., Haeberlin et al., 2002). These include the major Pataz-Parcoy gold districts that are situated within a regional scale dilational jog at the intersection of

the Famatinian suture and the Pataz Lineament, which has been suggested to form the continuation of the K'Mudku shear zone ("*PL*" in Figure 4F; Wiemer et al., 2022). The dilational jog formed during Carboniferous dextral strike-slip of the NNW-trending Rio Marañon fault (Wiemer et al., 2021a; 2022). Gold formation is dated at ca. 332 Ma (Re-Os molybdenite, Szappanosné-Vágó et al., 2010) and corresponds to a switch in the tectonic regime from compression to transtension (Voute et al., 2019; Wiemer et al., 2021a). Gold formation in Pataz-Parcoy was near-contemporaneous to orogenic gold deposit formation in the Santo Domingo, La Rinconada-Ananea, and Yani-Aucapata, as well as the Antofagasta, Amayapampa, and Cebadillas districts within the eastern Altiplano region of the Ordovician retro-arc platform (6 and 7 in Figure 4F; e.g., Haeberlin et al., 2002). This indicates a possible extended Carboniferous gold belt, approximately following the ancient basement tracts of the Famatinian Paracas collisional suture and the inferred Puncoviscana suture (see previous *Sections*).

The *Early* Gondwanide cycle culminated in regional metamorphism at ca. 315 Ma (e.g., Chew et al., 2016) and was succeeded by the *Late* Gondwanide orogeny that occurred during the Permian and witnessed the ca. 300–260 Ma intrusion of mostly A- and S-type granitoid plutons, followed by metamorphism at ca. 260 Ma, along the Peruvian Eastern Cordillera (Mišković et al., 2009; Chew et al., 2016). The preserved width and abundance (i.e., volume) of the Permian intrusive rocks increase, concomitant with an apparent younging of magmatism until the Triassic, towards the south. These A- and S-type magmatic suites indicate an incipient extensional regime and the decline of subduction related magma production, which may be ascribed to large-scale crustal relaxation after final Pangea assembly, and/or the development of post-Carboniferous back-arc extensional environments (e.g., Mišković et al., 2009; Wiemer et al., 2021a).

During the Triassic, continental rifting and extension affected most of the western South American margin, likely associated with the disassembly of West Gondwana/Pangea (Figure 4F; e.g., Spikings et al., 2016). In Peru, thick syn-rift shallow marine to continental sedimentary sequences of the ca. 245–220 Ma Mitu Group were deposited within NNW-trending grabens (e.g., Spikings et al., 2016). As mentioned in the introduction of Section 3, early Sub-Andean basin formation during syn-rift Mitu Group deposition was controlled by Paleozoic basement structural inhomogeneities, e.g., resulting in the formation of structural highs, such as the Iquitos arch, that represent sub-parallel, NNW-trending boundaries of basins or sub-basins (e.g., Marañon basin, Figure 2C; Zamora and Gil, 2018). Also, the reader is encouraged to compare the alignment of the Contaya arch with the sub-parallel Famatinian Paracas suture and the Rondonian-San-Ignacio and Sunsás orogenic fronts (Figure 3). Similarly, Jacques (2003) proposed that NE-trending sub-Andean basin boundaries can be geometrically correlated with the transverse fault segmentation of the Andean belt (compare Figures 2B, 4H).

Based on these insights, it may be argued that the extension dynamics led to the displacement of segments/blocks of the Paleozoic Eastern Cordillera, accommodated by NE-trending transverse faults, which either established during the Permian-Triassic rifting, or represented the reactivation of more ancient faults in the continental basement (i.e., Gondwana and/or Paracas-Arequipa-Antofalla). Indeed, Noble et al. (1978) suggested that peralkaline volcanic lavas within the Mitu Group indicate lithosphere-scale extension, but also remarked that the rather sporadic along-strike distribution of these lavas may document the onset of Triassic fragmentation of lithospheric blocks. In the case that the NE-trending transverse faults originated from the Gondwanan continental interior, it is noted that remarkably little Andean arc-parallel strike-slip offsets are observed.

3.7 Late Mesozoic to recent Andean orogenic cycles

Renewed commencement of subduction during the Late Triassic to Early Jurassic initiated the Andean orogeny (e.g., Clark et al., 1990; Mišković et al., 2009; Zentilli et al., 2018) that roughly coincided with the onset of the opening of the South Atlantic (Granot and Dyment, 2015; Figure 4G). The Andean orogeny witnessed several cycles of repeated convergence, extension, and deformation phases along the western margin of South America. The presence or absence, width, and distribution of i) deformational fronts, 2) magmatic belts and thermal/hydrothermal activity, and 3) metallogenic belts, display characteristic along-strike variations across major arc-perpendicular transverse lineaments and/or deflections (e.g., Huancabamba and Abancay deflection; Figures 4G–I; Sillitoe, 1976; Sillitoe, 2008; Love et al., 2004; Sillitoe and Perello, 2005). In general, major subduction and associated ore deposit formation occurred during following episodes along distinct arc segments: i) mid-late Jurassic (ca. 174–145 Ma), ii) early-mid Cretaceous (ca. 135–100 Ma), iii) Late Cretaceous to early Paleocene (ca. 80–52 Ma), iv) Paleocene-early Eocene (62–40 Ma), v) mid Eocene-early Oligocene (ca. 42–32 Ma), and vi) Miocene-early Pliocene (ca. 20–4 Ma; Figures 4G–I; e.g., Clark et al., 1990; Sillitoe, 1976; 2008; Sillitoe and Perello, 2005; Carlotto et al., 2009; and data and references presented in Section 4).

Allochthonous and/or parautochthonous terrane accretion during the Andean orogeny was largely restricted to the Cretaceous accretion of the Amotape-Tahuin block, the Late Cretaceous-Paleocene accretion of the Pacific and Caribbean oceanic terranes, and the following protracted collision of the Choco-Panama terranes, until the Miocene, all focusing on the Ecuador and Colombia margins (Figures 4G, H; e.g., Mourier et al., 1988; Cediel et al., 2003). In Ecuador, the northern limit of the clockwise rotation and Cretaceous accretion of the Amotape-Tahuin terrane spatially correlates with the southern demarcation of the strike-slip dominated Paleocene accretion of oceanic terranes (Figure 4G; e.g., Mourier et al., 1988; Cediel et al., 2003). In turn, this NE-trending structural corridor (i.e., Central Ecuador structural corridor, CEC) can be geometrically correlated with both the recent Grijalva fracture zone in the Nazca plate and the approximate southern limit of the Mesoproterozoic Putumayo orogenic front (Figure 4H). The possible existence of a long-lived inherited structural corridor and its control on ore deposit distribution in this area will be discussed in Section 4.2. The subsequent accretion of the Choco-Panama terranes in Colombia also appears to have been controlled by a pre-existing lithospheric inhomogeneity. Here, the southern edge of the incoming terranes, the former Triassic rift axis, and the inferred southern margin of the northward displaced

Maracaibo sub-plate (e.g., Cediel et al., 2003; Spikings et al., 2016) appear to lign-up along a common structural corridor that is highly endowed in Mesozoic-Cenozoic ore mineral systems (Figures 2C, 4H, I). Further details are provided and discussed in Section 4.1.

Another conspicuous Andean arc segment boundary, the NE-trending Abancay deflection, is observed in southern Peru. During the late stages of the Peruvian Coastal batholith emplacement at ca. 45–39 Ma, porphyry and skarn deposits formed in southern Peru, south of the deflection, and represent the northernmost extremity of the prominent Eocene-Oligocene porphyry belt of northern Chile (Figure 4I). The deflection also coincides with an apparent offset in Miocene magmatic activity and deposit formation (Figures 4H, I; e.g., Clark et al., 1990). The Abancay deflection approximately coincides with the northern region of the south Peruvian—Bolivian orocline (Clark et al., 1990; Clark et al., 1990; Sillitoe, 2008; Sillitoe, 2008). Development of the wide deformation belt that wraps around the orocline included clockwise rotation of crustal thrust slices during Eocene-Oligocene (i.e., Incaic deformation phase) shortening, but also sinistral transcurrent shear along pre-existing faults (Figure 4G; Roperch et al., 2011). This indicates that orocline formation represented the upper crustal amplification of an inherited basement feature that was likely established during the Mesoproterozoic. Interestingly, this area also delimits the approximate southernmost extent of present-day Peruvian flat-slab subduction (Figure 3). The Abancay fault/deflection offsets, and/or cuts, the Cusco-Vilcanota fault system (CVFS; Figure 4H) that extends SE-ward and marks a trans-lithospheric structure, separating different upper mantle domains, based on a Sm-Nd and Sr isotopic study of Cenozoic potassic volcanic rocks and intrusions (Carlier et al., 2005). The latter study found that the upper mantle domain to the NE of the CVFS is characterized by overall older depleted mantle Nd-isotopic model ages (i.e., Paleoarchean to Sunsás), compared to the lithospheric mantle to the SW (i.e., largely Sunsás age depleted mantle model ages), whereas in-between the two domains, an additional Neoproterozoic component (T_{DM} = 864–612 Ma), likely including an asthenospheric mantle contribution, was detected (Carlier et al., 2005). The Neoproterozoic model age overlaps the oceanic crust formation age of the Peruvian ophiolites. However, although the strike direction of the trans-lithospheric CVFS approximates the Famatinian Paracas suture and associated basement structural grain in central to northern Peru (Wiemer et al., 2021a; 2022), its position does not agree with a linear continuation of the Famatinian suture (Figure 4F). As mentioned in Section 3.6, the proposed westward displacement of basement blocks, hence including the CVFS, along transverse faults, may have resulted from the Permian-Triassic extension. Similarly, the westward displacement of the TUM ophiolitic vestiges relative to the northern Tomac ophiolite may be explained in this way. Indeed, for example, the cryptic Antamina transverse structural corridor ("*AC*" in Figure 4G) has been interpreted to be of at least Mesozoic origin (e.g., Love et al., 2004; McCuaig and Hronsky, 2014) and may represent a transverse structure that initially accommodated the Permian-Triassic extension. The Antamina structural corridor affects volcanic-sedimentary successions dating back to at least the Upper Jurassic, and its polyphase activity is inferred from varying degrees of deflection of the plunge of folds and the strike of folds and faults throughout the younger Cenozoic volcanic and sedimentary cover rocks (Love et al., 2004). A similar situation will be discussed in Section 4.3 with regards to the Pataz Lineament ("*PL*" in Figure 4G). Both the Antamina corridor and the Pataz Lineament are characterized by an unusual abundance of Cenozoic igneous intrusions and appear to play a significant role in controlling the localization of Miocene porphyry and related epithermal and skarn deposits (e.g., Love et al., 2004; Wiemer et al., 2022). NW/NNW-trending, strike-parallel normal faults that accommodated the Permian-Triassic extension and syn-rift sediment accumulation in southern Peru were reactivated, and/or nucleated the development of Andean thrust faults during progressive Cenozoic basin inversion and deformation (Perez et al., 2016).

Along the Chilean-Argentinian western margin of the South American Andes, an overall inverted, i.e., landward younging of magmatic and metallogenic belts (Cu porphyry) is observed (Figure 4I; Sillitoe and Perello, 2005). Within these belts, however, deposits and/or deposit clusters display a punctuated distribution, and particularly some of the younger Miocene volcanic centers and associated deposits are situated within, or in vicinity to, older pre-Andean magmatic and metamorphic belts, indicating the repeated magmatic-hydrothermal reactivation of older belts (e.g., Sillitoe and Perello, 2005). The punctuated distribution of deposits along the Chilean-Argentinian segment has been ascribed to intersections between arc-parallel and older transverse lineaments (e.g., Chernicoff et al., 2002; Richards, 2003; Hayward et al., 2018). The origin of the older transverse structures, however, remains unknown so far. In the context of the presented tectonic evolution of the western South American margin, these structures will be discussed in more detail in Section 4.4.

4 Case studies of multi-scale and polyphase structural inheritance and associated gold-rich deposit clusters

Below, selected areas (see maps indicated in Figures 2A, 4H) will be discussed in more detail, to highlight the distribution of ore deposits in the context of key geodynamic and geological features and the presented tectonic history.

4.1 Colombia

The temporal spatial distribution of ore deposits in Colombia overall follows the previously recognized main Cu porphyry belts of the Andes (Sillitoe and Perello, 2005; Sillitoe, 2008; compare Figures 4I, 5A). However, based on the presented tectonic evolution history (Figure 4; Section 3), the Colombian Andes are largely underlain by Mesoproterozoic and Paleozoic basement, so that a simple "onion-shell"-like accretion and crustal growth with respect to the Mesozoic-Cenozoic sub-parallel magmatic and metallogenic belts appears inadequate. Indeed, we propose below the existence of cryptic structural corridors, which host a particularly high abundance of deposits of various formation ages, i.e., belonging to distinct segments of various previously identified metallogenic belts, that may represent deposit superclusters controlled by larger-scale structural-geodynamic inheritance (after Wiemer et al., 2022).

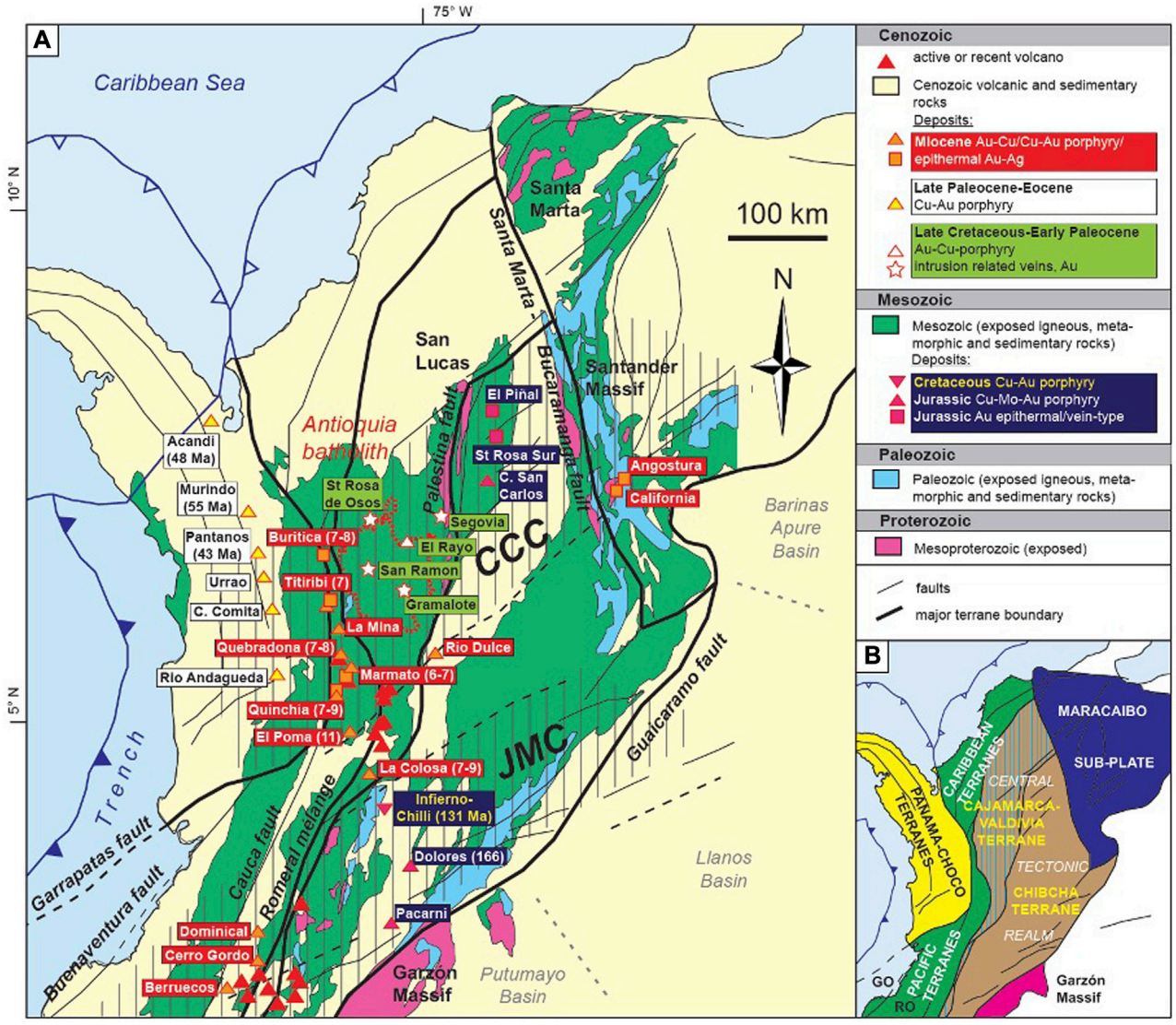

FIGURE 5
(A) Simplified geologic map of Colombia showing major faults and terrane boundaries, and the distribution of major deposits, grouped by age of mineralization (given in brackets, in *Ma*, where known) and deposit type (compiled and modified after Cediel et al., 2003; Sillitoe and Perello, 2005; Naranjo et al., 2018; Shaw et al., 2019; Gómez et al., 2019). Inferred cryptic inherited structural corridors are indicated by shaded (stripe pattern) areas and include the Central Colombian (CCC) and the Junin-Mocoa (JMC) structural corridors (compare to Figures 3, 4H). **(B)** Corresponding subdivision into major terranes and crustal blocks. Location of map shown in Figure 2A.

In NE Colombia, the Vetas-California-Angostura district deposits are overall hosted by partially migmatized Mesoproterozoic and Paleozoic basement gneiss and Jurassic-Cretaceous granitoids and metasedimentary rocks (Figure 5A). However, Miocene-Pleistocene Cu-Mo-Au porphyry, Au-Ag epithermal, and hydrothermal Au-Ag breccia type mineralization are spatially associated with local late Miocene intrusions, situated at significant distance to the main Miocene magmatic-metallogenic belt (Figure 5A). Auriferous veins of the Vetas-California-Angostura district follow NE-trending faults, such as the La Baja fault, sub-parallel to the foliation of the basement gneiss (e.g., Naranjo et al., 2018; Shaw et al., 2019; Scarpelli, 2021). The Vetas-California district is of similar age and displays similar types and styles of mineralization as the major Miocene Cauca belt (e.g., Quebradona, Marmato, La Colosa; Figure 5A), which is characterized by Au-Cu/Cu-Au porphyry and related epithermal Au-Ag, as well as minor intrusion-related Au veins and stockworks (e.g., Naranjo et al., 2018; Shaw et al., 2019). The roughly N-S-trending Cauca belt extends along almost the entire Colombian and Ecuadorian Andes and focusses along the Romeral mélange and sub-parallel Cauca fault, which mark the suture zone of the early phase of oceanic terrane accretion onto the Cajamarca-Valdivia continental margin during the Paleocene (Figures 4G, 5; e.g., Cediel et al., 2003; Naranjo et al., 2018). Importantly, however, the Cauca belt displays conspicuous mineralization gaps. Its mineralized Colombian northern section spans about 150–200 km, from the Buritica deposit in the north to the La Colosa deposit cluster in the south (Figure 5A). The southern limit of the northern Cauca belt approximates the

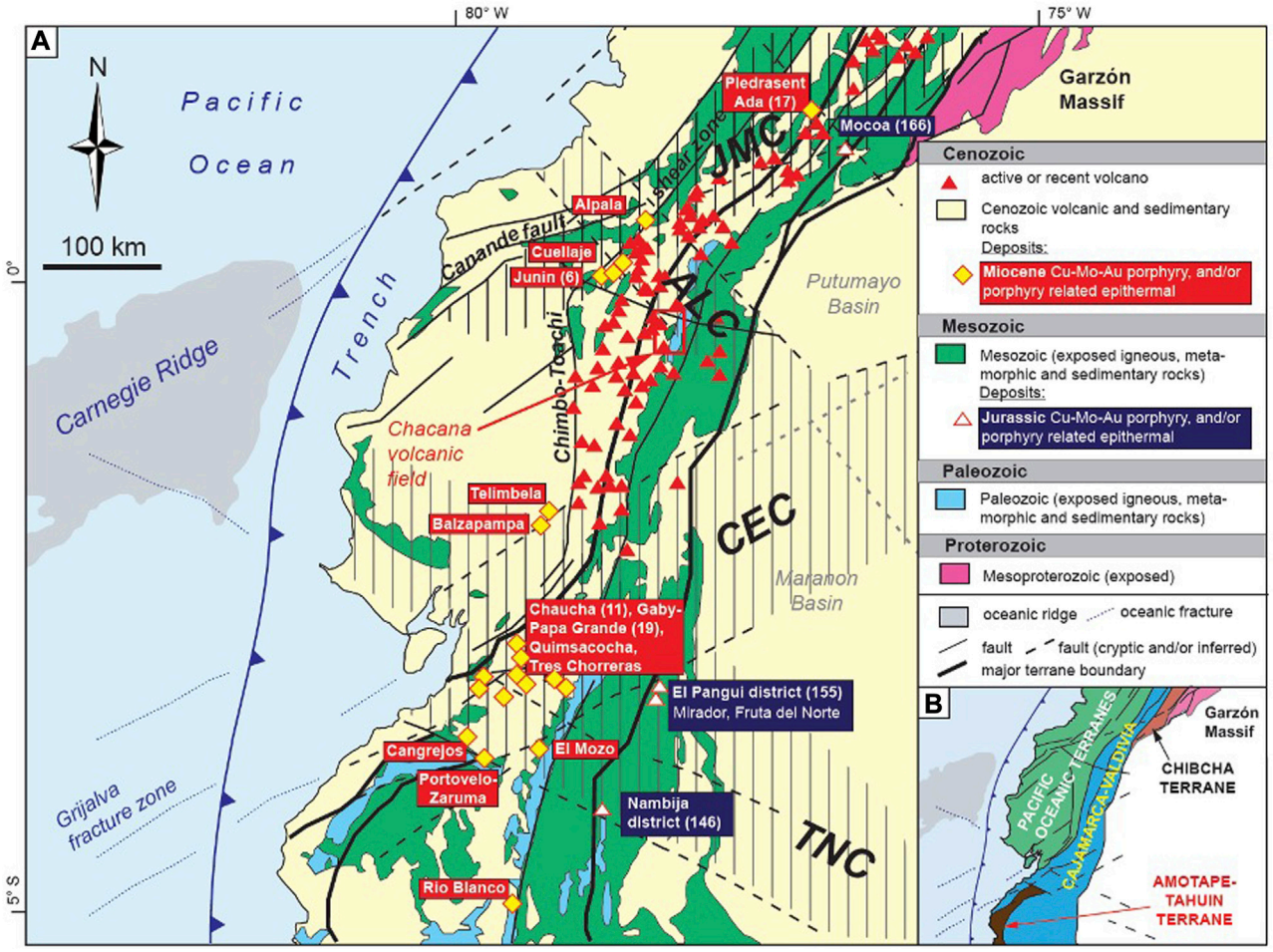

FIGURE 6
Simplified geologic map of Ecuador showing major faults and terrane boundaries, and the distribution of major deposits, grouped by age of mineralization (given in brackets, in *Ma*, where known) and deposit type (compiled and modified after Sillitoe and Perello, 2005; Schutte et al., 2012; Gómez et al., 2019). Inferred cryptic inherited structural corridors are indicated by shaded (stripe pattern) areas and include: ALC, Alpala corridor; CEC, Central Ecuador corridor; JMC, Junin-Mocoa corridor; TNC, Telimbela-Nambija corridor (compare to Figures 3, 4H). **(B)** Corresponding subdivision into major terranes and crustal blocks. Location of map shown in Figure 2A.

southern NE-trending demarcation of the Miocene Choco-Panama terrane accretion (i.e., Garrapatas fault) to the SW and the structurally bound Vetas-California deposits along NE-trending faults, as well as the sub-parallel NE-trending southern limit of the Maracaibo sub-plate to the NE (Figures 5A, B; e.g., Leal-Mejia et al., 2019). This southern limit of what is here referred to as the Central Colombian corridor (CCC), also marks a prominent deflection of the Cauca belt from ca. NNW-trending to the north towards ca. NNE-trending to the south. The deflection marks a region of the highest abundance of recent volcanoes in central Colombia (Figure 5A). The central part of the CCC, between the northern Cauca belt and the Santa Marta Bucaramanga fault, hosts an apparently isolated cluster of deposits that form the northernmost extremity of the Jurassic Cu-Au porphyry belt (e.g., Sillitoe and Perello, 2005; Naranjo et al., 2018). Furthermore, the Antioquia batholith intruded the central CCC, with a main phase of magmatic activity between ca. 96–70 Ma. Compared to other typically elongated magmatic belts, the Antioquia batholith displays a noticeably circular shape (Figure 5A). The batholith is associated with Late Cretaceous to early Paleocene gold-rich porphyry and intrusion related vein type mineralization (Figure 5A; e.g., Naranjo et al., 2018). Interestingly, prior to Late Mesozoic-Cenozoic mineral system formation along the CCC, Triassic rifting affected approximately the same corridor, at least in its southern south-west to central part (i.e., as a branch of the Payendé rift, Spikings et al., 2016).

The broad, up to 200-km-wide delineation of the CCC, as depicted in Figure 5A, however, cannot be realistically regarded as resulting from a single underlying basement TLF structure. It may be argued that a critical basement terrane boundary approximates the southern limit of the CCC, whereas the localizations of deposit clusters in the central part of the CCC were controlled by respective more narrow cross-structures and corridors, recording a more complex geodynamic interplay of basement and superimposed tectonic features.

Another cluster of Cretaceous and Jurassic deposits is spatially well separated from the Cretaceous and Jurassic deposits within the CCC, and may belong to another sub-parallel, ca. 150-km-wide

NE-trending corridor, here referred to as the Junin-Mocoa corridor (JMC, Figures 3, 4H, 5A). To the SW, the JMC marks the continuation of the Cauca belt in southern Colombia and northern Ecuador and approximates the location and strike of the Carnegie Ridge and associated sub-parallel oceanic fractures (Figures 5A, 6A).

4.2 Ecuador

The continuation of the middle section of the Miocene Cauca belt in northern Ecuador, as a part of the inferred JMC, is also interrupted by a mineralization gap to the south, which approximates another deflection, from NNE-to N-trending, of the overall Andean strike (Figure 6A). This deflection appears to mark an intersection between the deflected Andean strike (here, the eastern suture zone of the oceanic terranes and associated sub-parallel crustal-scale structures, such as the Chimbo-Toachi shear zone), the inferred, cross-belt cryptic JMC, which correlates with the NE-trending Canande fault that cuts through the oceanic terranes in northern Ecuador (e.g., Kerr et al., 2002), and another possible cryptic NW-trending lineament, here referred to as the Alpala corridor (ALC; Figures 4H, 6A). To the SE, the NW-trending Alpala corridor approximates the boundary between the Putumayo and the Marañon basins, and the Iquitos arch, respectively (Figure 3). Indeed, the high-grade porphyry Cu-Au Alpala deposit is located within a NW-trending sector of the roots of a structurally controlled lithocap (Rohrlach et al., 2015).

The ca. 250–300-km-wide mineralization gap to the south is characterized by a high abundance of recent volcanoes. The distribution of recent volcanoes displays a somewhat suspicious outlier cluster that appears to follow the ALC (Figure 6A). Furthermore, in vicinity to the ALC, the Chacana volcanic field produced sanukitoid-like lavas (Chiaradia et al., 2014) that will be discussed in Section 5.

In western central to south Ecuador, recent volcanoes are absent, whereas the area marks another possible deposit supercluster, previously proposed by Wiemer et al. (2022). This supercluster marks the intersection of the Andean belt with two inferred cryptic structural corridors, here referred to as the NE-trending Central Ecuador corridor and the NW-trending Telimbela-Nambija corridor (CEC and TNC in Figures 3, 4H, 6A). The proposed existence of the inferred structural corridors is based on following observations: 1) The NE-trending CEC forms the broadened extension of the boundary between the NE-striking suture along the southern tip of the accreted Pacific oceanic terranes and the northern limit of the preceding dextral strike-slip dominated Amotape-Tahuin terrane accretion, as well as the oceanic Grijalva fracture system in the Nazca plate (Figures 4G, 6A, B; e.g., Mourier et al., 1988; Cediel et al., 2003; Spikings et al., 2005; Schutte et al., 2012). Furthermore, in its proposed NE-ward extension, the CEC hosts a major cluster of Miocene Cu-Mo-Au porphyry and related epithermal deposits, in addition to the Jurassic Cu-Mo-Au porphyry and related epithermal deposits of the El Pangui district (Figure 6A). At its inferred northern limit, the CEC aligns with the NE-trending boundary between the Putumayo and Marañon basins in the Sub-Andes. On a larger scale, the CEC trend and location approximates the southern front of the Putumayo orogeny (and/or the northern limit of the Archean-Paleoproterozoic margin of the Amazonian Craton), and, indeed, the respective Andean segment is absent of known Mesoproterozoic basement inliers that are observed to the north (Figures 3, 4H, 6A). 2) The proposed TNC is interpreted to form the extension of NW-trending structures that cut through the Miocene deposit cluster (at the intersection of the TNC and CEC; e.g., Schutte et al., 2012) and equivalent recent oceanic fractures that appear to dextrally offset the tip of the Carnegie Ridge (Figure 6A). To the SE, the TNC runs through the Jurassic Nambija Cu-Au porphyry district. On the continental scale, the TNC may be correlated with the Contaya arch and with the NW-trending Mesoproterozoic Sunsás orogenic belts (compare Figure 3).

4.3 Peru

The Peruvian Andes comprise some of the most compelling evidence for ancient structural inheritance in controlling the distribution of mineral systems and ore deposits to date. This section focusses specifically on the north Peruvian gold supercluster (Figure 7), based on which the terminology “deposit supercluster” was originally introduced (Wiemer et al., 2022). The localization of the north Peruvian gold supercluster has been ascribed to the intersection of two major cryptic structural basement corridors, namely, i) the NE-trending Pataz Lineament (PL) and ii) the NW-trending Famatinian Paracas collisional suture (PCS), with the superimposed NNW-trending magmatic arcs of the Late Paleozoic Eastern and the Late Mesozoic-Cenozoic Western Andean Cordilleras (Figures 3, 4E–H, 7; Wiemer et al., 2022).

The structural intersection marks a prominent deflection of the trend of the post Famatinian Rio Marañon fault zone, demarcating a regional-scale ca. 40-km-wide dilational jog that hosts the world-class Carboniferous Pataz-Parcoy gold districts (Figures 4F, 8A; Wiemer et al., 2022; Villanes et al., 2023). The gold veins follow internal rheological contrasts within the host plutonic Pataz batholith (e.g., Schreiber et al., 1990; Haeberlin et al., 2004; Witt et al., 2013a; 2016; Wiemer et al., 2021a), which, in turn, can be correlated with pre-existing NW-trending faults and foliations that belong to the Famatinian basement (Wiemer et al., 2021b). The overall along-strike prominence of steep to medium NE-dipping (i.e., NW-striking) thrust faults and foliations of the basement indicate that the Pataz-Parcoy gold districts formed in the hanging wall of the cryptic Famatinian suture (Figure 8A; Wiemer et al., 2021a; 2022).

Importantly, the extrapolated cryptic Famatinian basement collisional orogen appears to control the localization of the Miocene Yanacocha Au-Cu porphyry and related Au-Ag epithermal deposits (Figure 8A). In fact, Sillitoe (2008) noted the presence of NW-trending faults in the Yanacocha deposit cluster, which otherwise is mainly controlled by the intersection of NNW-trending Andean faults and a NE-trending transverse structural corridor. Further to the north, the distribution of other related Miocene porphyry-epithermal deposits can also be correlated with extrapolated Famatinian structures in the Western Cordillera (Wiemer et al., 2022; Figure 7). It is noted that the inferred NE-inclined Famatinian suture that controls the localization of the Pataz-Parcoy gold system in its hanging-wall may have been

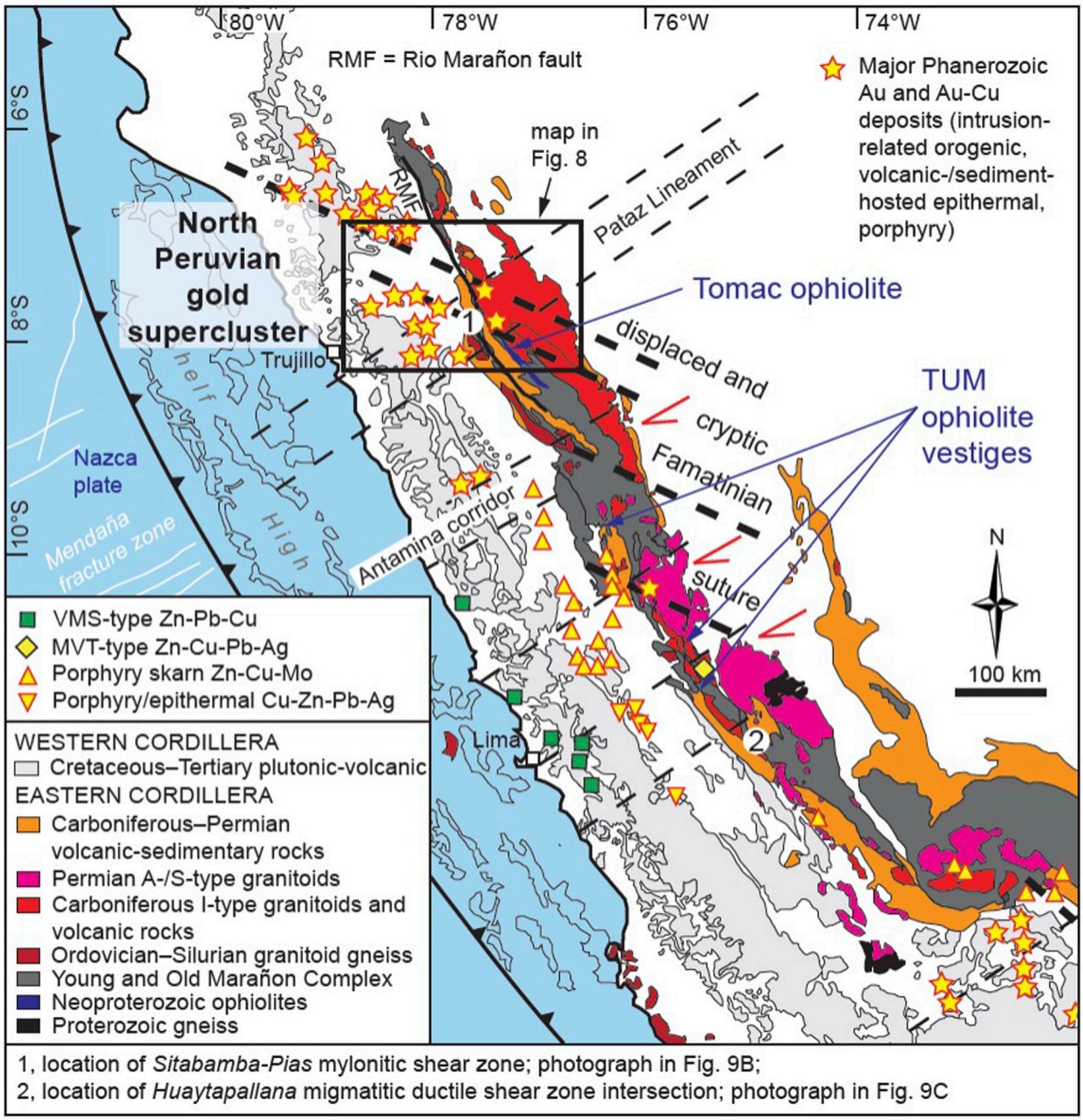

FIGURE 7
Simplified geologic map of Peru (adapted from Wiemer et al., 2022; based on Goméz et al., 2019). Note the NE-trending Pataz Lineament structural corridor, which is proposed to link the Mesoproterozoic K'Mudku shear zone with the recent Mendaña fracture zone (refer to Figure 4H). The North Peruvian gold supercluster is situated at the intersection of the Pataz Lineament with both the Famatinian Paracas collisional suture and the superimposed syn-to post-Carboniferous trend of the Andean orogen. Further to the south, the cryptic Famatinian suture is offset to the W/SW, likely due to dextral transverse fault kinematic movement (see red arrows), for example, along the Antamina corridor, sub-parallel to the Pataz Lineament. A Mesoproterozoic origin of the transverse structures remains to be tested; interestingly, the origin of the Antamina corridor has been demonstrated to date to at least the early Mesozoic (e.g., Love et al., 2004). In the absence of evidence for a Mesoproterozoic origin, it is proposed that the scissor-like southward widening of the Permo-Triassic continental rift system (Figure 4F) resulted in the formation of syn-rift transverse structures, such as the Antamina corridor. The westward displacement of the Famatinian suture to the south is supported by the location of the TUM (Tapo Ultramafic Massif) ophiolitic vestiges relative to the Tomac ophiolite (e.g., Tassinari et al., 2011; Wiemer et al., 2022). Location of the map in Figure 8 is indicated, and locations of photographs shown in Figures 9B, C are indicated.

offset dextrally in its NW-ward extrapolated continuation (see displaced Famatinian suture, Figure 8A). The proposed NW-ward continuation of the suture is not well constrained, but spatially matches the prominent El Cuello corridor of reactivated structures cutting through the Pataz area and the northernmost occurrence of Neoproterozoic ophiolitic remnants in vicinity to the

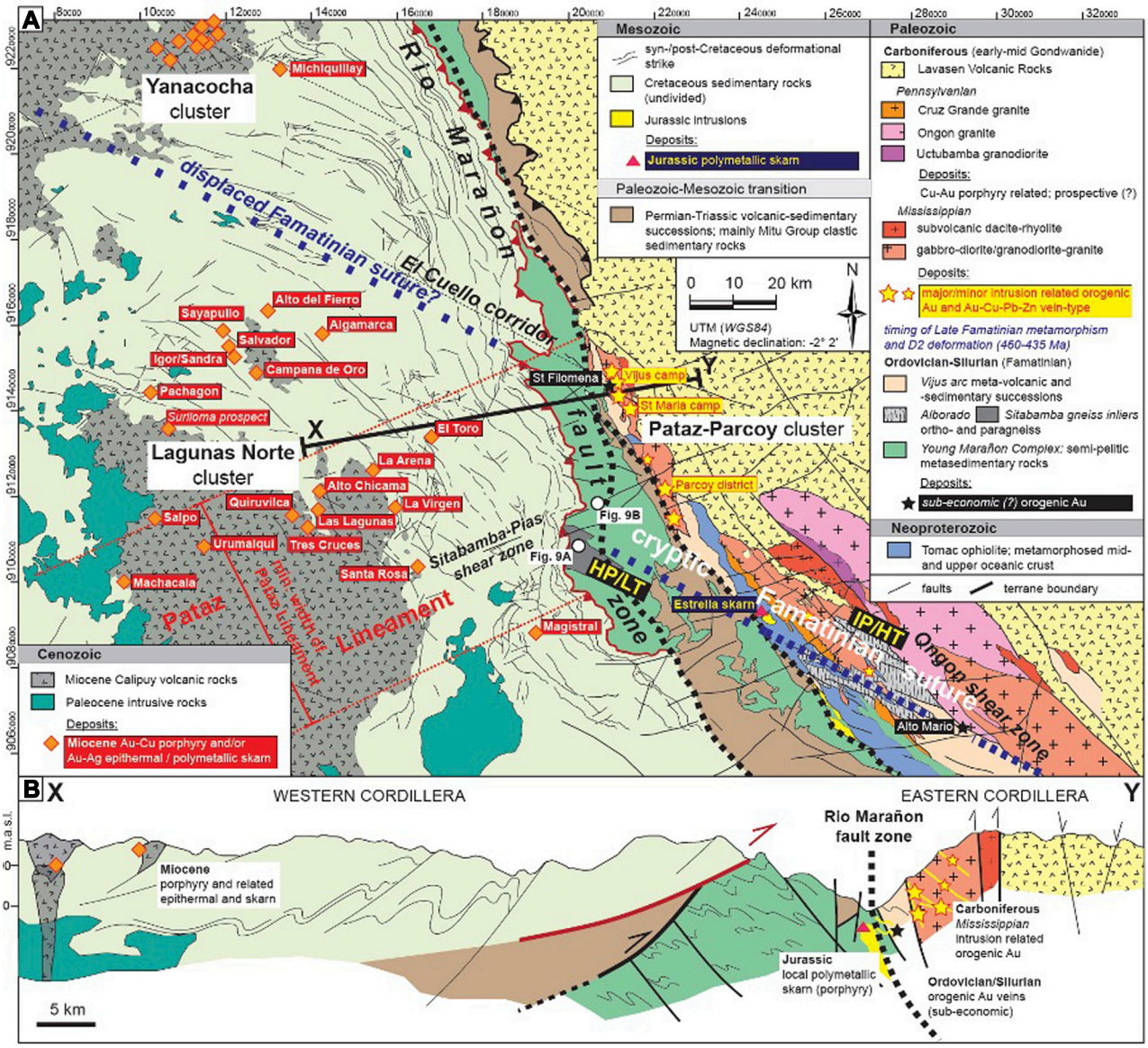

FIGURE 8
(A) Geologic map of the Pataz region and adjacent areas, northern Peru, showing the distribution of gold-rich Paleozoic and Miocene deposits (based on and modified after Wiemer et al., 2021a; Wiemer et al., 2022, Eastern Cordillera; and INGEMMET, Western Cordillera). Major cryptic inherited structures (NE-trending Pataz Lineament; NW-trending Famatinian suture and sub-parallel El Cuello corridor) are shown and extrapolated into the Western Cordillera. Major Carboniferous orogenic gold deposits (Pataz-Parcoy) are situated in the hanging-wall of the NE-dipping Famatinian suture (i.e., suture between Gondwana to the NE and the Paracas micro-terrane to the SW; Wiemer et al., 2022) and the associated fold-thrust-style Ordovician-Silurian basement orogen. The intersection between the inherited structures marks the location of a regional-scale dilational jog (see bend in the first-order Rio Marañon fault), which hosts the Pataz-Parcoy deposits. The extrapolated inherited structures and corridors are well-correlated with the location of the Miocene Yanacocha and Lagunas Norte deposit clusters. Importantly, although the Famatinian suture is well-constrained within the basement of the Eastern Cordillera (e.g., paired high-pressure/low-temperature, HP/LT—intermediate-pressure/high-temperature, IP/HT metamorphic belt; Wiemer et al., 2022), the inferred minimum total width of the cryptic Famatinian orogenic belt exceeds 80 km. Similarly, the structural corridor associated with the Pataz Lineament spans a minimum width of 50 km. Note that the occurrence of local Jurassic intrusions and related (sub-economic) polymetallic skarn within the Eastern Cordillera is spatially restricted to the vicinity of the Famatinian suture. Location of map indicated in Figures 2A, 7. Locations of photographs in Figures 9A, B are indicated. **(B)** Schematic cross-section illustrating the *thin-skinned* thrust style contact between the Eastern and the Western Cordillera, indicating the west-ward continuation of Paleozoic basement below the Mesozoic-Cenozoic nappes.

Rio Marañon fault zone (Wiemer et al., 2021a; Wiemer et al., 2022). Furthermore, the inclined nature of the Famatinian suture in combination with its proposed continuation as shown in Figure 8A, suggests a similar control of hanging-wall deposit localization in approximately 15-km-distance from the suture towards the NE for both the Pataz and the Yanacocha clusters.

The NE-trending Pataz Lineament may represent the link between the Mesoproterozoic intracratonic K'Mudku shear zone, and/or a branch thereof, in the Amazonian Craton and the recent (ca. 3.5 Ma, Huchon and Bourgois, 1990) oceanic Mendaña fracture system in the Nazca plate (Figures 3, 4H, 7; Wiemer et al., 2022). Furthermore, the Pataz Lineament approximates the boundary

between the Marañon and the Acre basins (Figure 2B), and it connects the Carboniferous Pataz-Parcoy gold districts with the Lagunas Norte cluster of Miocene Au-Cu porphyry and related epithermal and skarn deposits in the Western Cordillera. In fact, high grade gold shoots in the major Lagunas Norte mine display a consistent NE-trending strike/plunge (Evans et al., 2016). On the other hand, it is important to note that particularly the expressions of the epithermal gold deposits associated with the Lagunas Norte cluster are locally subject to significant lithologic control of hosting volcanic and sedimentary successions (e.g., Cerpa et al., 2013). As noted in Section 3.7, along the Pataz Lineament the exposed Miocene volcanic rocks and associated intrusions that are likely genetically related to the Lagunas Norte deposit cluster display an increased abundance (Figure 8A). In addition, the inferred boundaries of the Pataz Lineament not only intersect the northern and southern limit of the Pataz-Parcoy dilational jog, but also appear to be responsible for significant deflections of the beddings/foliations and fold plunge direction of the Cretaceous sedimentary rock successions in the Western Cordillera (Figure 8A).

Thus, it is important to note the similarity between the Pataz Lineament and the Antamina corridor. The Jurassic (or older) origin of the Antamina corridor, which displays similar features of strike deflection within younger cover rocks (e.g., Love et al., 2004; McCuaig and Hronsky, 2014), may be ascribed to the formation of a transfer structure that accommodated the Triassic extension episode (Section 3.7; Figures 4F, 7). Indeed, in contrast to the Pataz Lineament, the Antamina corridor cannot be readily correlated with any known structure within the Amazonian Craton, but is part of a set of NE-trending cryptic arc-normal fault corridors found throughout the central and southern Peruvian Andes. Wiemer et al. (2022) proposed that the Pataz Lineament may have already accommodated the Neoproterozoic detachment of the Paracas terrane as a propagated major oceanic transform fault during the Paracas oceanic basin opening, to subsequently delineate and accommodate the northern Paracas re-collision (Figures 4C, E). Thus, similar transverse structures, such as the Antamina corridor or Abancay deflection, may also originate from more ancient, pre-existing structures that accommodated the detachment and re-collision of the Paracas-Arequipa-Antofalla continental ribbon.

The proposed continuation of the pre-Carboniferous basement below the Western Andean Cordillera is schematically depicted in the cross-section of Figure 8B. The cross-section highlights the presence of Famatinian basement to the west of the superimposed major NNW-trending Rio Marañon fault zone. No distinct boundary between the Eastern and Western Cordillera is observed. The structurally bound occurrence of Permian-Triassic rift-related sedimentary sequences (Mitu Group) on both sides of the Rio Marañon fault zone attests to the fact that NNW-trending (i.e., Andean strike) horst-graben structural development that initiated in the Carboniferous was polyphase with more recent uplift activity during the Cenozoic (e.g., Witt et al., 2016; Wiemer et al., 2021a). During the Late Mesozoic to early Cenozoic, however, Cretaceous sedimentary rocks of the Western Cordillera were thrust NE-ward over the basement of the Famatinian orogen and the Carboniferous-Permian plutonic and volcanic rocks of the Eastern Cordillera along shallow thrust faults resembling a thin-skinned mode of tectonic emplacement (Figure 8B). The shallow thrust-style contact relationship between the Western and Eastern Cordillera lithologic-tectonic entities to the west of the Rio Marañon fault zone is shown in the photograph of Figure 9A. Just below the thin-skinned thrust contact, the Famatinian basement hosts the newly identified NE-trending Sitabamba-Pias shear zone, which appears to form part of the Pataz Lineament (Figure 8A). The mylonitic Sitabamba-Pias shear zone (Figure 9B, location indicated in Figures 7, 8A) aligns with NE-trending mafic dike swarms that crosscut the Pataz batholith between the Pataz and Parcoy districts to the east, and spatially correlates with significant strike deflections of structures within the over-thrusted Cretaceous sedimentary rocks.

Another critical insight stems from the recent discovery of a high-grade metamorphic migmatitic shear zone intersection within the Huaytapallana area of the Eastern Cordillera of central Peru (location shown in Figure 7; photograph in Figure 9C; this study). The shear zone intersection records at least three main episodes of deformation, corresponding to $S_{1/2}$, S_3 and S_4 foliations and associated isoclinal F_2 and superimposed tight F_3 folds, respectively (Figure 9C). The latest D_4 deformation is characterized by discontinuous narrow zones of S_4 foliation development that clearly cut through all previous deformation fabrics and follow a strike that can be correlated with the Andean strike direction. This D_4 event is ascribed to reactivation during the Andean orogeny but displays ductile fabric development. The earlier deformation events D_2 and D_3 are both associated with penetrative ductile foliation development along the hinges of associated F_2 and F_3 folds (Figure 9C). The strike trends of the S_2 and S_3 foliations are surprisingly well correlated with the large-scale NW-trending Famatinian orogen (S_2) and the NE-trending transverse structures, e.g., Pataz Lineament and Antamina corridor (S_3). Both D_2 and D_3 fabrics are associated with garnet-bearing metamorphic assemblages, whereas only D_2 experienced partial melting and leucosome formation. Overall, the observations support the notion of polyphase, stepwise uplift of the Eastern Cordillera basement, and the pre-Andean origin of both NW- and NE-trending structures. Ultimately, the garnet-bearing metamorphic assemblages associated with D_2 and D_3 were formed in deep crustal levels, whereas the rock currently outcrops at an elevation of ca. 4500 m altitude, juxtaposed against little deformed sub-greenschist Cenozoic metasedimentary rocks at lower altitude (ca. 3500 m), in which the same trend of structures is observed, but displays a brittle response. Hence, considering the thin-skinned thrust-style contact relationship between the Western and Eastern Cordillera as observed in the Pataz region (Figures 8B, 9A), a westward continuation of the Famatinian Paracas basement appears reasonable. North-west and NE-trending structures were reactivated and propagated vertically, possibly at multiple times during the Andean orogeny.

4.4 Chile and Argentina

The central to northern Chilean-Argentinian margin of South America hosts some of the world's largest copper mines, Collahuasi, Chuquicamata, and Escondida, which are part of the Eocene to early Oligocene Cu-Au porphyry and associated epithermal belt that follows the N-S trending arc-parallel trans-lithospheric Domeyko

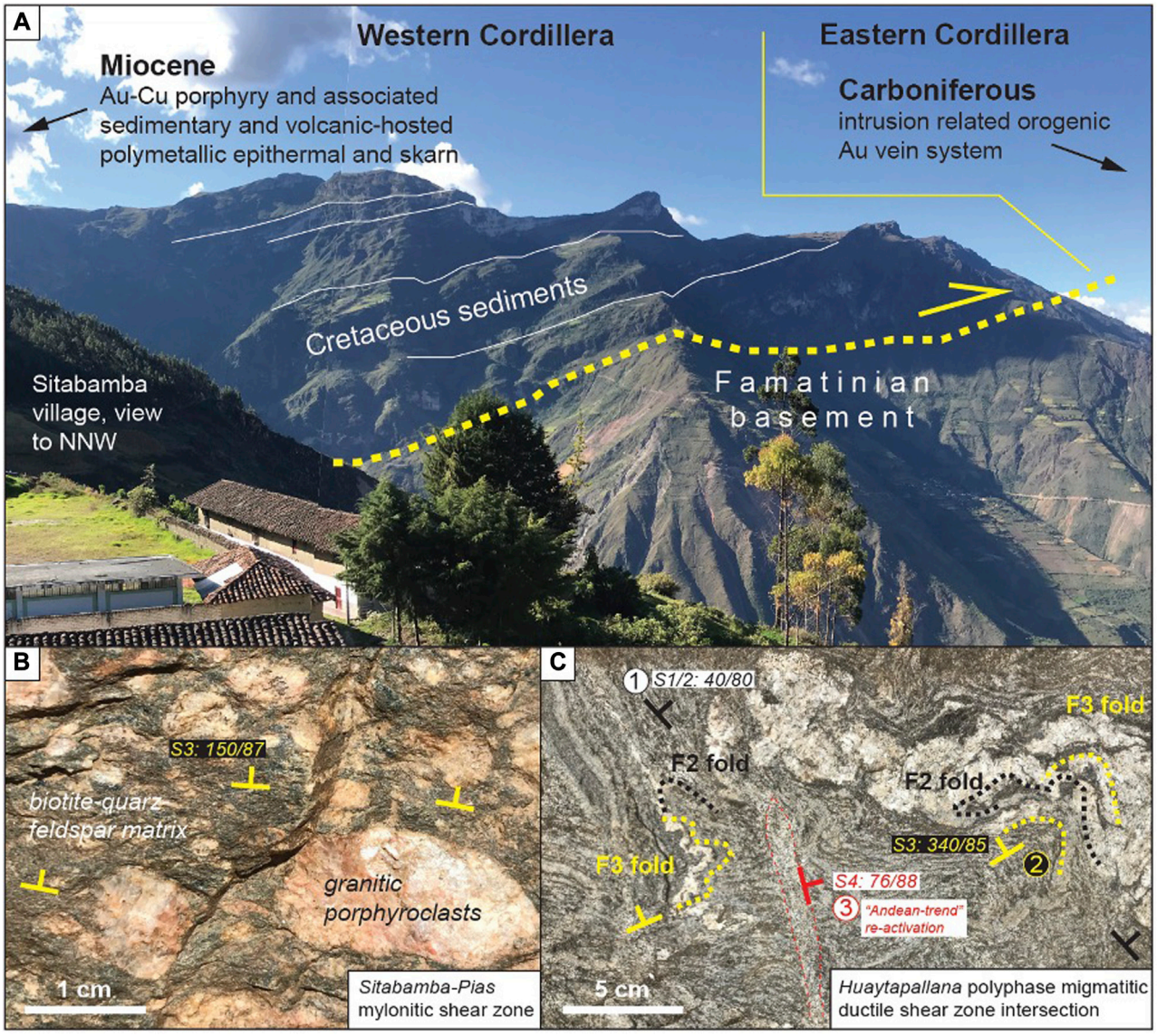

FIGURE 9
(A) Panorama photograph of the thrust-style contact between the Eastern and the Western Cordillera in the Pataz region, northern Peru (location of photograph given in Figure 8A; looking to the NNW; compare to cross-section in Figure 8B; this study). **(B)** Photograph from the newly defined (this study) *Sitabamba-Pias* mylonitic shear zone, northern Peru (location of photograph given in Figures 7, 8A). **(C)** Photograph of a polyphase migmatitic, ductile shear zone intersection, Huaytapallana area, south-central Peru (location of photograph given in Figure 7; this study). Note: values in **(B,C)** are given as *dip direction/dip angle* for average foliation measurements of S1/2, S3 and S4. The values correlate with the main structural trends of strike directions identified by Wiemer et al. (2022), i.e., ca. 115° for the Famatinian orogen (#1 in **(C)**), ca. 55° for the Pataz Lineament and other supposedly inherited cross-fault structures (#2 in **(C)**), and ca. 150° for the post-Famatinian Andean orogen (#3 in **(C)**).

fault system (Figure 10A). This belt has been subject to the debate about the role of structural inheritance and/or spatial periodicity in the distribution of major deposits (e.g., Chernicoff et al., 2002; Richards, 2003; Hayward et al., 2018). The southern termination (~29°S) of the Eocene–early Oligocene belt approximates the proposed northern demarcation of the Cuyania and Chilenia terranes and/or its intersection with the NE-trending Tucuman Transfer zone that roughly marks the northern limit of the recent Chilean flat-slab segment (Figures 4E, F, 10; e.g.; Kley et al., 2005; Iaffa et al., 2011). As mentioned in Section 3.7, the northernmost and less endowed part of this metallogenic belt is recognized in southern Peru, south of the Abancay fault and deflection (Figure 4I; e.g.; Clark et al., 1990; Sillitoe and Perello, 2005).

Overall, the belt is hosted within a corridor of NW-trending faults, here referred to as the North Chile-Argentina corridor (NCAC; Figures 3, 4H, 10). Major NW-trending faults within the NCAC have previously been recognized as ore deposit controlling structures, and include the Calama-Olacapato-El Toro, the Chorrillos, the Quevar, the Archibarca, and the Culampaja lineaments or faults (Figure 10A; e.g., Chernicoff et al., 2002; Richards, 2003; Hayward et al., 2018; Escuder-Viruete et al., 2022). The Chorrillos and Quevar faults have been regarded as branches of the Calama-Olacapato-El Toro fault (e.g., Escuder-Viruete et al., 2022). Another, so far

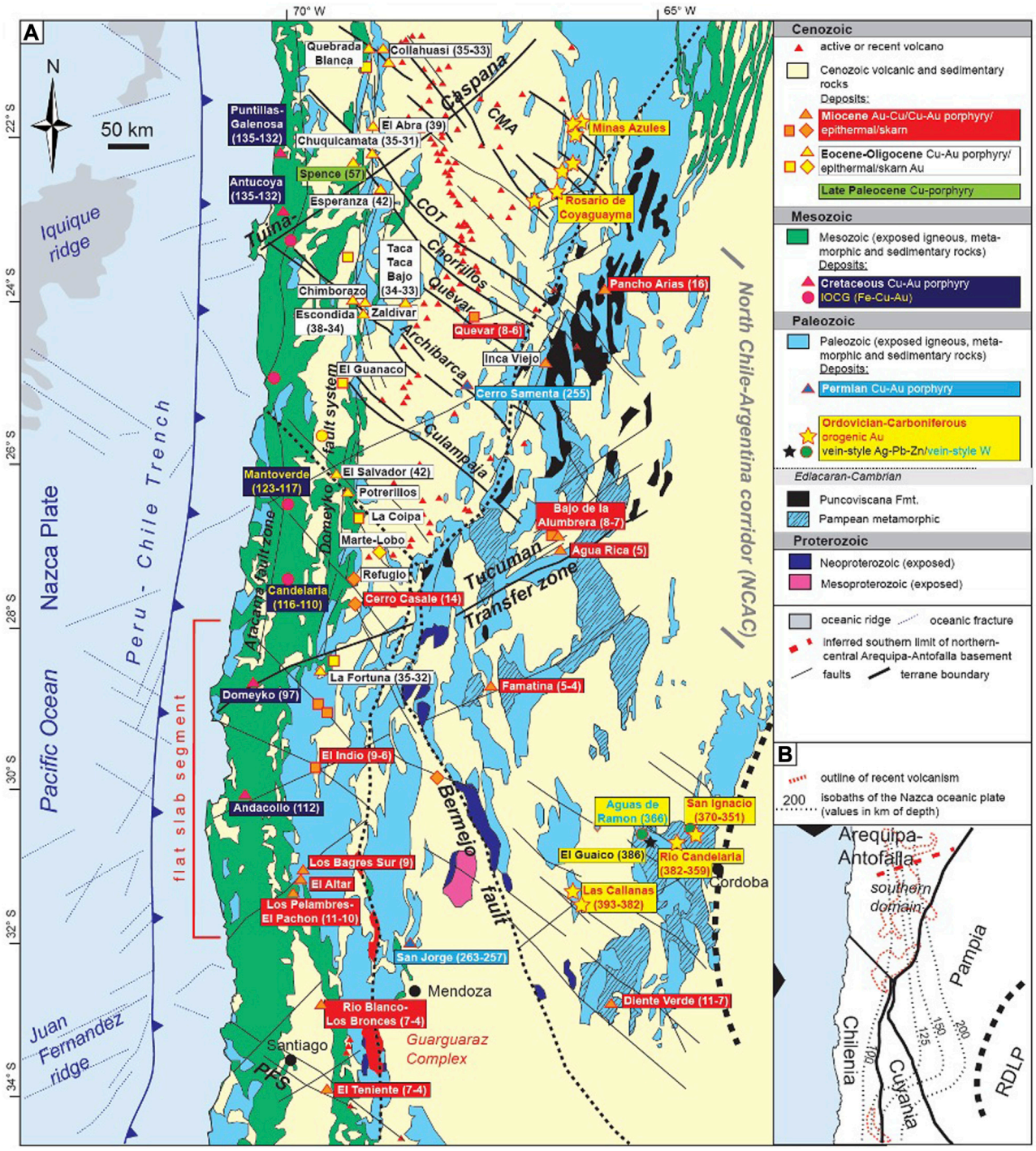

FIGURE 10
Simplified geologic map of north-central Chile and north-western Argentina showing major faults and terrane boundaries, and the distribution of major deposits, grouped by age of mineralization (given in brackets, in *Ma*, where known) and deposit type (compiled and modified after Skirrow et al., 2000; Rodríguez and Bierlein, 2002; Chernicoff et al., 2002; Sillitoe and Perello, 2005; Rapela et al., 2010; Willner et al., 2011; Escayola et al., 2011; Gómez et al., 2019; Piquer et al., 2021a; 2021b; Escuder-Viruete et al., 2022). Note that besides the Atacama fault zone and the Domeyko fault system, faults that strike sub-parallel to the overall N-S Andean strike direction are ommitted, for clarity. CMA, Collahuasi-Minas Azules fault zone; COT, Calama-Olacapato-El Toro fault; PFS, Piuquencillo fault system. **(B)** Corresponding subdivision into major terranes and crustal blocks. RDLP, Rio de la Plata craton Location of map shown in Figure 2A.

unnamed, but previously recognized (e.g., Chernicoff et al., 2002) sub-parallel broad fault zone that largely demarcates the northern boundary of the NCAC is here referred to as the Collahuasi-Minas Azules fault corridor (CMA; Figure 10A). The CMA corridor runs sub-parallel to the poorly defined northern NW-trending boundary of the Rio de la Plata Craton (Figures 3, 4H; e.g., Rapela et al., 2011).

The origin of the NW-trending faults within the NCAC remains unclear, noting that numerous studies have interpreted these transverse fault sets to date back to at least the late Paleozoic (Permo-Carboniferous) as arc-oblique transfer faults, which were variously reactivated as Mesozoic transtensional and normal faults (e.g., Chernicoff et al., 2002; Espinoza et al., 2021). It may be discussed that the southern limit of the NCAC correlates with the proposed sub-parallel NW-trending boundary of the northern Chilenia terrane (see Chilenia boundary after Ramos, 2008 in Figure 10). However, considering the presented tectonic history of South America (Section 3; Figure 4), and lack of conclusive evidence, the NW-trending northern boundary of the Chilenia terrane is not confirmed. A more reasonable explanation for the limiting boundaries of the Eocene to early Oligocene metallogenic belt may be found in a NE-trending structural corridor that includes the Tucuman Transfer zone and the Tuina-Caspana fault (Figures 4H, 10). Indeed, based on the integration of 3-D P-wave, V_P/V_S, and electrical resistivity tomographic models in northern Chile, a recent study by Contreras-Reyes et al. (2021) demonstrated the existence of zones of high permeability, fracturing and fluid content that correlate with the trans-lithospheric Atacama and Domeyko fault zones and the NE-trending Tuina-Caspana fault (Figure 10). The Tuina-Caspana trans-lithospheric fault approximates the structurally unspecified but geochronologic-isotopic broadly constrained boundary between the northern-central and the younger southern domain of the Arequipa-Antofalla terrane (Figure 10B; Loewy et al., 2004). Indeed, it appears that a critical knowledge gap in our understanding of causative relationships and processes in the origin and evolution of major trans-lithospheric fault zones and their role in ore deposit formation concerns a more comprehensive tectonic reconstruction and delineation of tectonic blocks. Based on intermediate-to-short wavelength gravity anomalies, a recent study by Carrizo and Herrera (2019) demonstrates the presence of widespread crustal-scale dense blocks in the Chilean fore-arc, arc, and back-arc. Investigation of the interplay between the dense crustal blocks and long-lived trans-lithospheric faults (TLF) suggests a spatial and genetic control on the emplacement of Cu-fertile magma along the flanks and edges of dense crustal blocks at their intersection with TLFs. It follows that a better understanding of the lithosphere-scale architecture and its evolution is crucial, requiring advanced integration of geophysical, geochronological, chemical-isotopic, and structural and geodynamic data sets.

Similar to the proposed deposit superclusters in Colombia, Ecuador and Peru (see previous *Sections*), both NW- and NE-trending transverse structures in central-northern Chile and Argentina are associated with deposits and deposit clusters of various type, style and age. For example, the CMA corridor that appears to control the localization of the giant Collahuasi Cu-Au porphyry deposit at its intersection with the Domeyko fault system can be traced SE-ward towards its intersection with the N/NNE-trending Famatinian belt and a spatially associated cluster of orogenic gold deposits (i.e., Minas Azules and Rosario de Coyaguayma districts, northern Sierra Rinconada; Figure 10A). Whereas structurally bound orogenic gold vein formation in the Minas Azules deposit is intimately associated with Late Famatinian N/NNE-striking fold-and-thrust belt development, and hosted within Ordovician metasedimentary rocks (i.e., turbidites), the localization of deposits and clusters along the belt appears to be controlled by NW-trending fault intersections (e.g., Rodríguez and Bierlein, 2002). Considering the close vicinity to the Pampean margin it may be argued that the NW-trending faults originated as transfer faults accommodating the closure of the Puncoviscana oceanic basin (Figures 4C–E, 10A). If true, the same scenario may explain the origin of the other sub-parallel NW-trending major TLF structures within the NCAC (i.e., Calama-Olcapato-El Toro, Archibarca, Culampaja). Ultimately, these TLF structures display a relatively regular spacing, are aligned near-perpendicular to the inferred suture that marks the closure of the Puncoviscana oceanic basin and they control the localization of deposits of various age dating back to at least the Late Mesozoic. Furthermore, the entire region has been shown to comprise basement of at least Late Mesoproterozoic age, supporting the notion of vertically accretive basement TLF inheritance and propagation (e.g., McCuaig and Hronsky, 2014).

Another noteworthy feature concerns the Chilean flat slab, its location, evolution, and effect on the volcanic arc migration and associated magmatic-hydrothermal systems during the Miocene. The sharp deflection of the present-day Benioff zone may be correlated with the progressive subduction of the Juan Fernandez ridge (Figures 10A, B). On the other hand, the location and alignment of the oceanic ridge itself raises the question whether the involvement of more ancient lithosphere-scale structures within the continent play a role. More importantly, associated isolated Miocene volcanic-hydrothermal centres and ore deposits appear to impinge on more ancient sites of lithospheric permeability. The Miocene Dente Verde Cu-Au porphyry deposit (~11.2 Ma; K-Ar hydrothermal illite; Urbina and Sruoga, 2008) is situated within a NNE-trending belt of Pampean metamorphic basement rocks and belongs to a narrow belt of isolated Miocene intrusions that follow a NW-striking trend (Figure 10A; e.g., von Gosen et al., 2002). The same NW-trending strike direction is also followed by faults that control the localization of the Devonian orogenic gold systems of the Rio Candelaria and Las Callanas districts at their intersection with the Pampean and superimposed Devonian-Carboniferous belt (Figure 10A; e.g., Skirrow et al., 2000).

In another example, Escuder-Viruete et al. (2022) show that Late Miocene (~7.7–6.3 Ma; $^{40}Ar/^{39}Ar$ whole rock) epithermal Ag-Pb-Zn mineralization associated with the Quevar Volcanic Complex marked the development of a Riedel-type fault network in between, and as a response to, sinistral reactivation of the Chorrillos and Quevar fault branches of the Calama-Olcapato-El Toro TLF (Figure 10 (Escuder-Viruete et al., 2022). The study demonstrates the importance of lower-order and potentially newly developed structural architectures adjacent to principal TLFs as sites of mineralization.

5 Geochemical evidence for trans-lithospheric connectivity and inherited pre-enriched mantle domains

In this Section, selected bulk-rock geochemical data is presented, focussing on magmatic parental rocks to particularly gold-rich mineral systems. In previous Sections, the importance of tectonic history, terrane boundaries and associated TLF structures and their

intersections as sites of increased permeability and associated high mass and energy fluxes has been highlighted. The review included both Cu- and Au-rich mineral systems. However, besides the fact that factors, such as the magmatic-hydrothermal transport behaviour of metal species, the volume, duration, and residence of magma and magmatic activity, physico-chemical parameters such as the redox state, the precipitation efficiency, and the transient stress state of the lithospheric mantle and crust play an important role in whether Cu- or Au-rich mineral systems form, it is commonly accepted that Cu and Au systems, respectively, require different magmatic source reservoirs, and or different processes of magma extraction (e.g., Loucks and Ballard, 2002; Hronsky et al., 2012; Loucks, 2014; 2021; Chiaradia, 2020). Compared to rather common subduction related magma genesis in Cu porphyry systems, noting that the confluence of various other parameters is required in the formation of economically significant Cu deposits (e.g., Loucks, 2014; 2021), the source and/or mode of source magma extraction in the generation of Au-rich systems has been associated with other specific geodynamic anomalies (e.g., Hronsky et al., 2012). Besides the mode of selective metal extraction as incompatible species at low degrees of partial melting of a reservoir, it is postulated that pre-enrichment of an upper mantle domain during a preceding or even ancient subduction event may produce a sufficiently fertilized (fossil) upper mantle reservoir subject to Au-rich magma generation upon reactivation (e.g., Xiong et al., 2021). Thus, structural TLF inheritance may be accompanied by inheritance of pre-fertilized mantle domains.

5.1 Identification of gold parental magmas

Bulk-rock geochemical data from unaltered/fresh plutonic and volcanic rocks and dike intrusions that are spatially and temporally associated with the Carboniferous Pataz gold vein system of northern Peru (location in Figures 7, 8A; discussed in Sections 3.5, 3.6 and 4.3) and its proposed extension in the Huachón gold prospective area in Central Peru (Défago et al., 2006) display an overall bimodal composition of mafic endmembers and differentiated felsic suites across a conspicuous silica gap (between ca. 57–65 wt% SiO_2; e.g., Witt et al., 2013b; Wiemer et al., 2020; Villanes et al., 2023). The mafic and felsic plutonic and volcanic suites are considered to be genetically related (Wiemer et al., 2020). Therefore, the silica gap is interpreted to represent a "Daly gap" (e.g., Daly, 1925; Bonnefoi et al., 1995). The origin of the Pataz "Daly gap" is subject to ongoing research, however, preliminary results from field observations, petrology and geochemistry indicate that deep crustal entrapment and fractionation processes led to the batch extraction of felsic magma from mafic parents, concomitant with ore-fluid release (Wiemer et al., 2021b; Villanes et al., 2023). Indeed, the primitive mafic endmember suite of the Pataz magmatic system displays a higher concentration in Cu compared to the differentiated felsic suite at comparable Au concentrations between the mafic endmembers and part of the felsic rocks (Figures 11A, B). Another group of the felsic rocks display a relative depletion in Au concentrations that may indicate that Au has been effectively removed. These observations challenge models that envisage gold enrichment as a primary result of differentiation of granitic magma with final magmatic-hydrothermal ore-fluid expulsion from highly evolved granitic systems (e.g., Mustard et al., 2006). The notion is important, because most often granitic systems are studied to argue for, or against, a magmatic origin of gold-rich mineral systems (e.g., orogenic gold; Goldfarb and Pitcairn, 2022). Instead, it appears more logical to focus on the source and genesis of parental mafic endmembers (Section 5.2) and the reason why these usually only represent voluminously subordinate components, compared to granitic intrusions, if they are exposed at all (Section 5.3).

5.2 Inheritance of pre-fertilized mantle source reservoirs

In the absence of evidence for post-magma extraction crustal contamination, in combination with the primitive character of both the Pataz and Huachón mafic endmembers, it is inferred that these rocks derived from a mantle source that was already enriched in incompatible species (including precious and base metals). The most primitive Pataz and Huachón rocks fall within the field for absarokite based on their elevated K_2O concentration (Figure 12A), at corresponding MgO contents of up to ca. 10 wt% (Figure 12B) indicating a mantle derived origin. The K-enriched mantle source is supported in comparison to a reference suite of primitive rocks from the Mariana arc. At similar SiO_2 and MgO concentrations, the Mariana rocks display K_2O contents along a typical basalt to basaltic andesite differentiation trend for rocks that derived from uncontaminated upper mantle (Figures 12A, B). In addition, a global data compilation of rocks belonging to the appinite-absarokite suite, or the primitive sanukitoid suite, are shown. All considered occurrences, spanning examples from the Neoarchean to the present, are genetically or at least spatially associated with gold-rich mineral systems, and overlap the K_2O and MgO vs. SiO_2 composition of the Pataz rocks. (Figures 12A, B; data sources: Ovejas batholith; Duque-Trujillo et al., 2019; Creixell et al., 2009; Graham et al., 2017; Absaroka Range; Iddings, 1895; Feeley, 2003; King River; Feldstein and Lange, 1999; Cripple Creek; Kelley et al., 1998; Mascota; Ownby et al., 2008; Ecuador; Chiaradia et al., 2014; Santos and Oliveiri, 2016; Wilkin and Bornhorst, 1993; Ach'Uaine; Fowler and Henney, 1996; Lobach-Zhuchenko et al., 2008; Larionova et al., 2007; Leslie et al., 2009; Damavand volcano; Liotard et al., 2008; Ireland; Murphy et al., 2019). Indeed, most of the compiled absarokite-appinite rocks are interpreted (by respective authors) to have been derived from upper mantle that was pre-enriched (i.e., pre-metasomatized) at the time of magma genesis/re-mobilization. In some cases, the subduction induced metasomatism of the upper mantle, responsible for the pre-enrichment preceded the remobilization event by 100s of million years.

The Pataz and Huachón primitive Au parental rocks along with the global absarokite-appinite data compilation are further discriminated in the (Ba/Zr)/(Sr/Y) vs. SiO_2 graph (Figure 12C), originally produced by Loucks and Ballard (2002) based on a global data set of least altered Phanerozoic rocks. The graph discriminates Au-, Cu-Au/Au-Cu-, and Cu-rich parental magmatic rocks, whereby Ba (normalized to Zr, as a commonly accepted immobile species) is used as an indicator for incompatible element enriched Au-rich sources and/or parental magmas, and the Sr/Y ratio that efficiently discriminates between Cu-Au- ore-productive compared to unproductive suites, whereby Y represents a

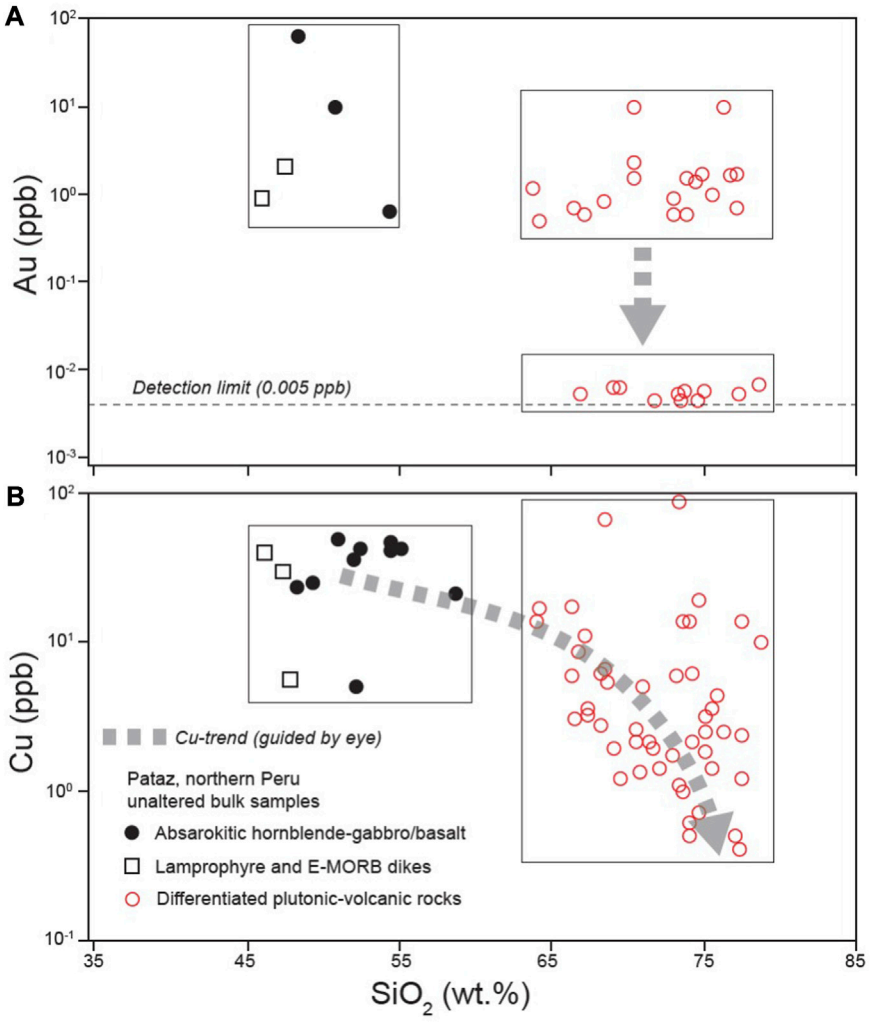

FIGURE 11
(A,B) Bulk-rock geochemistry discrimination diagrams of Carboniferous unaltered plutonic and volcanic host rocks to the Pataz intrusion related orogenic gold system. Au and Cu versus SiO_2, respectively, showing higher metal concentrations in the mafic (gabbro/basalt, lamprophyre dikes) endmembers (<57 wt% SiO_2), whereas the more differentiated granodiorite/dacite-granite/rhyolite association (>65 wt% SiO_2) is interpreted to have lost part of its metal cargo upon ore-fluid expulsion during magmatic fractionation and differentiation processes.

compatible species in minerals that are not significantly affected by high pressure or high H_2O content, such as hornblende, and Sr (similar to Eu) represents a compatible species in plagioclase, which is drastically suppressed at high pressure and high H_2O (Loucks and Ballard, 2002). In other words, both Au- and Cu-fertile parental magmas are hydrous and characterized by deep crustal onset of crystallization, whereby Au-parents require an incompatible element enriched source, or selective extraction of incompatible species. Furthermore, Loucks and Ballard (2002) demonstrated that the SiO_2 content (as an index of differentiation) of respective parental magmatic systems corresponds to variations in approximate onset of sulfide-saturation, i.e., ca. 50 wt% SiO_2 for Au magmas and ca. 55 wt% SiO_2 for Cu parental magmas.

Indeed, the data from the Carboniferous magmatic rocks from the Pataz and Huachón regions suggest that part of the northern and central Peruvian lithospheric mantle was pre-enriched/-metasomatized due to the preceding Famatinian orogeny (and/or the older Sunsás orogeny). A similar model has recently been proposed for post-subduction shoshonitic host rocks to major gold deposits in Fiji (Clarke et al., 2022). Clarke et al. (2022) argue that directly preceding subduction in Fiji was not sufficient in providing slab-derived sediment melt and fluid fluxing to produce observed enriched geochemical trends (including metals) within post-subduction shoshonitic magmas. Instead, an earlier episode of subduction best explains the formation of metal-enriched cumulate portions within the Fijian upper mantle and lower crustal lithosphere, which were subject to later partial melting. However, a zircon-based study on the Pataz absarokitic gabbros indicates that here respective magmas were some of the first to be generated and to intrude the lower to mid crust during Carboniferous subduction-related magmatic activity (Wiemer et al., 2020; 2023). Hafnium-in-zircon isotopic data with slightly negative εHf values (ca. −2) in early crystallized zircons from the Pataz absarokitic gabbros support the notion of Au-parental magma extraction from pre-enriched sub-continental lithospheric mantle since the onset of Carboniferous subduction (Wiemer et al., 2020; 2023). Re-melting of the pre-fertilized Pataz lithospheric mantle

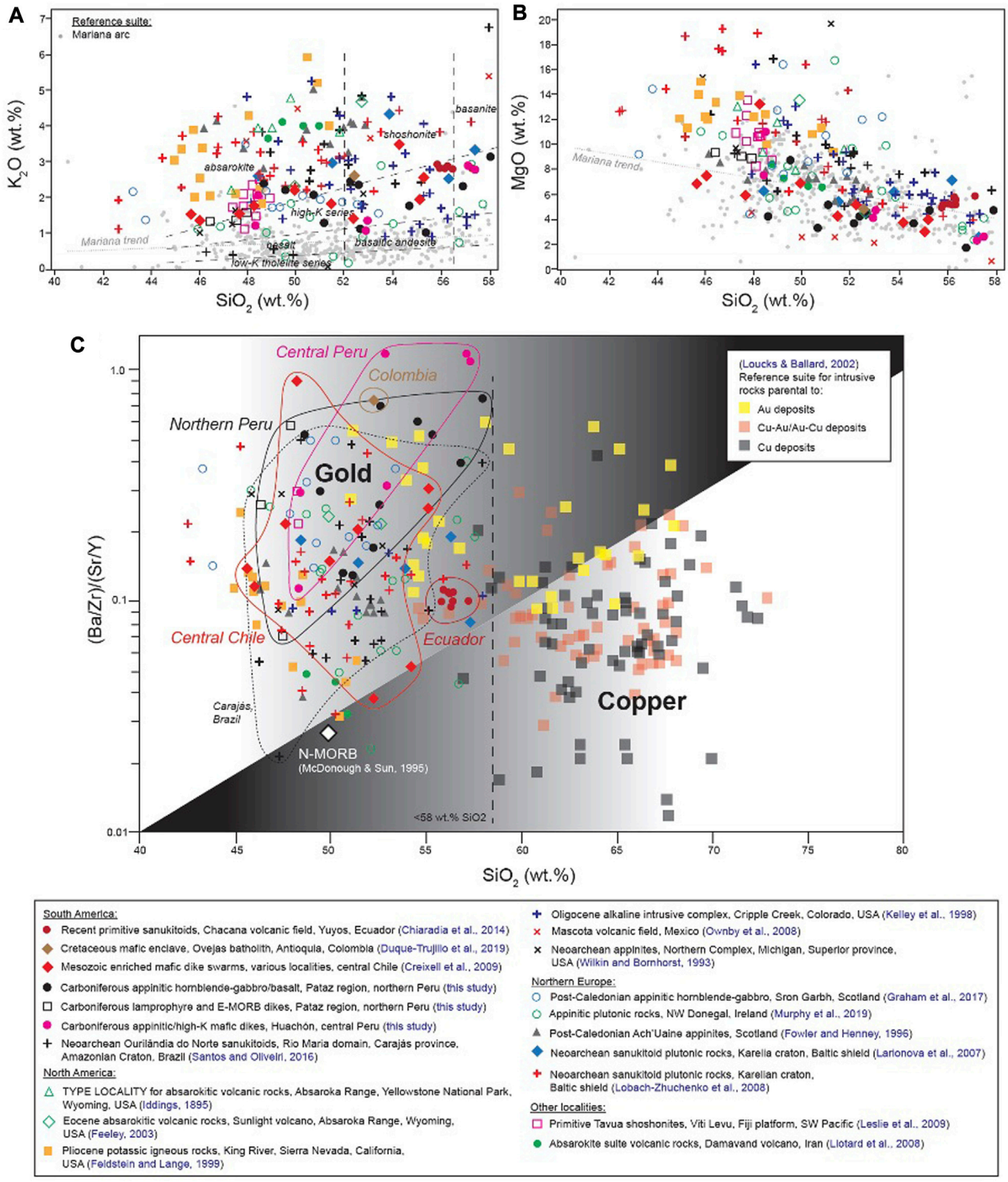

FIGURE 12
(A,B) K_2O and MgO versus SiO_2 bulk-rock geochemical diagrams, including data from South American and other appinite-absarokite and primitive sanukitoid localities (samples <58 wt% SiO_2) that occur in spatial association with gold-rich deposits (locations and references provided in the legend). The data suggest the direct derivation of mafic endmembers from a metasomatized lithospheric mantle, and all localities have witnessed preceding subduction related orogenic events at some point in geologic time. The interpretation is corroborated by comparison to a reference suite of most primitive rocks from the Mariana arc. **(C)** Bulk-rock (Ba/Zr)/(Sr/Y) versus SiO_2 discrimination diagram (based on a global reference suite provided in Loucks and Ballard (2002); see legend in upper right corner). Refer to text for discussion.

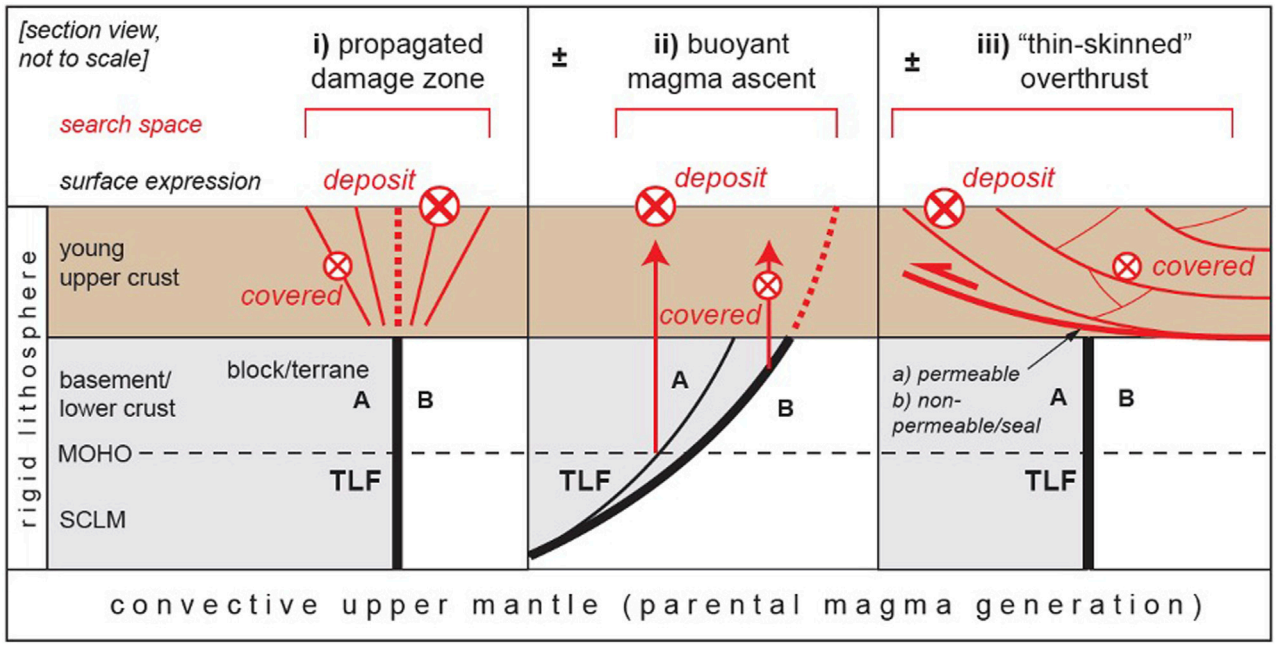

FIGURE 13
Schematic endmember scenarios of vertical inheritance and propagation of trans-lithospheric fault systems (TLF). See text for discussion.

may be explained as a result of subduction-drag and/or heat from concomitant subduction-related magmatism. Nevertheless, despite the specific geodynamic mode of melt generation, both the Fjian and the Pataz systems require the presence of pre-modified (and fertilized) upper mantle or lower crustal domains.

The presented compilation of data in Figure 12 also includes the primitive sanukitoids of the recent (ca. 30 ka) Yuyos lava flow from the Chacana volcanic field (location shown in Figure 6; data from Chiaradia et al., 2014). Interestingly, the Chacana volcanic field is situated at an intersection with the newly proposed Alpala corridor (ALC; Figure 6; Section 4.2) that hosts the Miocene Cu-Au porphyry Alpala deposit (Rohrlach et al., 2015). Considering the plotting of the Chacana data in the Cu-Au/Au-Cu field of Figure 12C, it may be argued that the Chacana volcanic field represents a Cu-Au/Au-Cu porphyry system "in-the-making."

Other data from South America include Jurassic-Cretaceous mafic dike swarms from the Coastal Range and Frontal Cordillera of central Chile, emplaced during a period of crustal extension (Creixell et al., 2009). Part of these dikes show geochemical signatures indicative of their derivation from a subduction-modified mantle source (Creixell et al., 2009). Although these dikes are not readily associated with any major deposits within the area, some of the dike swarms appear to follow major TLF systems (e.g., along the Piuquencillo fault system; Figure 10A).

Along the proposed Central Colombian structural corridor (CCC; Figure 5A), enriched mafic enclaves within the Cretaceous Ovejas satellite intrusion of the Antioquia batholith also display geochemical affinities to the enriched absarokitic-shoshonitic suite (Duque-Trujillo et al., 2019). Considering the presented tectonic history of the Colombian region, it may be argued that both the Putumayo and the subsequent Famatinian subduction-accretion episodes played a fundamental role in the modification and fertilization of respective upper mantle domains, which were repeatedly tapped during the prolonged Antioquia batholith magmatism.

5.3 Comment on the scarcity of gold parental igneous rocks

For decades, primitive potassic magmas have been considered as potential parents to gold rich ore deposits (e.g., Müller and Groves, 2019). However, the idea is often rejected due to the subordinate exposed volume of respective rock suites. In fact, mafic dikes (lamprophyric and other enriched basalt compositions) in the Pataz region are spatially restricted to the vicinity of the Ongon shear zone and the eastern- and westernmost exposed margin of the Pataz batholith (Figure 8A). Within the interior of the granodiorite to monzogranite-dominated batholith hardly any mafic dikes are observed. Similarly, both plutonic mafic rocks (appinitic/absarokitic gabbros) and their volcanic equivalents (appinitic lava flows) appear to focus on the western margin of the Pataz batholith and overlying volcanic pile (i.e., Lavasen Volcanic Rocks). The most voluminous granodiorite within the central parts of the Pataz batholith, however, comprises locally abundant appinitic mafic enclaves (e.g., Wiemer et al., 2021a; Villanes et al., 2023). These enclaves are chemically similar to those observed within the Antioquia batholith of central Colombia (Duque-Trujillo et al., 2019).

Based on insights from previous studies, Murphy (2020) presents a reasonable explanation for the overall scarcity and/or peri-batholithic restricted distribution of preserved intact appinite complexes and/or related dikes: The coeval formation of voluminous felsic granitoid magma, irrespective of process (e.g., fractionation of appinitic mafic parent, associated lower crustal anatexis, or

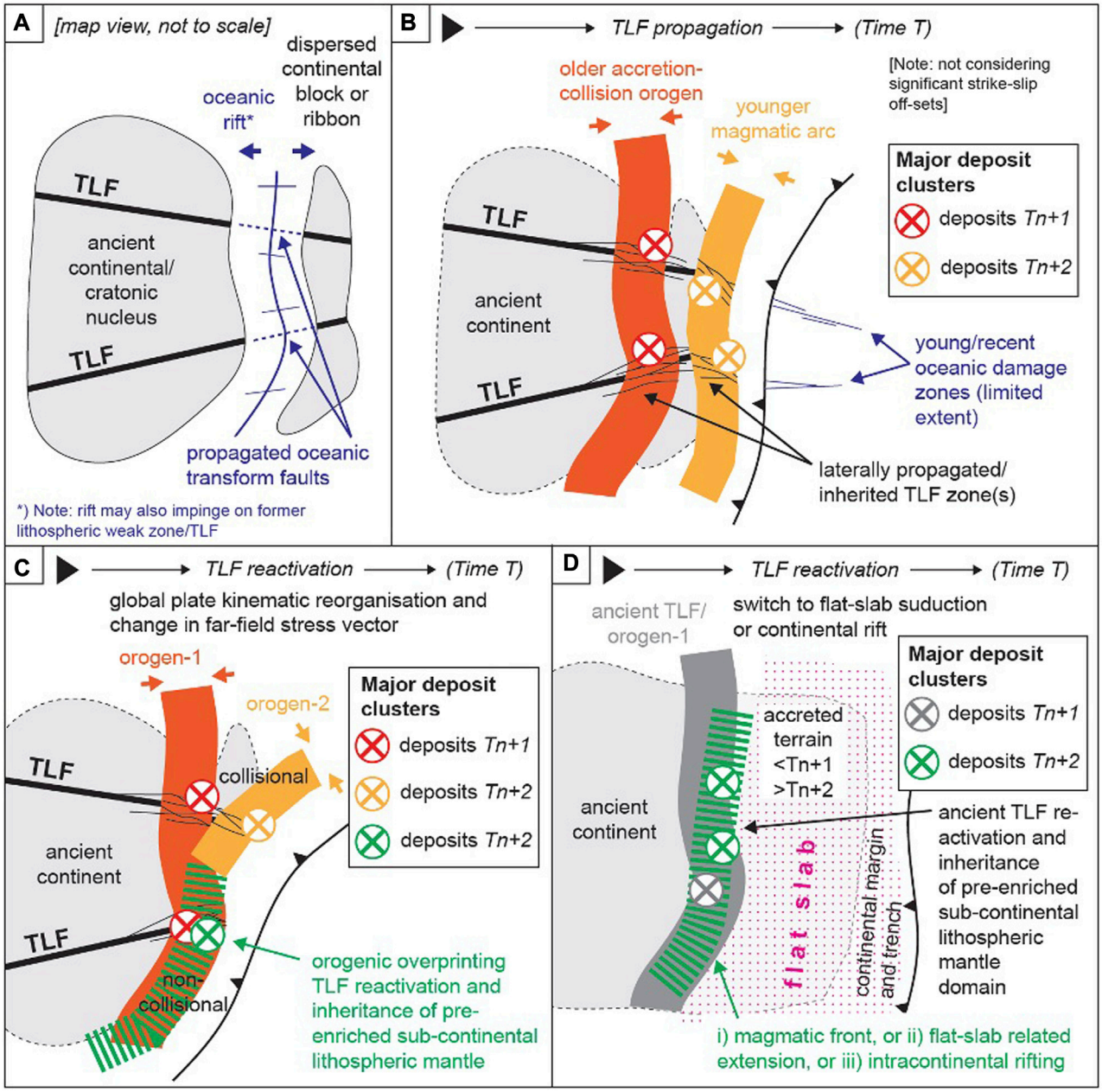

FIGURE 14
Schematic illustration of various modes of lateral inheritance, propagation, and reactivation of trans-lithospheric fault systems. **(A)** Rifting along pre-existing weak zones and/or seeding and propagation of oceanic transform faults originating from TLFs within older continental lithosphere. **(B)** Simple lateral TLF propagation during terrane accretion. **(C)** TLF reactivation during superimposed orogeny upon change in far-field stress and/or difference in collision versus non-collision dynamics across distinct arc segments. **(D)** TLF reactivation in continental interiors during switch in large-scale geodynamics. See text for discussion.

extraction from another source) that rise into mid-upper-crustal levels to form large magma chambers, causes a rheological barrier to the subsequent ascent of mafic magma. Thus, parental components often only occur in the form of mafic enclaves entrained in differentiated granitoids, as observed in Pataz (e.g., Murphy, 2020; Wiemer et al., 2021b).

Moreover, younger ore-endowed regions, such as in the case of the Miocene Cu-Au/Au-Cu porphyry and related skarn deposits along the western South American margin, mostly only provide insight into shallow level sub-volcanic rocks and surficial volcanic eruptive rocks of their respective crustal-scale magmatic system. In these cases, fruitful insight comes from variable compositions of mineral phenocrysts and/or their chemical zonation. In the Yanacocha district, northern Peru, for example, Chambefort et al. (2013) recorded the occurrence of early high-alumina amphibole phenocryst compositions that indicate crystallization from a volatile-rich mafic precursor magma at elevated depth.

6 Discussion and conclusion

In view of the concepts, observations, and data reviewed and presented in this paper, several conclusions can be drawn, but more importantly, critical points of discussion are highlighted, which may direct future research. Firstly, it is noted that it has most recently been stated that young gold-rich deposits are not underlain by older basement and/or lithosphere as part of an argument against both a magmatic and a mantle-derived source for orogenic gold deposits (e.g., Goldfarb and Pitcairn, 2022). This statement may be wrong. The here presented tectonic evolution of South America clearly indicates that almost the entire continent is underlain by pre-Andean, in fact mostly pre-Cambrian basement, including its western margin. Although no "young" orogenic gold deposits are known from South America, hardly any respective young mesothermal crustal levels are exposed at present.

Secondly, the western South American margin as a natural laboratory for the investigation of endmember models of deposit distribution (i.e., self-organization and structural inheritance) is recalled. The presented tectonic history implies that significant strike-slip off-sets or impacts of plate tectonic reorganization were limited on the continental to regional scale to typically <50 km along-strike, allowing for the reconstruction of successive geodynamic events of particular regions over Earth-scale geologic time. Indeed, it appears likely that not only prominent ancient structural grains (e.g., the NW-trend of the Paleoproterozoic Transamazonian orogen, Amazonian Craton), but also widespread remnants of ancient mantle lithosphere comprising components of Proterozoic or older age, fundamentally affected the geodynamic evolution, including ore genesis, of South America until the present day. The critical review of the tectonic history and the presented case studies highlight the importance of further investigation. In some of the presented case studies, deposit supercluster formation as a result of polyphase structural inheritance appears very likely and the origin of respective inherited TLFs can be traced back to specific geodynamic events, tectonic boundaries and/or terrane sutures. In other cases, the proposed existence of cryptic TLF corridors remains speculative. Nevertheless, this paper documents an integrated approach towards the delineation of potential inherited structural corridors that are recommended for more detailed investigation to explore further causative relationships and processes of TLF inheritance.

With regards to the end-member models of ore deposit distribution, i.e., structural inheritance and self-organization, the following first-order knowledge gaps are put forth: 1) How do overlapping scales of self-organization (fractal geometry) interact and relate to applicable spatial framework solutions, 2) What is the interplay between temporally superimposed "spontaneous" self-organization events (likely at various scale), and 3) What are the boundaries and the effects of boundaries of/on self-organizing systems? The latter knowledge gap may be the most straight forward to address. For example, if the Eocene-Oligocene porphyry belt of Chile displays spatial periodicity (Figure 1B), where geologic and structural features are only observed internally, within the belt, it can be expected that internally the belt is characterized by a certain degree of homogeneity. Among all complexity, such homogeneity and its boundaries must be defined and parameterized to validate the operation of self-organization. This, in turn, leads to the fact that knowledge of tectonic histories and lithosphere-scale structural architecture and lithologic anatomy is key.

The documented or proposed inherited structures or structural corridors, irrespective of the origin of respective TLFs are cryptic in nature and mostly not readily observed in their surface expression. Nevertheless, various modes of TLF inheritance can be identified based on presented case studies and examples and will be discussed in the next Section.

6.1 Modes of trans-lithospheric fault inheritance

Two general modes of trans-lithospheric fault inheritance and propagation are discussed below, comprising vertical and lateral endmembers and sub-types. These modes are not mutually exclusive.

6.1.1 Vertical TLF inheritance and propagation

Three possible endmember modes of vertical structural inheritance and propagation are identified and conceptually summarized in Figure 13. The Figure schematically illustrates the wide lateral mid-to upper crustal exploration targeting search space resulting from vertical modes of TLF propagation. The endmember modes of vertical inheritance are summarized below, noting that these endmembers may work in conjunction and that changes in the stress field during TLF reactivation may significantly alter the upper crustal propagated fault zone in 3D space.

The first endmember mode (Figures 13–i) describes the upward propagation of a vertical TLF into younger overlying cover rocks, as has been conceptualized previously based on the Antamina corridor in central Peru (Figure 1C; McCuaig and Hronsky, 2014). Other examples presented in this paper include the Atacama and Domeyko fault zones in NW Chile, which represent steep/sub-vertical TLF systems, branching into the upper crust (Figure 10A; e.g., Contreras-Reyes et al., 2021). Indeed, particularly the somewhat discontinuous and/or anastomosing nature of the relatively broad Domeyko fault zone system demonstrates this mode of vertical TLF propagation. More complex examples include both the Pataz gold vein system in northern Peru (Figure 8A; Wiemer et al., 2021a) and the epithermal polymetallic Quevar deposit in Argentina (Figure 10A; Escuder Viruete et al., 2022). In both cases, not only a branching of strike-parallel faults occurred, but in-between the main fault branches, strike-slip induced lower-order structural systems evolved, which host most of the economic ore mineralization. In this case, exploration targeting must symmetrically focus on both sides of the TLF.

In the second endmember mode, an inclined and/or listric-shaped TLF is reactivated as a principal magma/fluid conduit (Figures 13–ii). An inclined geometry of TLFs may not be unusual, considering the shape of subduction zones and associated sutures and major thrust faults in accretion to collisional orogens. Magma ascent along such inclined TLF conduit would eventually depart as sufficiently buoyant differentiated magma evolves. The buoyant upward rise (path of least resistance) of magma and in consequence the localization of associated mineral deposits may be expected in quite some distance

from the actual TLF and its surface expression but can be expected to focus on the hanging-wall (Figures 13–ii). The locations of the Pataz-Parcoy intrusion related orogenic gold districts in northern Peru, for example, are clearly spatially restricted to the hanging-wall of the medium to steeply NE-inclined Famatinian suture (Wiemer et al., 2022; Figure 8A). In this endmember mode of vertical inheritance, exploration targeting strategies must acknowledge the asymmetric nature with preference of deposits situated in the hanging-wall of the TLF, but still in relative proximity.

Lastly, thin-skinned over-thrusting must be considered. Here, basement and TLF underly younger tectonic nappes characterized by distinct possibly entirely unrelated structural architecture Figures 13–iii). This case is demonstrated in the contact between the Western and Eastern Cordillera in the Pataz region, northern Peru (Figures 8A, B, 9A). The over-thrusted Western Cordillera sedimentary successions are intruded by Miocene subvolcanic and volcanic rocks associated with Au-Cu mineralization, which can be overall correlated with inferred/extrapolated and/or cryptic TLFs (Famatinian Paracas suture and Pataz Lineament). However, local fluid flow and mineralization are controlled by the structural-lithologic anatomy of the sedimentary nappes. In addition, however, the sedimentary-nappe internal structural architecture is significantly affected by superimposed deformation that is interpreted to mark the reactivation of the underlying TLF. This can be observed in the deflection of the strike of foliations and folds in the Cretaceous sedimentary rocks (Figure 8A). Therefore, in the case of over-thrusting of upper crustal tectonic slices, the exploration search space may drastically vary depending on the internal structural and permeability architecture of respective thrust nappes and/or its interplay with the underlying TLF during tectonic reactivation. Ultimately, the over-thrusting of tectonic nappes may also lead to the sealing of a basement TLF (see a and b in Figures 13–iii).

6.1.2 Lateral TLF inheritance and propagation

The lateral inheritance and propagation of TLFs may even be more difficult to detect within complex tectonic histories. Case studies concerned with more recent geodynamic events provide fruitful insights. For example, the opening of the North Atlantic as reconstructed by Schiffer et al. (2020) nicely demonstrates that the initial continental break-up occurred along former weak zones that can be correlated with the Caledonian and Variscan orogens, and even older, Precambrian structures propagated into, or led to the nucleation sites of newly formed transforms in the oceanic crust. The concept has been adopted by Wiemer et al. (2022) to explain the opening of the Paracas oceanic basin (i.e., along former Sunsás orogen-parallel weak zones) and associated detachment and later re-collision of the Paracas micro-terrane with emphasis on its northern demarcation along and accommodated by a proposed oceanic lithosphere-scale transfer fault (i.e., Pataz Lineament), which may have propagated and/or nucleated from the K'Mudku shear zone, and or a branch thereof, within the Amazonian Craton (Figures 4C–E). In support of Wiemer et al.'s (2022) reconstruction, NW-striking transform faults associated with Rodinia break-up and Iapetus opening that segment the Laurentian (i.e., Grenville) margin of eastern North America are observed (e.g., Allen et al., 2010). The Laurentian transform faults segment the Grenvillian orogen at similar relative angle (i.e., after back-rotation of global plate kinematic reorganizations). Future advanced paleogeographic reconstructions may be able to correlate the Pataz Lineament with its Laurentian transform fault counterpart.

The issue of lateral structure propagation and/or inheritance is furthermore exemplified in the case of the Triassic intracontinental rifting that affected most of the South American margin (e.g., Spikings et al., 2016; Figure 4F). Could it be that structures, such as the central Peruvian Antamina corridor, originated as syn-rift accommodation zones near-perpendicular to inferred rift axes, or do they represent even more ancient propagated and inherited Precambrian basement structures? Similarly, the initial formation of the major fault zones of the North Chile-Argentina corridor (NCAC) may be discussed in the light of the former Neoproterozoic opening of the Puncoviscana oceanic basin (Figures 4C, D, 10).

Approaching lateral TLF propagation and inheritance in a generalized fashion, the reader is referred to various scenarios as depicted schematically in Figures 14A–D. Lateral TLF inheritance and propagation is best documented in examples of intracontinental rifts and oceanic basin opening. Here, the rift zone may impinge on former lithospheric weak zones and/or pre-existing TLFs within the continent may seed the propagation of transform faults within the newly forming oceanic lithosphere (Figure 14A; e.g., Thomas, 2006; Phillips et al., 2019; van den Broek et al., 2020; Muñoz-Barrera et al., 2020; Schiffer et al., 2020; Stephenson et al., 2021; Zwaan et al., 2021; Wiemer et al., 2022). A future challenge in understanding lateral TLF inheritance includes improved mechanical-structural models of inter-terrane fault propagation during episodes of terrane accretion and collision. In a simple case of lateral TLF propagation during near-perpendicular terrane accretion, deposit localization can be expected to approximate linear damage zones that propagate through time and space (Figure 14B). However, either global kinematic reorganisation, or superimposed non-collisional subduction episodes may result in the reactivation of TLF systems and their lithospheric roots, whereby overprinting structural-hydrothermal systems may represent a combination of vertical and lateral fault propagation (Figure 14C). The latter scenario may be documented in the Carboniferous overprinting and reactivation of Famatinian structures in the Pataz region of northern Peru (Wiemer et al., 2021a; Wiemer et al., 2022). Finally, as depicted in Figure 14D, lateral modes of TLF reactivation may include a change from normal or steep to flat-slab subduction, whereby tectonic-magmatic activity switches from trench proximal towards reactivation of ancient orogens and TLFs within the continental interior. In view of the Wilson Cycle of plate tectonic operation, the generalized types of lateral inheritance, propagation, and reactivation (Figures 14A–D) provide clues to an underlying mechanism of recycling of gold reservoirs throughout Earth's history (e.g., Griffin et al., 2013).

6.2 Integrated geodynamics perspective on gold cluster formation and localization

The here presented case studies of identified and/or proposed inheritance of trans-lithospheric fault systems highlight the importance of early structural architectures, which may have initially formed and subsequently developed over 100s of million years prior to reactivation and gold formation (e.g., Yang and Santosh, 2020; Wiemer et al., 2022). However, of equal importance appears to

be the type of a respective TLF structure (i.e., terrane boundary or suture, transform fault, or rift) and/or its mode of reactivation (e.g., superimposed subduction, strike-slip reactivation, etc.). Numerous recent examples world-wide highlight the multistage subduction histories of regions that are particularly highly endowed in gold, whereby early subduction-induced metasomatism fertilized the lithospheric mantle or lower crust (e.g., North China craton, Xiong et al., 2021; Clarke et al., 2022). Multistage subduction histories support the notion that the critical fundamental control on gold metallogeny is the presence of a gold-enriched lithospheric upper mantle region as either a source reservoir, or a passage for deeper generated ascending magma (Hronsky et al., 2012; Griffin et al., 2013). Although the Au content of metasomatized sub-continental lithospheric mantle is only slightly higher compared to unmodified counterparts, the metasomatized domains are characterized by a heterogeneous mineralogical-chemical composite, including more readily fusible fractions promoting selective and efficient release of metals into respective hydrous parental magmas (e.g., Tassara et al., 2017; Wang et al., 2019). In other words, mantle regions surrounding the deeper roots of TLF structures that represent former subduction- or accretion-related terrane boundaries are likely to have undergone a pre-mineral stage of mineralogical-chemical redistribution and segregation of incompatible species and metal enriched, melt-accessible portions (e.g., gold-rich veins in metasomatized mantle xenoliths; Tassara et al., 2017; enriched cumulates in the lower crust; Clarke et al., 2022).

As part of the non-convective lithospheric upper mantle or lower crust, these fertilized domains may remain hidden for extensive periods of geologic time until the respective TLF structure is reactivated, and the readily fusible metal-enriched portions are scavenged by partial melts. The presented global geochemical data compilation identifies the most primitive end-member Au-parental rock suites (i.e., appinite/absarokite and primitive sanukitoids) associated with regions that were subject to multistage subduction histories prior to gold deposit formation. In the case of the South American examples, i.e., absarokitic-shoshonitic enclaves in the Cretaceous Antioquia batholith, central Colombia (Duque-Trujillo et al., 2019), recent primitive sanukitoid lavas from the Chacana volcanic field, Ecuador (Chiaradia et al., 2014), Carboniferous absarokitic gabbro intrusions and mafic dikes in the Pataz and Huachón areas of northern and central Peru (Wiemer et al., 2020; 2023), and Mesozoic enriched dike swarms in central Chile (Creixell et al., 2009), the presented tectonic reconstructions of respective areas are consistent with the here envisaged model of protracted geodynamic inheritance: all regions display evidence of TLF inheritance and have undergone multiple subduction or accretion episodes that are likely to have modified the lithospheric mantle or lower crust.

Nevertheless, structural, geochronological, geochemical, and isotopic data are lacking in various key regions along the western South American margin to refine tectonic histories and shed further light on the inheritance of TLF structures and accompanying fertile lithospheric domains in controlling the genesis and spatial and temporal distribution of gold-rich mineral systems.

Author contributions

DW came up with the idea and conceptualisation of this paper, based on discussions with SH, NH, GB, and JH. DW prepared all figures and the draft text and performed all data analyses and data compilation. All authors contributed to the article and approved the submitted version.

Funding

This article is based on a project conceived by DW and SH through the Center for Exploration Targeting, University of Western Australia, which was fully funded by the Compañia Minera Poderosa S.A. (Lima, Perú).

Acknowledgments

DW and SH express their deepest thanks to D. Sologuren Arias and F. Cueva (Compañia Minera Poderosa S.A.) for their continued support in this research.

Conflict of interest

NH was employed by Predict Ore Pty Ltd. GB was employed by Minerals Targeting International Pty Ltd. JH was employed by Western Mining Services Pty Ltd. CV was employed by Compañia Minera Poderosa S. A.

The remaining authors declare that the research was conducted in the absence of any commercial or financial relationships that could be construed as a potential conflict of interest.

Publisher's note

References

Allen, J. S., Thomas, W. A., and Lavoie, D. (2010). "The Laurentian margin of northeastern North America," in *From Rodinia to Pangea: The lithotectonic record of the appalachian region*. Editors R. P. Tollo, M. J. Bartholomew, J. P. Hibbard, and P. M. Karabinos (Geological Society of America Memoir 206), 71–90.

Angerer, T., Kemp, A. I. S., Hagemann, S. G., Witt, W. K., Santos, J. O., Schindler, C., et al. (2018). Source component mixing controls the variability in Cu and Au endowment along strike of the Eastern Andean Cordillera in Peru. *Contributions Mineralogy Petrology* 173, 1–34. doi:10.1007/s00410-018-1462-5

Astini, R. A., and Davila, F. D. (2004). Ordovician back arc foreland and Ocloyic thrust belt development on the western Gondwana margin as a response to Precordillera terrane accretion. *Tectonics* 23 (TC4008), 1–19. doi:10.1029/2003tc001620

Bak, P., (1996). *How nature works: The science of self-organized criticality*. Copernicus, Springer-Verlag, Ney York, 212.

Bettencourt, J. S., Juliani, C., Xavier, R. P., Monteiro, L. V. S., Neto, A. C. B., Klein, E. L., et al. (2016). Metallogenetic systems associated with granitoid magmatism in the amazonian craton: an overview of the present level of understanding and exploration significance. *J. S. Am. Earth Sci.* 68, 22–49. doi:10.1016/j.jsames.2015.11.014

Bettencourt, J. S., Leite, W. B., Ruiz, A. S., Matos, R., Payolla, B. L., and Tosdal, R. M. (2010). The rondonian-san Ignacio province in the SW amazonian craton: an overview. *J. S. Am. Earth Sci.* 29, 28–46. doi:10.1016/j.jsames.2009.08.006

Bierlein, F. P., Murphy, F. C., Weinberg, R. F., and Lees, T. (2006). Distribution of orogenic gold deposits in relation to fault zones and gravity gradients: targeting tools applied to the eastern Goldfields, Yilgarn craton, western Australia. *Miner. Deposita* 41, 107–126. doi:10.1007/s00126-005-0044-4

Bogossian, J., Kemp, A. I. S., and Hagemann, S. G. (2021). Linking gold systems to the crust-mantle evolution of Archean crust in central Brazil. *Minerals* 11, 944. doi:10.3390/min11090944

Bonilla, A., Cramer, T., Grave, J. D., Alessio, B., Glorie, S., and Kroonenberg, S. (2021). The NW amazonian craton in guainía and vaupés departments, Colombia: transition between orogenic to anorogenic environments during the paleo-mesoproterozoic. *Precambrian Res.* 360, 106223. doi:10.1016/j.precamres.2021.106223

Bonnefoi, C. C., Provost, A., and Albarède, F. (1995). The 'Daly gap' as a magmatic catastrophe. *Nature* 378, 270–272. doi:10.1038/378270a0

Calderon, Y., Baby, P., Hurtado, C., and Brusset, S. (2017). Thrust tectonics in the andean retro-foreland basin of northern Peru: permian inheritances and petroleum implications. *Mar. Petroleum Geol.* 82, 238–250. doi:10.1016/j.marpetgeo.2017.02.009

Cardona, A., Cordani, U. G., Ruiz, J., Valencia, V. A., Armstrong, R., Chew, D., et al. (2009). U-Pb zircon geochronology and Nd isotopic signatures of the pre-mesozoic metamorphic basement of the eastern Peruvian Andes: growth and provenance of a late neoproterozoic to carboniferous accretionary orogen on the northwest margin of Gondwana. *J. Geol.* 117, 285–305. doi:10.1086/597472

Carlier, G., Lorand, J. P., Liégeois, J. P., Fornari, M., Soler, P., Carlotto, V., et al. (2005). Potassic-ultrapotassic mafic rocks delineate two lithospheric mantle blocks beneath the southern Peruvian Altiplano. *Geology* 33, 601–604. doi:10.1130/g21643.1

Carlotto, V., Quispe, J., Acosta, H., Rodríguez, R., Romero, D., Cerpa, L., et al. (2009). Dominios geotectónicos y metalogénesis del Perú. *Bol. Soc. Geol. del Peru* 103, 1–89.

Carrizo, G. Y., and Herrera, O. R. (2019). Crustal dense blocks in the fore-arc and arc region of Chilean ranges and their role in the magma ascent and composition: breaking paradigms in the andean metallogeny. *J. Aouth Am. Earth Sci.* 93, 51–66. doi:10.1016/j.jsames.2019.04.006

Casquet, C., Dahlquist, J. A., Verecchia, S. O., Baldo, E. G., Galindo, C., Rapela, C. W., et al. (2018). Review of the cambrian pampean orogeny of Argentina: a displaced orogen formerly attached to the saldania belt of South Africa? *Earth-Science Rev.* 177, 209–225. doi:10.1016/j.earscirev.2017.11.013

Casquet, C., Hervé, F., Pankhurst, R. J., Baldo, E., Calderón, M., Fanning, C. M., et al. (2014). The Mejillonia suspect terrane (northern Chile): late triassic fast burial and metamorphism of sediments in a magmatic arc environment extending into the early jurassic. *Gondwana Res.* 25, 1272–1286. doi:10.1016/j.gr.2013.05.016

Casquet, C., Rapela, C. W., Pankhurst, R. J., Baldo, E. G., Galindo, C., Fanning, C. M., et al. (2012). A history of proterozoic terranes in southern southSouth America: from Rodinia to Gondwana. *Geosci. Front.* 3, 137–145. doi:10.1016/j.gsf.2011.11.004

Caxito, F. d. A., Santos, L. C. M. D. L., Ganade, C. E., Bendaoud, A., Fettous, E. H., and Bouyo, M. H. (2020). Toward an integrated model of geological evolution for NE Brazil–NW africa: the Borborema province and its connections to the trans-saharan (benino-Nigerian and Tuareg shields) and central african orogens. *Braz. J. Geol.* 50, 1–38. doi:10.1590/2317-4889202020190122

Cediel, F., Shaw, R. P., and Cáceres, C. (2003). "Tectonic assembly of the northern andean block," in *The circum-gulf of Mexico and the caribbean: Hydrocarbon habitats, basin formation, and plate tectonics: AAPG memoir 79*. Editors C. Bartolini, R. T. Buffler, and J. Blickwede, 815–848.

Cerpa, L. M., Bissig, T., Kyser, K., McEwan, C., Macassi, A., and Rios, H. W. (2013). Lithologic controls on mineralization at the Lagunas Norte high-sulfidation epithermal gold deposit, northern Peru. *Miner. Deposita* 48, 653–673. doi:10.1007/s00126-013-0455-6

Chadam, J., and Ortoleva, P. (1990). Morphological instabilities in physico chemical systems. *Earth-Science Rev.* 29, 175–181. doi:10.1016/0012-8252(0)90035-t

Chambefort, I., Dilles, J. H., and Longo, A. A. (2013). Amphibole geochemistry of the Yanacocha volcanics, Peru: evidence for diverse sources of magmatic volatiles related to gold ores. *J. Petrology* 54, 1017–1046. doi:10.1093/petrology/egt004

Chernicoff, C. J., Richards, J. P., and Zappettini, E. O. (2002). Crustal lineament control on magmatism and mineralization in northwestern Argentina: geological, geophysical, and remote sensing evidence. *Ore Geol. Rev.* 21, 127–155. doi:10.1016/s0169-1368(02)00087-2

Chew, D. M., Pedemonte, G., and Corbett, E. (2016). Proto-andean evolution of the eastern Cordillera of Peru. *Gondwana Res.* 35, 59–78. doi:10.1016/j.gr.2016.03.016

Chew, D. M., Petrus, J. A., and Kamber, B. S. (2014). U–Pb LA-ICPMS dating using accessory mineral standards with variable common Pb. *Chem. Geol.* 363, 185–199. doi:10.1016/j.chemgeo.2013.11.006

Chew, D. M., Schaltegger, U., Košler, J., Whitehouse, M. J., Gutjahr, M., Spikings, R. A., et al. (2007). U-Pb geochronologic evidence for the evolution of the Gondwanan margin of the north-central Andes. *GSA Bull.* 119, 697–711. doi:10.1130/b26080.1

Chiaradia, M. (2020). Gold endowments of porphyry deposits controlled by precipitation efficiency. *Nat. Commun.* 11, 1–10. doi:10.1038/s41467-019-14113-1

Chiaradia, M., Müntener, O., and Beate, B. (2014). Quaternary sanukitoid-like andesites generated by intracrustal processes (Chacana caldera complex, Ecuador): implications for archean sanukitoids. *J. Petrology* 55, 769–802. doi:10.1093/petrology/egu006

Cingolani, C. A., and Ramos, V. A. (2017). "Pre-carboniferous tectonic evolution of the san Rafael block, mendoza province," in *Pre-carboniferous evolution of the san Rafael block, Argentina*. Editor C. A. Cingolani (Springer Earth System Sciences), 239–255.

Clark, A. H., Farrar, E., Kontak, D. J., Langridge, R. J., Arenas F., M. J., France, L. J., et al. (1990). Geologic and geochronologic constraints on the metallogenic evolution of the Andes of southeastern Peru. *Econ. Geol.* 85, 1520–1583. doi:10.2113/gsecongeo.85.7.1520

Clarke, R., Smith, D., and Naden, J. (2022). Source controls on mineralisation: regional geology and magmatic evolution of Fiji. *Lithos* 432-433, 1–25. doi:10.1016/j.lithos.2022.106897

Contreras-Reyes, E., Díaz, D., Bello-González, J. P., Slezak, K., Comte, D., Maksymowicz, A., et al. (2021). Subduction zone fluids and arc magmas conducted by lithospheric deformed regions beneath the central Andes. *Sci. Rep.* 11, 23078. doi:10.1038/s41598-021-02430-9

Cordani, U. G., Fraga, L. M., Reis, N., Tassinari, C. C. G., and Brito-Neves, B. B. (2010). On the origin and tectonic significance of the intra-plate events of grenvillian-type age in South America: a discussion. *J. S. Am. Earth Sci.* 29, 143–159. doi:10.1016/j.jsames.2009.07.002

Cordani, U. G., Pimentel, M. M., Araújo, C. E. G. d., Basei, M. A. S., Fuck, R. A., and Girardi, V. A. V. (2013). Was there an ediacaran Clymene Ocean in central South America? *Am. J. Sci.* 313, 517–539. doi:10.2475/06.2013.01

Cordani, U. G., Sato, K., Sprossner, W., and Fernandes, F. S. (2016). U-Pb zircon ages of rocks from the Amazonas Territory of Colombia and their bearing on the tectonic history of the NW sector of the Amazonian Craton. *Braz. J. Geol.* 46, 5–35. doi:10.1590/2317-4889201620150012

Cordani, U. G., and Teixeira, W., (2007). Proterozoic accretionary belts in the amazonian craton. 4-D framework of continental crust200, p. 297–320.

Creixell, C., Parada, M. A., Morata, D., Roperch, P., and Arriagada, C. (2009). The genetic relationship between mafic dike swarms and plutonic reservoirs in the mesozoic of central Chile (30°-33°45'S): insights from AMS and geochemistry. *Int. J. Earth Sci.* 98, 177–201. doi:10.1007/s00531-007-0240-9

Da Silva, L. R., Oliveira, D. C., and Santos, M. N. S. (2018). Diversity, origin and tectonic significance of the Mesoarchean granitoids of Ourilândia do Norte, Carajás province (Brazil). *J. S. Am. Earth Sci.* 82, 33–61. doi:10.1016/j.jsames.2017.12.004

Daly, R. A. (1925). The geology of ascension island. *Proc. Am. Acad. Arts Sci.* 60, 3–80. doi:10.2307/25130043

De Castro, D. L., Fuck, R. A., Phillips, J. D., Vidotti, R. M., Bezerra, F. H. R., and Dantas, E. L. (2014). Crustal structure beneath the Paleozoic Parnaíba Basin revealed by airborne gravity and magnetic data, Brazil. *Braz. Tectonophys.* 614, 128–145. doi:10.1016/j.tecto.2013.12.009

Défago, M., Robert, M., and Jesus, P., (2006). "The Huachón gold prospect, eastern andean Cordillera of Peru: the southern extension of a 400 km long carboniferous orogenic gold province?," in 4th Swiss Geosci. Meet. Bern. 1–3.

Doutre, R., Micklethwaite, S., Kovesi, P., McCuaig, C. T., Ford, A., and Hayward, N., (2015). "Multi-scale spacing and endowment of orogenic gold deposits," in Proceedings 13th SGA Biennial Meeting 1, 81–84.

Duque-Trujillo, J., Bustamante, C., Solari, L., Gómez-Mafla, A., Toro-Villegas, G., and Hoyos, S. (2019). Reviewing the Antioquia batholith and satellite bodies: a record of late cretaceous to Eocene syn-to post-collisional arc magmatism in the central Cordillera of Colombia. *Andean Geol.* 46, 82–101. doi:10.5027/andgeoV46n1-3120

Eisenlohr, B. N., Groves, D., and Partington, G. A. (1989). Crustal-scale shear zones and their significance to Archaean gold mineralization in Western Australia. *Miner. Deposita* 24, 1–8. doi:10.1007/bf00206714

Escayola, M. P., van Staal, C. R., and Davis, W. J. (2011). The age and tectonic setting of the Puncoviscana Formation in northwestern Argentina: an accretionary complex related to early cambrian closure of the Puncoviscana Ocean and accretion of the arequipa-antofalla block. *J. S. Am. Earth Sci.* 32, 438–459. doi:10.1016/j.jsames.2011.04.013

Escuder-Viruete, J., Molina, E. A., Chinchilla, D., Gabites, J., Seggiaro, R., Marquetti, C. A., et al. (2022). Structural and temporal relationships between volcanic activity, hydrothermal alteration, epithermal Ag-Pb-Zn mineralization and regional stress regime in the Quevar Volcanic Complex (Puna plateau, Salta Province, NW Argentina). *J. Struct. Geol.* 158, 104582. doi:10.1016/j.jsg.2022.104582

Espinoza, M., Oliveros, V., Vásquez, P., Giambiagi, L., Morgan, L., González, R., et al. (2021). Gondwanan inheritance on the building of the western and central Andes (Domeyko Range, Chile): structural and thermochronological approach (U-Pb and ^{40}Ar/^{39}Ar). *Tectonics* 40, e2020TC006475. doi:10.1029/2020TC006475

Evans, L., Miranda, H., and Scholey, B. (2016). *Technical report on the Lagunas Norte mine, La libertad region, Peru*. Barrick Gold Corporation, 1–204. report NI 43-101.

Feeley, T. C. (2003). Origin and tectonic implications of across-strike geochemical variations in the Eocene Absaroka Volcanic province, United States. *J. Geol.* 111, 329–346. doi:10.1086/373972

Feldstein, S. N., and Lange, R. A. (1999). Pliocene potassic magmas from the kings River region, Sierra Nevada, California: evidence for melting of a subduction-modified mantle. *J. Petrology* 40, 1301–1320. doi:10.1093/petroj/40.8.1301

Fowler, M. B., and Henney, P. J. (1996). Mixed caledonian appinite magmas: implications for lamprophyre fractionation and high Ba-Sr granite genesis. *Contributions Mineralogy Petrology* 126, 199–215. doi:10.1007/s004100050244

Goldfarb, R. J., Hart, C. J. R., and Marsh, E. E. (2008). "Orogenic gold and evolution of the Cordilleran orogen," in *Ores and orogenesis: Circum-Pacific tectonics, geologic evolution, and ore deposits*. Editors J. E. Spencer and S. R. Titley (Arizona Geological Society Digest), 22, 311–323.

Goldfarb, R. J., Phillips, G. N., and Nokleberg, W. J. (1998). Tectonic setting of synorogenic gold deposits of the Pacific Rim. *Ore Geol. Rev.* 13, 185–218. doi:10.1016/s0169-1368(97)00018-8

Goldfarb, R. J., and Pitcairn, I. (2022). Orogenic gold: is a genetic association with magmatism realistic? *Miner. Deposita* 58, 5–35. doi:10.1007/s00126-022-01146-8

Gómez, J., Schobbenhaus, C., Montes, N. E., and compilers, (2019). Geological map of SouthSouth America 2019. Scale 1:5000000. Commission for the geological map of the world (CGMW). *Colombian Geol. Surv. Geol. Surv. Braz.* doi:10.32685/10.143.2019.929

González, P. D., Naipauer, M., Sato, A. M., Varela, R., Basei, M. A. S., Cábana, M. C., et al. (2021). Early Paleozoic structural and metamorphic evolution of the Transpatagonian Orogen related to Gondwana assembly. *Int. J. Earth Sci.* 110, 81–111. doi:10.1007/s00531-020-01939-0

Gow, P. A., and Walshe, J. L. (2005). The role of preexisting geologic architecture in the formation of giant porphyry-related Cu ± Au deposits: examples from new Guinea and Chile. *Econ. Geol.* 100, 819–833. doi:10.2113/gsecongeo.100.5.819

Graham, S. D., Holwell, D. A., McDonald, I., Jenkin, G. R. T., Hill, N. J., Boyce, A. J., et al. (2017). Magmatic Cu-Ni-pge-Au sulfide mineralisation in alkaline igneous systems: an example from the sron garbh intrusion, tyndrum, scotland. *Ore Geol. Rev.* 80, 961–984. doi:10.1016/j.oregeorev.2016.08.031

Granot, R., and Dyment, J. (2015). The cretaceous opening of the South atlantic ocean. *Earth Planet. Sci. Lett.* 414, 156–163. doi:10.1016/j.epsl.2015.01.015

Griffin, W. L., Begg, G. C., and O'Reilly, S. Y. (2013). Continental-root control on the genesis of magmatic ore deposits. *Nat. Geosci.* 6, 905–910. doi:10.1038/ngeo1954

Groves, D. I., Santosh, M., Goldfarb, R. J., and Zhang, L. (2018). Structural geometry of orogenic gold deposits: implications for exploration of world-class and giant deposits. *Geosci. Front.* 9, 1163–1177. doi:10.1016/j.gsf.2018.01.006

Groves, D. I., and Santosh, M. (2016). The giant Jiadong gold province: the key to a unified model for orogenic gold deposits? *Geosci. Front.* 7, 409–417. doi:10.1016/j.gsf.2015.08.002

Haeberlin, Y., Moritz, R., Fontboté, L., and Cosca, M. (2004). Carboniferous orogenic gold deposits at Pataz, eastern andean Cordillera, Peru: geological and structural framework, paragenesis, alteration, and ^{40}Ar/^{39}Ar geochronology. *Econ. Geol.* 99, 73–112. doi:10.2113/99.1.73

Haeberlin, Y., Moritz, R., and Fontboté, L. (2002). Paleozoic orogenic gold deposits in the eastern Central Andes and its foreland, South America. *Ore Geol. Rev.* 22, 41–59. doi:10.1016/s0169-1368(02)00108-7

Hagemann, S. G., and Brown, P. E. (2000). Gold in 2000. *Rev. Econ. Geol.* 13, 1–559. doi:10.5382/Rev.13

Hagemann, S. G., Lisitsin, V. A., and Huston, D. L. (2016). Mineral system analysis: quo vadis. *Ore Geol. Rev.* 76, 504–522. doi:10.1016/j.oregeorev.2015.12.012

Hayward, N., Doutre, R., and Micklethwaite, S. (2018). Spatial periodicity in self-organized ore systems. *Seg. Spec. Publ.* 21, 1–24. doi:10.5382/SP.21.01

Hronsky, J. M. A., Groves, D. I., Loucks, R. R., and Begg, G. (2012). A unified model for gold mineralisation in accretionary orogens and implications for regional-scale exploration targeting methods. *Miner. Deposita* 47, 339–358. doi:10.1007/s00126-012-0402-y

Hronsky, J. M. A. (2011). Self-organized critical systems and ore formation: the key to spatial targeting? *Soc. Econ. Geol. Newsl.* 84, 14–16.

Huchon, P., and Bourgois, J. (1990). Subduction-induced fragmentation of the Nazca plate off Peru: mendana fracture zone and trujillo trough revisited. *J. Geophys. Res.* 95, 8419–8436. doi:10.1029/jb095ib06p08419

Iaffa, D. N., Sàbat, F., Bello, D., Ferrer, O., Mon, R., and Gutierrez, A. A. (2011). Tectonic inversion in a segmented foreland basin from extensional to piggy back settings: the tucumán basin in NW Argentina. *J. S. Am. Earth Sci.* 31, 457–474. doi:10.1016/j.jsames.2011.02.009

Ibanez-Mejia, M., Ruiz, J., Valencia, V. A., Cardona, A., Gehrels, G. E., and Mora, A. R. (2011). The Putumayo orogen of Amazonia and its implications for Rodinia reconstructions: new U-Pb geochronological insights into the proterozoic tectonic evolution of northwestern South America. *Precambrian Res.* 191, 58–77. doi:10.1016/j.precamres.2011.09.005

Iddings, J. P. (1895). Absarokite-shoshonite-banakite series. *J. Geol.* 3, 935–959. doi:10.1086/607398

Jacques, J. M. (2003). A tectonostratigraphic synthesis of the sub-andean basins: implications for the geotectonic segmentation of the andean belt, *J. Geol. Soc.* 160. 687–701. doi:10.1144/0016-764902-088

Juliani, C., Assis, R. R., Monteiro, L. V. S., Fernandes, C. M. D., Martins, J. E. Z. S., and Costa, J. R. C. (2021). Gold in paleoproterozoic (2.1 to 1.77 Ga) continental magmatic arcs at the Tapajós and Juruena mineral provinces (amazonian craton, Brazil): a new frontier for the exploration of epithermal–porphyry and Related deposits. *Minerals*11, 714. doi:10.3390/min11070714

Kelley, K. D., Romberger, S. B., Beaty, D. W., Pontius, J. A., Snee, L. W., Stein, H. J., et al. (1998). Geochemical and geochronological constraints on the genesis of Au-Te deposits at Cripple Creek, Colorado. *Econ. Geol.* 93, 981–1012. doi:10.2113/gsecongeo.93.7.981

Kerr, A. C., Aspden, J. A., Tarney, J., and Pilatasig, L. F. (2002). The nature and provenance of accreted oceanic terranes in western Ecuador: geochemical and tectonic constraints, *J. Geol. Soc.* 159. 577–594. doi:10.1144/0016-764901-151

Kley, J., Rossello, E. A., Monaldi, C. R., and Habighorst, B. (2005). Seismic and field evidence for selective inversion of Cretaceous normal faults, Salta rift, northwest Argentina. *Tectonophysics* 399, 155–172. doi:10.1016/j.tecto.2004.12.020

Klipfel, P. (2007). *Summary report on the Incahuasi gold project, northwest Argentina*. Cardero Resources Corporation report.

Kroonenberg, S. B., de Roever, E. W. F., Fraga, L. M., Reis, N. J., Faraco, T., Lafon, J.-M., et al. (2016). Paleoproterozoic evolution of the Guiana Shield in Suriname: a revised model. *Neth. J. Geosciences* 95, 491–522. doi:10.1017/njg.2016.10

Kroonenberg, S. B. (2019). "The proterozoic basement of the western Guiana Shield and the northern Andes," in *Geology and tectonics of northwestern South America. Frontiers in Earth sciences*. Editors F. Cediel and R. P. Shaw, 115–192.

Larionova, Y. O., Samsonov, A. V., and Shatagin, K. N. (2007). Sources of archean sanukitoids (high-Mg subalkaline granitoids) in the Karelian craton: sm-Nd and Rb-Sr isotopic-geochemical evidence. *Petrology* 15, 530–550. doi:10.1134/s0869591107060021

Leal-Mejia, H., Shaw, R. P., and Draper, J. C. M. (2019). "Spatial-temporal migration of granitoid magmatism and the Phanerozoic tectono-magmatic evolution of the Colombian Andes," in *Geology and tectonics of northwestern South America. Frontiers in Earth sciences*. Editors F. Cediel and R. P. Shaw, 253–410.

Leslie, R. A. J., Danyushevsky, L. V., Crawford, A. J., and Verbeeten, A. C. (2009). Primitive shoshonites from Fiji: geochemistry and source components. *Geochem. Geophys. Geosystems* 10, Q07001. doi:10.1029/2008GC002326

Liotard, J. M., Dautria, J. M., Bosch, D., Condomines, M., Mehdizadeh, H., and Ritz, J.-F. (2008). Origin of the absarokite–banakite association of the Damavand volcano (Iran): trace elements and Sr, Nd, Pb isotope constraints. *Int. J. Earth Sci.* 97, 89–102. doi:10.1007/s00531-006-0159-6

Lobach-Zhuchenko, S. B., Rollinson, H., Chekulaev, V. P., Savatenkov, V. M., Kovalenko, A. V., Martin, H., et al. (2008). Petrology of a late archaean, highly potassic, sanukitoid pluton from the baltic Shield: insights into late archaean mantle metasomatism. *J. Petrology* 49, 393–420. doi:10.1093/petrology/egm084

Loewy, S. L., Connelly, J. N., and Dalziel, I. W. D. (2004). An orphaned basement block: the arequipa-antofalla basement of the central andean margin of SouthSouth America. *GSA Bull.* 116, 171–187. doi:10.1130/b25226.1

López, C. A., Álvarez, J. J. R., Scharff, M. W., Jiménez, F. A. C., Botelho, N. F., Mejía, M. I., et al. (2020). The Guaviare complex: new evidence of mesoproterozoic (ca. 1.3 Ga) crust in the Colombian amazonian craton. *Bol. Geológico* 47, 5–34. doi:10.32685/0120-1425/boletingeo.47.2020.502

Loucks, R. R., and Ballard, J. R. (2002). "Predictive guides to copper and gold mineralization at circum-pacific convergent plate margins," in *Report 2A: Distinguishing characteristics, petrogenesis and tectonic habitat of copper ore-forming arc magmas*, 1–105.

Loucks, R. R. (2021). Deep entrapment of buoyant magmas by orogenic tectonic stress: its role in producing continental crust, adakites, and porphyry copper deposits. *Earth-Science Rev.* 220, 103744. doi:10.1016/j.earscirev.2021.103744

Loucks, R. R. (2014). Distinctive composition of copper-ore-forming arcmagmas. *Aust. J. Earth Sci.* 61, 5–16. doi:10.1080/08120099.2013.865676

Love, D. A., Clark, A. H., and Glover, J. K. (2004). The lithologic, stratigraphic, and structural setting of the giant Antamina copper-zinc skarn deposit, ancash, Peru. *Econ. Geol.* 99, 887–916. doi:10.2113/gsecongeo.99.5.887

Marcaillou, B., Collot, J.-Y., Ribodetti, A., d'Acremont, E., Mahamat, A.-A., and Alvarado, A. (2016). Seamount subduction at the North-Ecuadorian convergent

margin: effects on structures, inter-seismic coupling and seismogenesis. *Earth Planet. Sci. Lett.* 433, 146–158. doi:10.1016/j.epsl.2015.10.043

McCuaig, T. C., Beresford, S., and Hronsky, J. M. A. (2010). Translating the mineral systems approach into an effective exploration targeting system. *Ore Geol. Rev.* 38, 128–138. doi:10.1016/j.oregeorev.2010.05.008

McCuaig, T. C., and Hronsky, J. M. A. (2014). The mineral system concept: the key to exploration targeting. *Econ. Geol. Spec. Publ.* 18, 153–175. doi:10.1080/03717453.2017.1306274

McDonough, W. F., and Sun, S.-S. (1995). The composition of the Earth. *Chem. Geol.* 120, 223–253. doi:10.1016/0009-2541(94)00140-4

Melo, R. P. d., Oliveira, M. A. F. d., Goldfarb, R. J., Johnson, C. A., Marsh, E. E., Xavier, R. P., et al. (2022). Early neoproterozoic gold deposits of the Alto Guaporé province, southwestern Amazon craton, western Brazil. *Econ. Geol.* 117, 127–163. doi:10.5382/econgeo.4852

Micklethwaite, S. (2007). The significance of linear trends and clusters of fault-related mesothermal lode gold mineralization. *Econ. Geol.* 102, 1157–1164. doi:10.2113/gsecongeo.102.6.1157

Mišković, A., and Schaltegger, U. (2009). Crustal growth along a non-collisional cratonic margin: a Lu-Hf isotopic survey of the eastern cordilleran granitoids of Peru. *Earth Planet. Sci. Lett.* 279, 303–315. doi:10.1016/j.epsl.2009.01.002

Mišković, A., Spikings, R. A., Chew, D. M., Košler, J., Ulianov, A., and Schaltegger, U. (2009). Tectonomagmatic evolution of western Amazonia: geochemical characterization and zircon U-Pb geochronologic constraints from the Peruvian eastern cordilleran granitoids. *GSA Bull.* 121, 1298–1324. doi:10.1130/b26488.1

Motta, J. G., Souza Filho, C. R., Carranza, E. J. M., and Braitenberg, C. (2019). Archean crust and metallogenic zones in the Amazonian Craton sensed by satellite gravity data. *Sci. Rep.* 9 (2565), 2565–2610. doi:10.1038/s41598-019-39171-9

Mourier, T., Laj, C., Mégard, F., Roperch, P., Mitouard, P., and Medrano, A. F. (1988). An accreted continental terrane in northwestern Peru. *Earth Planet. Sci. Lett.* 88, 182–192. doi:10.1016/0012-821x(88)90056-8

Müller, D., and Groves, D. I. (2019). "Potassic igneous rocks and associated gold-copper mineralization," in *Mineral resource reviews*. Editor J. Slack (USA: Springer), 1–430.

Muñoz-Barrera, J. M., Rotevatn, A., Gawthorpe, R. L., Henstra, G. A., and Kristensen, T. B. (2020). The role of structural inheritance in the development of high-displacement crustal faults in the necking domain of rifted margins: the klakk fault complex, frøya high, offshore mid-Norway. *J. Struct. Geol.* 140, 104163. doi:10.1016/j.jsg.2020.104163

Murphy, J. B. (2020). Appinite suites and their genetic relationship with coeval voluminous granitoid batholiths. *Int. Geol. Rev.* 62, 683–713. doi:10.1080/00206814.2019.1630859

Murphy, J. B., Nance, R. D., Gabler, L. B., Martell, A., and Archibald, D. A. (2019). Age, geochemistry and origin of the Ardara appinite plutons, northwest Donegal, Ireland. *Geosci. Can.* 46, 31–48. doi:10.12789/geocanj.2019.46.144

Mustard, R., Ulrich, T., Kamenetsky, V. S., and Mernagh, T. (2006). Gold and metal enrichment in natural granitic melts during fractional crystallization. *Geology* 34, 85–88. doi:10.1130/g22141.1

Naranjo, A., Horner, J., Jahoda, R., Diamond, L. W., Castro, A., Uribe, A., et al. (2018). La Colosa Au porphyry deposit, Colombia: mineralization styles, structural controls, and age constraints. *Econ. Geol.* 113, 553–578. doi:10.5382/econgeo.2018.4562

Nedel, I. M., Fuck, R. A., Ruiz, A. S., Matos-Salinas, G. R., and Ferreira, A. d. C. D. (2021). Timing of proterozoic magmatism in the sunsas belt, Bolivian precambrian Shield, SW amazonian craton. *Geosci. Front.* 12, 101247–101317. doi:10.1016/j.gsf.2021.101247

Neumayr, P., Ridley, J. R., McNaughton, N. J., Kinny, P. D., Barley, M. E., and Groves, D. I. (1998). Timing of gold mineralization in the Mt York district, Pilgangoora greenstone belt, and implications for the tectonic and metamorphic evolution of an area linking the western and eastern Pilbara Craton. *Precambrian Res.* 88, 249–265. doi:10.1016/s0301-9268(97)00071-5

Nicolis, G., and Prigogine, I. (1977). *Self-organization in non-equilibrium systems: From dissipative structures to order through fluctuations*. New York: Wiley, 491.

Noble, D. C., Silberman, M. L., Megard, F., and Bowman, H. R. (1978). Comendite (peralkaline rhyolite) and basalt in the Mitu group, Peru: evidence for permian-triassic lithospheric extension in the central Andes. *J. Res. U.S. Geol. Surv.* 6, 453–457.

Ownby, S. E., Lange, R. A., and Hall, C. M. (2008). The eruptive history of the Mascota volcanic field, western Mexico: age and volume constraints on the origin of andesite among a diverse suite of lamprophyric and calc-alkaline lavas. *J. Volcanol. Geotherm. Res.* 177, 1077–1091. doi:10.1016/j.jvolgeores.2008.08.002

Paixão, M. A. P., Nilson, A. A., and Dantas, E. L. (2008). The Neoproterozoic Quatipuru ophiolite and the Araguaia fold belt, central-northern Brazil, compared with correlatives in NW Africa. *Geol. Soc. Lond. Spec. Publ.* 294, 297–318. doi:10.1144/SP294.16

Perez, N. D., Horton, B. K., and Carlotto, (2016). Structural inheritance and selective reactivation in the central Andes: cenozoic deformation guided by pre-andean structures in southern Peru. *Tectonophysics* 671, 264–280. doi:10.1016/j.tecto.2015.12.031

Phillips, T. B., Fazlikhani, H., Gawthorpe, R. L., Fossen, H., Jackson, C. A. L., Bell, R. E., et al. (2019). The influence of structural inheritance and multiphase extension on rift development, the northern North Sea. *Tectonics* 38, 4099–4126. doi:10.1029/2019tc005756

Piquer, J., Rivera, O., Yáñez, G., and Oyarzún, N. (2021b). The Piuquencillo fault system: a long-lived, andean-transverse fault system and its relationship with magmatic and hydrothermal activity. *Solid earth.* 12, 253–273. doi:10.5194/se-12-253-2021

Piquer, J., Sanchez-Alfaro, P., and Pérez-Flores, P. (2021a). A new model for the optimal structural context for giant porphyry copper deposit formation. *Geology* 49, 597–601. doi:10.1130/g48287.1

Quadros, M. L. d. E. S., Giustina, M. E. S. D., Rodrigues, J. B., and Souza, V. d. S. (2021). Geology and LA-ICP-MS U–Pb geochronology of the Nova brasilândia belt, SW amazonian craton: new ages, re-evaluation of existing geochronological data, and implications for the evolution of the Sunsás orogen. *J. S. Am. Earth Sci.* 109, 103220. doi:10.1016/j.jsames.2021.103220

Ramos, V. A., Escayola, M., Leal, P., Pimentel, M. M., and Santos, J. O. S. (2015). The late stages of the pampean orogeny, Córdoba (Argentina): evidence of postcollisional early cambrian slab break-off magmatism. *J. S. Am. Earth Sci.* 64, 351–364. doi:10.1016/j.jsames.2015.08.002

Ramos, V. A. (2008). The basement of the central Andes: the Arequipa and related terranes. *Annu. Rev. Earth Planet. Sci.* 36, 289–324. doi:10.1146/annurev.earth.36.031207.124304

Ramos, V. A. (2018). "The famatinian orogen along the protomargin of western Gondwana: evidence for a nearly continuous ordovician magmatic arc between Venezuela and Argentina," in *The evolution of the Chilean-argentinean Andes*. Editors (Springer Earth System Sciences), 154–183.

Rapela, C. W., Fanning, C. M., Casquet, C., Pankhurst, R. J., Spalletti, L., Poiré, D., et al. (2011). The Rio de la Plata craton and the adjoining pan-african/brasiliano terranes: their origins and incorporation into south-west Gondwana. *Gondwana Res.* 20, 673–690. doi:10.1016/j.gr.2011.05.001

Rapela, C. W., Pankhurst, R. J., Casquet, C., Baldo, E., Galindo, C., Fanning, C. M., et al. (2010). The western Sierras Pampeanas: protracted grenville-age history (1330-1030 Ma) of intra-oceanic arcs, subduction-accretion at continental-edge and AMCG intraplate magmatism. *J. S. Am. Earth Sci.* 29, 105–127. doi:10.1016/j.jsames.2009.08.004

Richards, J. P. (2003). Tectono-magmatic precursors for porphyry Cu-(Mo-Au) deposit formation. *Econ. Geol.* 98, 1515–1533. doi:10.2113/gsecongeo.98.8.1515

Rizzotto, G. J., and Hartmann, L. A. (2012). Geological and geochemical evolution of the Trincheira Complex, a Mesoproterozoic ophiolite in the southwestern Amazon craton, Brazil. *Lithos* 148, 277–295. doi:10.1016/j.lithos.2012.05.027

Rocha, L. G. d. M., Correa, R. T., Silva, A. B. d., and Matos, D. R. (2019). Geophysical reassessment of the azimuth 125° lineament: emplacement model and propagation of its dikes. *J. Geol. Surv. Braz.* 2, 87–98. doi:10.29396/jgsb.2019.v2.n1.6

Rodríguez, G. A., and Bierlein, F. P. (2002). The Minas Azules deposit – an example of orogenic lode gold mineralization in the Sierra de Rinconada, northern Argentina. *Int. Geol. Rev.* 44, 1053–1067. doi:10.2747/0020-6814.44.11.1053

Rohrlach, B., Poma, O., Rosero, B., Silva, J., and Ward, J. (2015). "High-grade porphyry copper-gold mineralisation in north-west Ecuador – the Alpala Cu-Au porphyry discovery," in PACRIM 2015 Congress, Hong Kong, China, 369–376.

Romero, D., Valencia, K., Alarcón, P., Peña, D., and Ramos, V. A. (2013). The offshore basement of Perú: evidence for different igneous and metamorphic domains in the forearc. *J. S. Am. Earth Sci.* 42, 47–60. doi:10.1016/j.jsames.2012.11.003

Roperch, P., Carlotto, V., Ruffet, G., and Fornari, M., (2011). Tectonic rotations and transcurrent deformation south of the Abancay deflection in the Andes of southern Peru. *Tectonics* 30, TC2010. doi:10.1029/2010tc002725

Rosenbaum, G., Giles, D., Saxon, M., Betts, P. G., Weinberg, R. F., and Duboz, C. (2005). Subduction of the Nazca Ridge and the inca plateau: insights into the formation of ore deposits in Peru. *Earth Planet. Sci. Lett.* 239, 18–32. doi:10.1016/j.epsl.2005.08.003

Salfity, J. A. (1985). Lineamientos transversales al rumbo andino en el noroeste argentino. IV Congreso Geológico Chileno. *Actas* 2, 119–137.

Santos, J. O. S., Rizzotto, G. J., Potter, P. E., McNaughton, N. J., Matos, R. S., Hartmann, L. A., et al. (2008). Age and autochthonous evolution of the Sunsás orogen in west Amazon craton based on mapping and U–Pb geochronology. *Precambrian Res.* 165, 120–152. doi:10.1016/j.precamres.2008.06.009

Santos, J. O. S., van Breemen, O. B., Groves, D. I., Hartmann, L. A., Almeida, M. E., McNaughton, N. J., et al. (2004). Timing and evolution of multiple paleoproterozoic magmatic arcs in the Tapajós domain, Amazon craton: constraints from SHRIMP and TIMS zircon, baddeleyite and titanite U–Pb geochronology. *Precambrian Res.* 131, 73–109. doi:10.1016/j.precamres.2004.01.002

Santos, M. N. S., and Oliveira, D. C. (2016). Rio Maria granodiorite and associated rocks of ourilândia do Norte – carajás province: petrography, geochemistry and implications for sanukitoid petrogenesis. *J. S. Am. Earth Sci.* 72, 279–301. doi:10.1016/j.jsames.2016.09.002

Sato, A. M., Tickyi, H., Llambías, E. J., and Sato, K. (2000). The las Matras tonalitic-trondhjemitic pluton, central Argentina: grenvillian age constraints, geochemical

characteristics, and regional implications. *J. S. Am. Earth Sci.* 13, 587–610. doi:10.1016/s0895-9811(00)00053-5

Sawkins, F. J. (1972). Sulfide ore deposits in relation to plate tectonics. *J. Geol.* 80, 377–397. doi:10.1086/627762

Scarpelli, W. (2021). The corridor of mineralization in the California gold district, in the Santander Department of Colombia. *J. Geol. Surv. Braz.* 4, 23–41. doi:10.29396/jgsb.2021.v4.n1.2

Schutte, P., Chiaradia, M., Barra, F., Villagómez, and Beate, B. (2012). Metallogenic features of Miocene porphyry Cu and porphyry-related mineral deposits in Ecuador revealed by Re-Os, 40Ar/39Ar, and U-Pb geochronology. *Miner. Deposita* 47, 383–410. doi:10.1007/s00126-011-0378-z

Schiffer, C., Doré, A. G., Foulger, G. R., Franke, D., Geoffroy, L., Gernigon, L., et al. (2020). Structural inheritance in the North atlantic. *Earth-Science Rev.* 206, 102975. doi:10.1016/j.earscirev.2019.102975

Schneider, E. D., and Dorion, S. (2005). *Into the cool: Energy flow, thermodynamics and life*. Chicago: The University of Chicago Press, 362.

Schreiber, D. W., Fontboté, L., and Lochmann, D. (1990). Geologic setting, paragenesis, and physicochemistry of gold quartz veins hosted by plutonic rocks in the Pataz region. *Econ. Geol.* 85, 1328–1347. doi:10.2113/gsecongeo.85.7.1328

Shaw, R. P., Leal-Mejía, H., and Draper, J. C. M. (2019). "Phanerozoic metallogeny in the Colombian Andes: a tectono-magmatic analysis in space and time," in *Geology and tectonics of northwestern South America. Frontiers in Earth sciences*. Editors F. Cediel and R. P. Shaw, 411–550.

Sibson, R. H. (1985). A note on fault reactivation. *J. Struct. Geol.* 7, 751–754. doi:10.1016/0191-8141(85)90150-6

Sibson, R. H. (1992). Fault-valve behavior and the hydrostatic-lithostatic fluid pressure interface. *Earth-Science Rev.* 32, 141–144. doi:10.1016/0012-8252(92)90019-p

Sillitoe, R. H. (1976). Andean mineralization: a model for the metallogeny of convergent plate margins. *Geol. Assoc. Can. Special Pap.* 14, 59–100.

Sillitoe, R. H., and Perello, J. (2005). Andean copper province: tectonomagmatic settings, deposit types, metallogeny, exploration, and discovery. *Econ. Geol. 100th Anniv.*, 845–890.

Sillitoe, R. H. (2008). Special paper: major gold deposits and belts of the North and southSouth American Cordillera: distribution, tectonomagmatic settings, and metallogenic considerations. *Econ. Geol.* 103, 663–687. doi:10.2113/gsecongeo.103.4.663

Skirrow, R. G., Camacho, A., Lyons, P., Pieters, P. E., Sims, J. P., Stuart-Smith, P. G., et al. (2000). Metallogeny of the southern Sierras Pampeanas, Argentina: geological, 40Ar-39Ar dating and stable isotope evidence for devonian Au, Ag-Pb-Zn and W ore formation. *Ore Geol. Revies* 17, 39–81. doi:10.1016/s0169-1368(00)00004-4

Souza, V. d. S., de Souza, A. G. H., Dantas, E. L., and Valério, C. d. S. (2015). K'Mudku A-type magmatism in the southernmost Guyana Shield, central-north Amazon craton (Brazil): the case of pedra do gavião syenogranite. *Braz. J. Geol.* 45, 293–306. doi:10.1590/23174889201500020008

Spikings, R. A., Winkler, W., Hughes, R. A., and Handler, R. (2005). Thermochronology of allochthonous terranes in Ecuador: unravelling the accretionary and post-accretionary history of the northern Andes. *Tectonophysics* 399, 195–220. doi:10.1016/j.tecto.2004.12.023

Spikings, R., Reitsma, M. J., Boekhout, F., Mišković, A., Ulianov, A., Chiaradia, M., et al. (2016). Characterisation of Triassic rifting in Peru and implications for the early disassembly of western Pangaea. *Gondwana Res.* 35, 124–143. doi:10.1016/j.gr.2016.02.008

Stephenson, R., Yegorova, T., and Stovba, S. (2021). An investigation of how intracratonic rifting is "seeded": case study of the late devonian Dniepr-Donets basin rift within the east European craton. *Precambrian Res.* 362, 106305. doi:10.1016/j.precamres.2021.106305

Stern, R. J., and Gerya, T. (2018). Subduction initiation in nature and models: a review. *Tectonophysics* 746, 173–198. doi:10.1016/j.tecto.2017.10.014

Szappanosné-Vágó, E., Moritz, R., and Barra, F. (2010). *Fluid inclusion investigation and Re-Os dating of the Pataz-Parcoy intrusion-hosted gold deposits, Eastern Cordillera, Peru. EG51, Crustal fluids and gold*, 260.

Tassara, S., González-Jiménez, J. M., Reich, M., Schilling, M. E., Morata, D., Begg, G., et al. (2017). Plume-subduction interaction forms large auriferous provinces. *Nat. Commun.* 843, 843–847. doi:10.1038/s41467-017-00821-z

Tassinari, C. C. G., Castroviejo, R., Rodrigues, J. F., Acosta, J., and Pereira, E. (2011). A Neoproterozoic age for the chromitite and gabbro of the Tapo ultramafic Massif, Eastern Cordillera, Central Peru and its tectonic implications. *J. S. Am. Earth Sci.* 32, 429–437. doi:10.1016/j.jsames.2011.03.008

Tedeschi, M. T., Hagemann, S. G., Kemp, A. I. S., Kirkland, C. L., and Ireland, T. R. (2020). Geochronological constrains on the timing of magmatism, deformation and mineralization at the Karouni orogenic gold deposit: guyana, South America. *Precambrian Res.* 337, 105329. doi:10.1016/j.precamres.2019.04.015

Teixeira, J. B. G., Misi, A., and da Silva, M. d. G. (2007). Supercontinent evolution and the proterozoic metallogeny of SouthSouth America. *Gondwana Res.* 11, 346–361. doi:10.1016/j.gr.2006.05.009

Teixeira, W., Geraldes, M. C., Matos, R., Ruiz, A. S., Saes, G., and Vargas-Mattos, G. (2010). A review of the tectonic evolution of the Sunsás belt, SW Amazonian Craton. *J. S. Am. Earth Sci.* 29, 47–60. doi:10.1016/j.jsames.2009.09.007

Thébaud, N., Sugiono, D., LaFlamme, C., Miller, J., Fisher, L., Voute, F., et al. (2018). Protracted and polyphased gold mineralisation in the agnew district (Yilgarn craton, western Australia). *Precambrian Res.* 310, 291–304. doi:10.1016/j.precamres.2018.02.013

Thomas, W. A. (2006). Tectonic inheritance at a continental margin. *GSA Today* 16, 4–11. doi:10.1130/1052-5173(2006)016[4:tiaacm]2.0.co;2

Tohver, E., Cawood, P. A., Rossello, E. A., and Jourdan, F. (2021). Closure of the Clymene Ocean and formation of West Gondwana in the cambrian: evidence from the Sierras australes of the southernmost Rio de la Plata craton, Argentina. *Gondwana Res.* 21, 394–405. doi:10.1016/j.gr.2011.04.001

Trevisan, V. G., Hagemann, S. G., Loucks, R. R., Xavier, R. P., Motta, J. G., Parra-Avila, L. A., et al. (2021). Tectonic switches recorded in a paleoproterozoic accretionary orogen in the alta floresta mineral province, southern amazonian craton. *Precambrian Res.* 364, 106324. doi:10.1016/j.precamres.2021.106324

Trunfull, E. F., Hagemann, S. G., Xavier, R. P., and Moreto, C. P. N. (2020). Critical assessment of geochronological data from the Carajás mineral province, Brazil: implications for metallogeny and tectonic evolution. *Ore Geol. Rev.* 121, 103556. doi:10.1016/j.oregeorev.2020.103556

Urbina, N. E., and Sruoga, P. (2008). *K-Ar mineral age constraints on the Diente Verde porphyry deposit formation, San Luis, Argentina*. San Carlos de Bariloche, Argentina: VI South American Symposium on Isotope Geology, 1–4.

Valdiya, K. S. (1976). Himalayan transverse faults and folds and their parallelism with subsurface structures of north Indian plains. *Tectonophysics* 32, 353–386. doi:10.1016/0040-1951(76)90069-x

Van den Broek, J. M., Magni, V., and Buiter, S. J. H. (2020). The formation of continental fragments in subduction settings: the importance of structural inheritance and subduction system dynamics. *J. Geophys. Res. Solid Earth* 125, e2019JB018370. doi:10.1029/2019JB018370

Villanes, C., Wiemer, D., and Hagemann, S. G. (2023). *4D tectonic-magmatic evolution and regional implications for the Pataz gold deposits, Eastern Andean Cordillera, northern Peru* in Proceedings of the 26th World Mining Congress, Brisbane, Australia, 1474–1485.

Von Gosen, W., Loske, W., and Prozzi, C. (2002). New isotopic dating of intrusive rocks in the Sierra de San Luis (Argentina): implications for the geodynamic history of the eastern Sierras Pampeanas. *J. S. Am. Earth Sci.* 15, 237–250. doi:10.1016/s0895-9811(02)00016-0

Voute, F., Hagemann, S. G., Kemp, A. I. S., Thébaud, N., Evans, N. J., and Villanes, C. (2019). Protracted evolution of the Marañón Valley Au Belt magmatic complex in the Peruvian Andes using zircon oxygen isotopes, Lu-Hf and U-Pb analyses. *Lu-Hf U-Pb analyses Lithos* 338, 34–57. doi:10.1016/j.lithos.2019.03.036

Wang, Z., Cheng, H., Zong, K., Geng, X., Liu, Y., Yang, J., et al. (2019). Metasomatized lithospheric mantle for Mesozoic giant gold deposits in the North China craton. *Geology* 48, 169–173. doi:10.1130/g46662.1

Weinberg, R. F., Van der Borgh, P., Bateman, R. J., and Groves, D. I. (2005). Kinematic history of the boulder-lefroy shear zone system and controls on associated gold mineralization, Yilgarn craton, western Australia. *Econ. Geol.* 100, 1407–1426. doi:10.2113/gsecongeo.100.7.1407

Wesselingh, F. P., Hoorn, M. C., Guerrero, J., Räsänen, M. E., Pittmann, L. R., and Salo, J. (2006). The stratigraphy and regional structure of Miocene deposits in western Amazonia (Peru, Colombia and Brazil), with implications for late Neogene landscape evolution. *Scr. Geol.* 133, 291–321.

Wiemer, D., Hagemann, S. G., Hronsky, J., Kemp, A. I. S., Thébaud, N., Ireland, T., et al. (2022). Ancient structural inheritance explains gold deposit clustering in northern Peru. *Geology* 50, 1197–1201. doi:10.1130/g50208.1

Wiemer, D., Hagemann, S. G., Kemp, A. I. S., Hronsky, J., Martin, L., Ireland, T., et al. (2023). "Superimposed orogeny as key to gold hotspot formation at the Peruvian Gondwana margin," in 17th SGA conference (Zürich, Switzerland: Extended Abstract), 1–4.

Wiemer, D., Hagemann, S. G., Kemp, A. I. S., Thébaud, N., Ireland, T., and Villanes, C. (2021b). "Timescales and processes of Au and Cu fertile magmatic-hydrothermal reservoir accumulation in continental arcs," in SEG100 Conference: Celebrating a Century of Discovery, Lindgren's Legacy – Ore Deposits in Depth, 1–2. abstract 4154.

Wiemer, D., Hagemann, S. G., Thébaud, N., Villanes, C., and Cueva, F. (2020). *4D tectonic-structural framework for gold mineralization in Pataz, Eastern Andean Cordillera, northern Peru: Implications for field and analytical exploration targeting*. Compañia Minera Poderosa S.A., 1–442. Unpublished company report.

Wiemer, D., Hagemann, S. G., Thébaud, N., and Villanes, C. (2021a). Role of basement structural inheritance and strike-slip fault dynamics in the formation of the Pataz gold vein system, Eastern Andean Cordillera, northern Peru. *Econ. Geol.* 116, 1503–1535. doi:10.5382/econgeo.4839

Wilkin, R. T., and Bornhorst, T. J. (1993). Archean appinites from the northern complex, Michigan. *J. Geol.* 101, 107–114. doi:10.1086/648199

Willner, A. P., Gerdes, A., Massonne, H.-J., Schmidt, A., Sudo, M., Thomson, S. N., et al. (2011). The geodynamics of collision of a microplate (Chilenia) in Devonian times deduced by the pressure-temperature-time evolution within part of a collisional belt (Guarguaraz Complex, W-Argentina). *Contributions Mineralogy Petrology* 162, 303–327. doi:10.1007/s00410-010-0598-8

Willner, A. P., Tassinari, C. C. G., Rodrigues, J. F., Acosta, J., Castroviejo, R., and Rivera, M. (2014). Contrasting Ordovician high- and low-pressure metamorphism related to a microcontinent-arc collision in the Eastern Cordillera of Perú (Tarma province). *J. S. Am. Earth Sci.* 54, 71–81. doi:10.1016/j.jsames.2014.05.001

Witt, W. K., Hagemann, S. G., and Villanes, C. (2013b). Geochemistry and geology of spatially and temporally associated calc-alkaline (I-type) and K-rich (A-type) magmatism in a Carboniferous continental arc setting, Pataz gold-mining district, northern Peru. *Aust. J. Earth Sci.* 61, 17–42. doi:10.1080/08120099.2013.797025

Witt, W. K., Hagemann, S. G., Villanes, C., and Qingtao, Z. (2013a). New geochronological results and structural evolution of the Pataz gold mining district: implications for the timing and origin of the batholith-hosted veins. *Ore Geol. Rev.* 50, 143–170. doi:10.1016/j.oregeorev.2012.10.007

Witt, W. K., Hagemann, S. G., Villanes, C., Vennemann, T., Zwingmann, H., Laukamp, C., et al. (2016). Multiple gold mineralizing styles in the northern Pataz district, Peru. *Econ. Geol.* 111, 355–394. doi:10.2113/econgeo.111.2.355

Wyborn, L. A. I., Heinrich, C. A., and Jaques, A. I. (1994). "Australian proterozoic mineral systems: essential ingredients and mappable criteria," in Australian Institute of Mining and Metallurgy Annual Conference, Melbourne, 109–115.

Wyman, D. A., Cassidy, K. F., and Hollings, P. (2016). Orogenic gold and the mineral systems approach: resolving fact, fiction and fantasy. *Ore Geol. Rev.* 78, 322–335. doi:10.1016/j.oregeorev.2016.04.006

Xiong, L., Zhao, X. F., Zhao, S. R., Lin, H. T., Lin, Z. W., Zhu, Z. X., et al. (2021). Formation of giant gold provinces by subduction-induced reactivation of fossilized, metasomatized continental lithospheric mantle in the North China Craton. *Chem. Geol.* 580, 120362. doi:10.1016/jchemgeo.2021.120362

Yang, C.-X., and Santosh, M. (2020). Ancient deep roots for mesozoic world-class gold deposits in the north China craton: an integrated genetic perspective. *Geosci. Front.* 11, 203–214. doi:10.1016/j.gsf.2019.03.002

Young, A., Flament, N., Maloney, K., Williams, S., Matthews, K., Zahirovic, S., et al. (2019). Global kinematics of tectonic plates and subduction zones since the late Paleozoic Era. *Geosci. Front.* 10, 989–1013. doi:10.1016/j.gsf.2018.05.011

Zamora, G., and Gil, W. (2018). "The marañón basin: tectonic evolution and paleogeography," in *Petroleum basins and hydrocarbon potential of the Andes of Peru and Bolivia*. Editors G. Zamora, K. R. McClay, and V. A. Ramos (AAPG Memoir), 117, 121–144.

Zentilli, M., Maksaev, V., Boric, R., and Wilson, J. (2018). Spatial coincidence and similar geochemistry of late triassic and eocene–oligocene magmatism in the Andes of northern Chile: evidence from the MMH porphyry type Cu–Mo deposit, Chuquicamata district. *Int. J. Earth Sci.* 16 (2), 1097–1126. doi:10.1007/s00531-018-1595-9

Zwaan, F., Chenin, P., Erratt, D., Manatschal, G., and Schreurs, G. (2021). Competition between 3D structural inheritance and kinematics during rifting: insights from analogue models. *Basin Res.* 34, 824–854. doi:10.1111/bre.12642